FAILURE MECHANISMS IN A QUASI-ISOTROPIC CERAMIC COMPOSITE LAMINATE UNDER TENSILE FATIGUE LOADING

THESIS

Gregory D. Tracy

Captain, USAF

AFIT/GAE/ENY/90D-30

DEPARTMENT OF THE AIR FORCE
AIR UNIVERSITY
AIR FORCE INSTITUTE OF TECHNOLOGY

Wright-Patterson Air Force Base, Ohio

AFIT/GAE/ENY/90D-30

FAILURE MECHANISMS IN A QUASI-ISOTROPIC CERAMIC COMPOSITE LAMINATE UNDER TENSILE FATIGUE LOADING

THESIS

Gregory D. Tracy

Captain, USAF

AFIT/GAE/ENY/90D-30

Approved for public release; distribution unlimited

AFIT/GAE/ENY/90D-30

FAILURE MECHANISMS IN A QUASI-ISOTROPIC CERAMIC COMPOSITE LAMINATE UNDER TENSILE FATIGUE LOADING

THESIS

Presented to the Faculty of the School of Engineering
of the Air Force Institute of Technology
Air University
In Partial Fulfillment of the
Requirements for the Degree of
Master of Science in Aeronautical Engineering

Gregory D. Tracy
Captain, USAF

December 1990

Preface

The purpose of this study was to investigate the fatigue failure mechanisms present in a symmetric quasi-isotropic Nicalon-CASII ceramic composite. Ceramic composites have been the receipients of an increasing amount of attention in the search for materials that can meet the requirements of future aerospace applications.

The study was conducted in two parts. First, an experimental testing station had to be developed and tested.. Then, $(0/\pm 45/90)s$ quasi-isotropic Nicalon-CASII ceramic composite specimens were placed in the station and subjected to sinusoidal tensile fatigue loading at various stress levels. The results were then compared to theoretical and analytical models to see how closely they correlated.

Many people contributed to this project. I wish to thank my advisor Dr. Shankar Mall for his help and guidance during my stay at AFIT. Next, I thank George Hartman and Larry Zawada of University of Dayton Research Institute, for all of their assistance and patience. Also, I thank Jay Anderson and the other technicians of the AFIT Laboratory for their help in the use of the lab facilities, and Tim Hancock and the craftsmen of the AFIT workshop for their manufacturing expertise. Finally, I thank my wife Kate, for her patience and understanding during this time, but most of all, I thank the Lord for getting me through this.

Gregory D. Tracy

Table of Contents

List of Figures

List of Tables

List of Symbols

Symbol	Definition
E_1	Principal direction axial modulus of elasticity for lamina
E_2	Principal direction transverse modulus of elasticity for lamina
G_{12}	Shear modulus for the composite lamina
ν_{12}	Poissons ratio for lamina
C_{ij}	Stiffness matrix
S_{ij}	Compliance matrix
Q_{ij}	Reduced stiffness matrix
A_{ij}	Extensional stiffness matrix
B_{ij}	Coupling stiffness matrix
D_{ij}	Bending stiffness matrix
N_x	Longitudinal tensile load
E_x	Principal modulus of elasticity for laminate
E_{x0}	Initial modulus of elasticity
σ	Applied stress
σ_{max}	Maximum applied stress
σ_{min}	Minimum applied stress
R	Stress ratio ($\sigma_{min}/\sigma_{max}$)
ϵ_x	Principal direction strain

ABSTRACT

A study was conducted to experimentally investigate the tensile fatigue damage mechanisms in a quasi-isotropic ceramic matrix composite (Corning's Nicalon/CASII). The goals of this study were to (1) develop a grip fixture for a servo-hydraulic MTS test machine capable of applying an axial tensile load in a small composite specimen without inducing any twisting or bending moments and (2) conduct tests with $(0/\pm45/90)_s$ Nicalon/CASIII specimens subjected to tensile fatigue loading to study their fatigue damage growth mechanisms.

The grip fixture that offered the best compromise between cost and accuracy was a servo-hydraulic grip fixture that has been developed by the Wright Research and Development Center's Materials Laboratory. This system consisted of an air-driven hydraulic compressor which applied pressure on the grip assembly via a yoke and piston arrangement. The alignment of the grip fixture was maintained by a Woods metal plug and cylinder assembly. An anti-rotation device was constructed to prevent the piston of the MTS hydraulic mechanism from rotating during testing. The fixture was built, tested and found to have less than 5% strain due to bending.

Eight different specimens were tested in the test station. Each specimen was subjected to tensile fatigue

cycling at a given stress level. These eight stress levels were chosen based upon work done on the same material by Mall and Kim (8). In this prior study, first ply failure had been determined to occur at 5.8 KSI (40 MPa). A further decrease in the stiffness of the material had been observed at 13.1 KSI (90 MPa). The other tests were run at stresses between or above these. During the tests, replicas of the edge of the specimens were taken at points of significant modulus decrease in the fatigue cycling to obtain a permanent visual record of the damage initiation and progression for each specimen. Measurements of the principal axial modulus of elasticity (E_1) were measured at regular intervals with an extensometer and a load cell to monitor the decrease in stiffness.

The material had an average initial elastic modulus of 17.1 MSI (117.78 MPa). All of the specimens tested at stresses below 13.1 KSI (90 MPa) lasted for more than 1,000,000 cycles, while all of the specimens tested at or above 13.1 KSI (90 MPa) lasted less than 700 cycles. The stress level of 13.1 KSI (90 MPa) corresponded with the level of second stiffness decrease noted by Mall and Kim. Residual strength decreased as applied stress increased. Most of the damage in the tests occurred in the early stages of cycling, with the modulus stabilizing to within 10 percent of the final value after 1000 cycles. A complete history of damage initiation and progression was recorded for all tests in order to explain the

observed behavior of the test specimens.

The "Critical Element Approach" developed by Reifsnider (1) was used to model the residual fatigue life of the material. The critical elements of the material were the 0 degree plies. As long as these plies remain undamaged, the material remained intact. Classical laminated plate theory, using a total ply discount method, was used to depict, in a simplified manner, the residual fatigue life of the material as was done previously by Rousseau (2). The material also followed the trend of the composite fatigue damage model suggested by Reinsnider (8), when the damage parameter of the failed specimens were plotted as a function of the percent life.

INVESTIGATION OF FAILURE MODES IN A QUASI-ISOTROPIC NICALON-CASII CERAMIC COMPOSITE LAMINATE UNDER TENSILE FATIGUE LOADING

I. Introduction

Ceramic matrix composites (CMCs) have come under an increased amount of investigation as engineers look for new materials to meet the requirements being generated by the National Aerospace Plane (NASP) and advanced propulsion systems. While it is generally known that CMC's retain their high strength at high temperatures, they are relatively brittle, and much remains to be discovered about their fatigue life properties before these materials can be used in practical applications.

There are many variables involved in the construction of a composite laminate. Factors such as fiber and matrix material properties, fiber and matrix volume fractions, type of bond between matrix and fiber, and the number and orientation of lamina, must be taken into account. This makes accurate prediction of a given ceramic composite's material properties through analytical methods difficult. Current theoretical models cannot completely describe the fatigue life

properties of a given ceramic matrix composite. Therefore, in order to obtain accurate fatigue life information for a given CMC, experimental testing must be done. Not only do the results describe the properties of the material, they can also be used to refine the analytic models.

The fatigue failure mechanisms of ceramic matrix composite laminates are not completely available, and are possibly influenced by temperature, stress, and environment. These damage mechanisms need to be fully understood before the material can be used in practical applications.

This research was done to contribute to the body of knowledge of fatigue failure mechanisms in ceramic matrix composite laminates. A quasi-isotropic symmetric Nicalon /CASIII laminate manufactured by Corning Glass Works was tested. Nicalon, manufactured by Nippon Carbon Co., is an amorphous crystallite predominantly silicon carbon fiber (SiC) commonly available in a 1800 denier tow. CASIII is a calcium-alumino- silicate crystalline glass-ceramic used for the matrix (6). It is one of the few good model ceramic composite materials available.

A. Background

The amount of experimentation involving failure investigation in ceramic based composites has been quite limited over

the past few years. Reifsnider and Stinchcomb (1) have suggested that the "Critical Element" analytical theory developed for polymer composites could be used for ceramics. Rousseau (2) used this apprach when he examined the fatigue behavior in Nicalon/CASII $[0/90]_{2S}$ laminates at room temperature and at elevated temperature. Prewo, Layden and Minford (3) studied a Nicalon silicon carbide fiber reinforced lithium aluminosilicate (LAS) glass ceramic system over a wide range of conditions, including fatigue, to prepare it for use in high temperature applications. Mandell, Grande, and Edwards (4) have studied the cyclic fatigue stress-strain response of unidirectional glass ceramic composites at high temperatures. Hartman (5) developed a low-cost, high-precision fatigue grip fixture system and, Zawada and Butkus (6) used it to conduct room and elevated temperature fatigue tests of $[0]_{10}$ and $[0/90]_3$ SiC/1723. Until now, there has been no comprehensive study of fatigue damage mechanisms in quasi-isotropic symmetric lay-up ceramic matrix composites. Such a study would require a grip fixture that would allow for precise permanent alignment of small ceramic specimens.

B. Purpose of This Study

This research focused on the study tensile fatigue failure mechanisms in $[0/\pm45/90]_S$ Nicalon/CASIII laminates.

Specifically, this study involved (1) the development of a grip fixture to hold small samples of ceramic matrix composite, (2) the testing of the Nicalon/CAS specimens in the grip fixture, (3) the observation of damage initiation and progression as a function of applied load and cycle count, and (4) the comparison of the test results with theoretical and analytical models.

C. Approach

The first step taken was the construction of a grip fixture that would maintain a high degree of alignment throughout the duration of the testing. A suitable test station has been in operation at the USAF Material Laboratory, Wright-Patterson Air Force Base, Ohio (5). This test station was adapted to one of the existing MTS test stands in the AFIT Laboratory. After the new grip fixture was built, it was aligned and tested for accuracy.

Nicalon/CasIII quasi-isotropic composite specimens were fatigue tested at various load levels to investigate in a systematic way damage initiation and progression as a function of cycle count. The composite specimens were cut from a single panel using a diamond saw, then polished on one edge to allow acetate film replications to be taken. The specimens had fiberglass tabs epoxied to them to act as stress reliefs and

then were mounted into the test station. Tensile fatigue tests were performed at eight different stress levels; 5.80 Ksi (40MPa), 8.70 Ksi (60 MPa), 10.15 Ksi (70 MPa), 11.6 Ksi (80MPa), 12.33 Ksi (85 MPa), 13.05 Ksi (90 MPa), 13.78 Ksi (95 MPa), and 14.5 Ksi (100 MPa). These stress levels were determined from static tension testing done previously on the same material by Mall and Kim (7). The 5.8 Ksi (40 MPa) stress was observed to be the first ply failure point of the material, and 13.05 Ksi (90 MPa) was the stress at which further modulus decrease was noticed. Strain was measured using an MTS extensometer, stress was measured by a load cell, and replications were taken at various cycle counts to record damage initiation and progression. The specimens that remained intact after the fatigue cycling were tested for residual strength. The results of the tests were then compared to current theoretical and analytical models.

Chapter II will describe the research that has already been conducted in this area of interest and will detail the analytical models that are currently being used to evaluate fatigue life for polymer composite laminates. There are no theoretical models for the estimation of fatigue life of ceramic composites. It has been demonstrated that some polymer composite residual fatigue life theories can be applied to ceramic composites and that static laminated plate theories

can be used to model modulus deterioration in fatigue.

Chapter III will review the development and construction of the grip fixture and explain the experimental method employed during the testing of the Nicalon/CASIII samples

Chapter IV will deliberate on the results of the tests and will show how these results compare with theory.

Chapter V and VI will offer conclusions and recommendations from this research.

II. Background

Nicalon/CASIII is a relatively new ceramic matrix composite. The foremost attribute of this material is the ability to retain high strength at elevated temperatures. Lately, much research has been done on the material to determine its characteristic properties.

This chapter will review some of the previous studies which are related to the present investigation. The analytical models that deal with composite strength, laminate fatigue damage characteristics, and the critical element approach will be presented in order to apply them to this material.

A. Experimental Background

There has been some research recently that had been dedicated to the study of fatigue in ceramic matrix composites, but, there has not been any fatigue research done with $[0/\pm 45/90]_S$ Nicalon/CASIII utilizing acetate replications to systematically record crack initiation and growth as a function of load and cyclic duration.

Reifsnider and Stinchcomb (1) proposed a residual fatigue life estimation method called the "Critical Element Approach" This method suggested that, for polymeric based

composites, the residual fatigue life was not dependant upon the lay-up of the material, but upon the critical plies of the material, usually the on-axis plies. If these critical plies remained intact, the material survived, if these plies failed, the material failed. The other plies defined the state of stress in the critical elements of the material and were sub-critical elements.

Reifsnider and Stinchcomb (8) also investigated fatigue damage progression for a large class of polymer-based composite systems. They developed a model that suggested damage progressed as a function of percent of life through a series of sequential modes that consisted of; (a) primary matrix cracking in the off-axis plies, (b) crack coupling with secondary cracks developing off the primaries, (c) delamination caused by mixed-mode crack growth, (d) fiber breaking in on-axis or near on-axis plies, and finally, (e) fracture.

Rousseau, (2) experimentally observed the room and elevated temperature quasi-static and cyclic behavior of $(0/90)_{2S}$ and $(\pm 45)_{2S}$ Nicalon/CASII laminates, and applied the "Critical Element" approach to fatigue-life characterization. A major premise of this study was that a parallel could be drawn between ceramic and polymeric composites, in other words, that the method Reifsnider et al. used for residual fatigue life estimation for polymeric composites could be

applied to ceramic composites. In the $(0/90)_{2S}$ laminate, the 0^0 plies were found to be the critical life-limiting elements of laminate behavior and the 90^0 plies were sub-critical elements.

Prewo, Layden and Minford (3) performed a series of studies using a Nicalon fiber reinforced lithium aluminosilicate (LAS) glass ceramic system over a wide range of conditions, including fatigue, to prepare it for use in high temperature applications. Mandell, Grande, and Edwards (4) studied the cyclic fatigue stress-strain response of unidirectional glass ceramic composites at elevated temperatures.

Hartman (5) devised a unique, low-cost, high degree of alignment precision grip fixture that featured a pair of servo-hydraulic grips in conjunction with a Woods metal alignment assembly. Zawada and Butkus (6) used this arrangement to observe the room and elevated temperature fatigue characteristics of Sic/1723 $(0/90)_{3S}$ and $(0)_{10}$ laminates. This study demonstrated how the materials acted in a dichotomous manner, that is, when tested below a critical fatigue stress limit for that material, the material could be fatigued indefinitely, but when the material was tested above this limit the material life span was very limited. This study indirectly confirmed that the Critical Element model approach could be used for ceramic composite materials.

Mall and Kim (7) studied failure mechanisms in a quasi-isotropic $[0/\pm 45/90]_S$ laminate of Nicalon/CASIII composite under static tensile loading. They observed that cracking initiated in the 90^0 and 45^0 plies in a random fashion well below the proportional limit. However, there were no cracks spanning the width of the whole specimen. They used classical laminated plate theory to predict the behavior of the tested laminate and achieved good agreement between the theory and the experimental results.

Daniel, Anastassopoulos, and Lee (9) conducted tests on unidirectional Nicalon/CAS under longitudinal and transverse static tensile loading. They observed how failure under transverse loading consisted of radial and interfacial cracks, while failure under longitudinal loading involved transverse matrix cracking of increasing density, followed by fiber fracture and debonding.

Fink (10) did a similar study in which Nicalon/CASII was statically tested at several off-axis (15, 30, 45, 60, and 90 degree) orientations. The principal longitudinal and transverse material modulii and the Poisson's ratio for the lamina were experimentally determined as a result of the testing. The material tested was identical to the material studied in this report, so the material properties that were experimentally determined for the lamina in that study were used to find the

theoretical material properties of the laminate using classical laminated plate theory in this investigation.

B. Theoretical Models

There were no theoretical models dedicated to ceramic matrix composite laminate fatigue damage propagation or residual fatigue life estimation. That is, no numeric solutions were available to predict how or when a given composite would fail during cyclic tensile fatigue loading. However, there were empirical models that have been used to estimate residual fatigue life. Classical static laminated plate theory, with total ply discount methods, while originally intended to be used for static problems, has been validated as a technique for the prediction of modulus degradation and therefore, damage progression and residual fatigue life in a simplified fashion (12-14).

1. Classical Laminated Plate Theory

If the values for principal modulus of elasticity (E_1 and E_2), principle Poisson's ratio (ν_{12}) and principal shear modulus (G_{12}), for the Nicalon/CAS unidirectional lamina are known, then the material properties for the $(0/\pm45/90)_s$ laminate can be formulated using laminated plate theory as detailed in Jones (11:48-186).

The stress-strain relationship for an anisotropic (no

planes of symmetry) material were formulated using generalized Hooke's Law. In contracted notation:

$$\sigma_i = C_{ij} * e_j \qquad (i,j=1,..6) \tag{1}$$

In the above equation, C_{ij} is the stiffness matrix which has 36 independent constants for an anisotropic material. This equation was inverted to give strain in terms of stress.

$$e_j = S_{ij} * \sigma_i \qquad (i,j=1,...6) \tag{2}$$

Here the inverse of the stiffness matrix was denoted as S_{ij}, and was called the compliance matrix. For an anisotropic material, this matrix was comprised of 21 independent constants. If two planes of a material were symmetric with respect to a third mutually orthogonal plane, then that material was defined as an orthotropic material. Due to this symmetry, the number of independent constants was reduced from 21 to 9 and the next equation resulted:

$$S_{ij} = S_{ji} \qquad (i,j = 1,..6) \tag{3}$$

It was assumed that the material was subjected to a state of plane stress. When engineering constants were substituted into the orthogonal compliance matrix, the following equations resulted.

$$S_{ij} = \begin{vmatrix} S_{11} & S_{12} & 0 \\ S_{12} & S_{22} & 0 \\ 0 & 0 & S_{66} \end{vmatrix} \tag{4}$$

$$S_{ii} = \frac{1}{E_i} \qquad (i = 1,..2) \tag{5}$$

$$S_{ij} = - \frac{\nu_{ij}}{E_i} \qquad (i,j=1,..2) \tag{6}$$

$$S_{66} = \frac{1}{G_{12}} \tag{7}$$

Equations 3 and 4 allowed for the determination of Poisson's ratio in the longitudinal direction below.

$$\nu_{21} = \nu_{12} * \frac{E_2}{E_1} \tag{8}$$

From the inverted S_{ij} matrix, the reduced stiffness matrix Q_{ij} was formed.

$$\begin{vmatrix} \sigma_1 \\ \sigma_2 \\ \tau_{12} \end{vmatrix} = \begin{vmatrix} Q_{11} & Q_{12} & 0 \\ Q_{12} & Q_{22} & 0 \\ 0 & 0 & Q_{66} \end{vmatrix} * \begin{vmatrix} \epsilon_1 \\ \epsilon_2 \\ \gamma_{12} \end{vmatrix} \tag{9}$$

Where,

$$Q_{ii} = \frac{E_i}{1-\nu_{12}\nu_{21}} \qquad (i = 1,2) \tag{10}$$

$$Q_{12} = \frac{\nu_{21} * E_1}{1 - \nu_{12}*\nu_{21}} \tag{11}$$

$$Q_{66} = G_{12} \tag{12}$$

The Q_{ij} matrix for each lamina in the laminate was transformed to account for the rotation of the fiber direction in the off-axis plies with respect to the load direction axis (Figure 1) .

$$|\bar{Q}| = |T|^{-1} * |Q| * |T|^{-T} \tag{13}$$

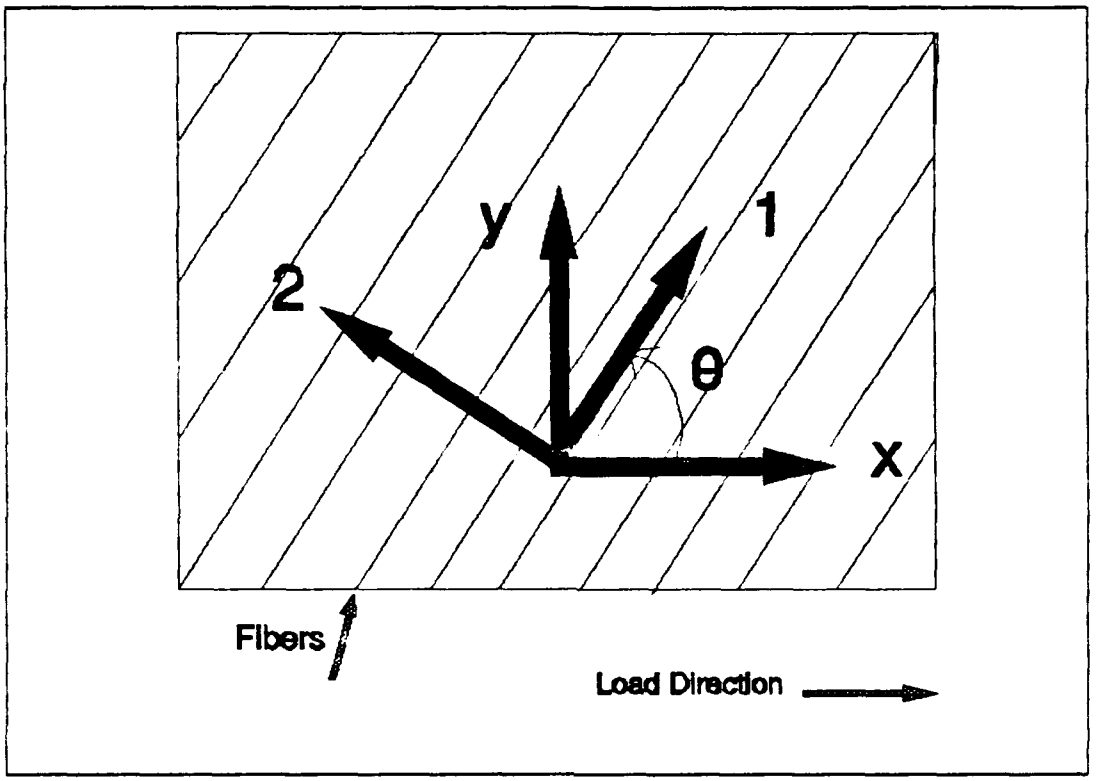

Figure 1 Transformation From Fiber Direction Axis (1-2) to Load Direction Axis (x-y)

$$|T| = \begin{vmatrix} \cos^2\theta & \sin^2\theta & -2\sin\theta\cos\theta \\ \sin^2\theta & \cos^2\theta & 2\sin\theta\cos\theta \\ \sin\theta\cos\theta & -\sin\theta\cos\theta & \cos^2\theta-\sin^2\theta \end{vmatrix} \qquad (14)$$

$$\begin{vmatrix} \sigma_x \\ \sigma_y \\ \tau_{xy} \end{vmatrix} = \begin{vmatrix} \bar{Q}_{11} & \bar{Q}_{12} & 0 \\ \bar{Q}_{12} & \bar{Q}_{22} & 0 \\ 0 & 0 & \bar{Q}_{66} \end{vmatrix} * \begin{vmatrix} \epsilon_x \\ \epsilon_y \\ \gamma_{xy} \end{vmatrix} \qquad (15)$$

After the transformed reduced stiffness matrix had been

created, the extensional stiffness $[A_{ij}]$ matrix, the coupling stiffness $[B_{ij}]$ matrix, and the bending stiffness $[D_{ij}]$ matrix for the laminate.

$$A_{ij} = \sum (\bar{Q}_{ij})_k (z_k - z_{k-1}) \qquad (k = 1, ..N) \qquad (16)$$

$$B_{ij} = \frac{1}{2}\sum (\bar{Q}_{ij})_k (z^2{}_k - z^2{}_{k-1}) \qquad (k = 1, ..N) \qquad (17)$$

$$D_{ij} = \frac{1}{3}\sum (\bar{Q}_{ij})_k (z^3{}_k - z^3{}_{k-1}) \qquad (k = 1, ..N) \qquad (18)$$

Where n was the number of plies and z_k was the distance of the ply boundary to the mid-plane of the laminate. (Figure 2) The combined stress-strain matrix for the laminate was then formed. The middle surface forces N, and moments M, for the laminate were found as a function of the middle surface strains, ϵ_0, and curvatures k.

$$\begin{vmatrix} N \\ M \end{vmatrix} = \begin{vmatrix} A & B \\ B & D \end{vmatrix} * \begin{vmatrix} e^o \\ \kappa \end{vmatrix} \qquad (19)$$

The material modulii were then determined.

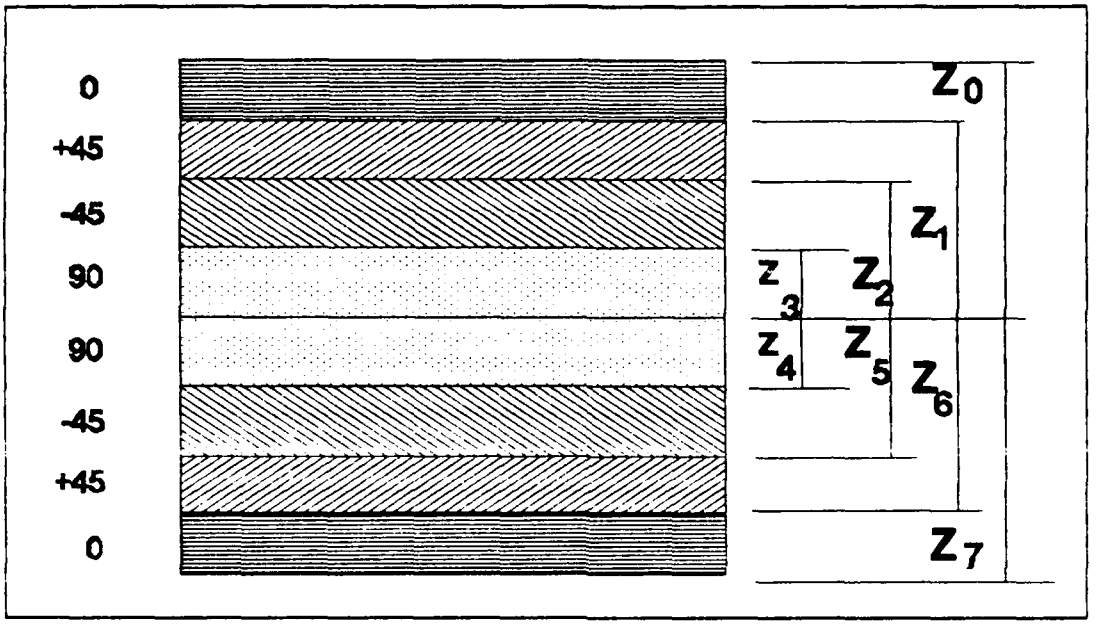

Figure 2 Schematic Representation of Distances From Mid-Plane (Z_k) In $(0/\pm 45/90)_S$ Laminate

$$[A_1] = [A^{-1}] + [A^{-1}] * [B] * ([D] - [B] * [A^{-1}] * [B])^{-1} * [B] * [A^{-1}] \quad (20)$$

$$[B_1] = -[A^{-1}] * [B] * ([D] - [B] * [A^{-1}] * [B])^{-1} \quad (21)$$

$$[C_1] = -([D] - [B] * [A^{-1}] * [B])^{-1} * [B] * [A^{-1}] \quad (22)$$

$$[D_1] = ([D] - [B] * [A^{-1}] * [B])^{-1} \quad (23)$$

From the above equations the principal modulii for the laminate were evaluated for different levels of ply failure using total ply discount methods. These were used predict the

residual fatigue life of the laminate in the critical element approach. Given a pure tensile load along the longitudinal axis (N_1), the value in the first column of the first row of the A_1 matrix was calculated as the principal modulus of elasticity (E_1) for the laminate. By assuming total ply failure in the 90^0 plies, a calculated residual strength value can be compared with the material strength experimentally determined after fatigue cycling at the first ply failure stress of the material. Likewise, by assuming total ply failure in all of the 90^0 and 45^0 plies, another calculated limit can be compared with the experimental results. See chapter 4 for the application of the method.

2. Analytical Models

In Rousseau's study of fatigue damage in Nicalon/CASII ceramic composites (2), the results validated the use of polymer based composite fatigue life prediction methods for ceramic matrix composites. In particular, Rousseau asserted that "Critical Element" approach as suggested by Reifsnider (1) et. al., could be used to predict the residual fatigue life of weak fiber-matrix bond, brittle ceramic matrix composites as well as for strong fiber-matrix bond, polymer-based composites. The "critical element approach" identified critical (life limiting) elements of a laminate, elements that directly affected the fatigue life of the material, modeled

the critical element as a function of cumulative sub-critical element damage and then estimated the remaining fatigue life of the composite. The critical element was modeled using the classical laminated plate theory, with the total ply discount method, as described above, to estimate the current state of sub-critical damage in the material.

Several studies have shown the usefulness of monitoring modulus degredation as a means of characterizing the damage progression during fatigue testing (2,3,4,13,14). Talreja (12) noted that "In order to predict fatigue life it is necessary not only to establish the sequential development of the damage mechanisms, but also to quantify the growth rates of the mechanisms. This can only be done when the physical processes controlling the growth rates are understood in sufficent detail".

Reifsnider et al. (8) have developed an analytical approach for fatigue damage analysis in composite materials. This approach detailed five modes in the development of damage in polymeric laminates in fatigue. The first damage mode was matrix cracking in off-axis plies. A series of cracks parallel to the direction of the fiber in the off-axis plies would occur. The next mode consisted of crack coupling where small secondary cracks extend perpendicularly from the primary cracks. The third damage mode was delamination between plies

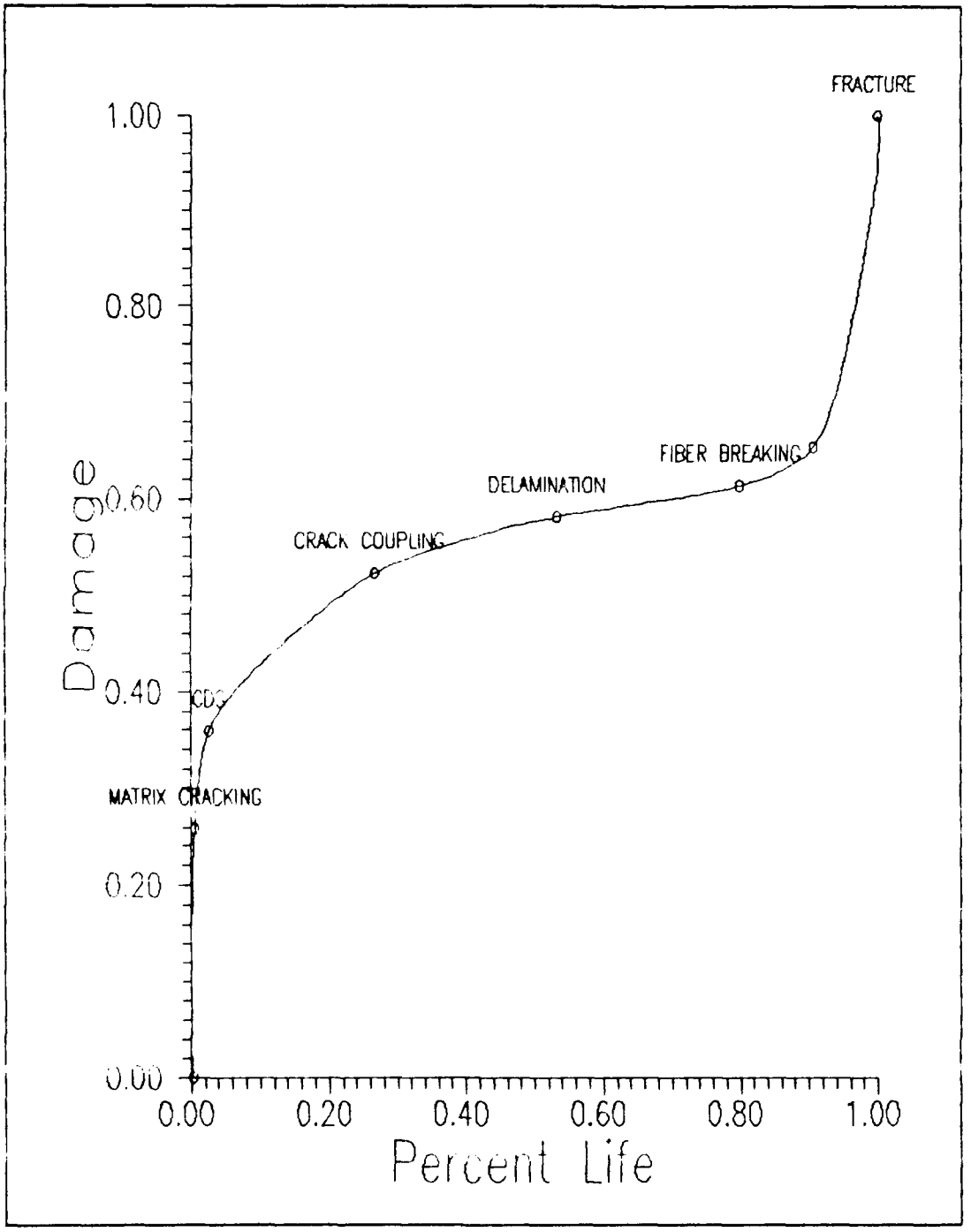

Figure 3 Fatigue Damage Modes in Composite Laminates (From Reifsnider et al. [8])

caused by mixed mode growth of interlaminar cracks. The fourth mode was characterized by a rapid increase in crack growth culminating in a critical local state of stress leading to the final mode of failure. The schematic representation is shown in Figure 3. The damage parameter is a number which is equal to the negative of the normalized modulus added to one.

$$\text{Damage} = 1 - E_I / E_{I0}$$

This parameter was used by Reifsnider and others as a way of non-dimensionalizing stiffness for the purpose of accurately comparing individual specimens.

III. Experimental Procedure

This chapter will discuss experimental test station development and construction, sample preparation, test procedures and data reduction.

A. Test Station Development

The ceramic matrix composites studied were relatively brittle materials and there was a limited amount of testing material available. Therefore, before any experimental testing could be attempted, a grip fixture that could fatigue small specimens without inducing bending or twisting had to be developed. The requirements for this fixture were, (a) be able to maintain a high degree of alignment precision and stability, (b) be easy to obtain and build, (c) be able to adapt to an existing MTS test stand and, (d) be affordable. Several alternatives were examined, and the one that would fit the requirements best was a grip fixture that was already in operation at the USAF Material Laboratory, at Wright Patterson AFB, Ohio. George Hartman (5) of the University of Dayton Research Institute, had developed a highly accurate, low-cost, grip system for testing small samples of ceramic composites. This self-contained system (Figure 4) features an air-driven fluid pump that takes pressurized air from the laboratory air

system and converts the air pressure into hydraulic pressure.

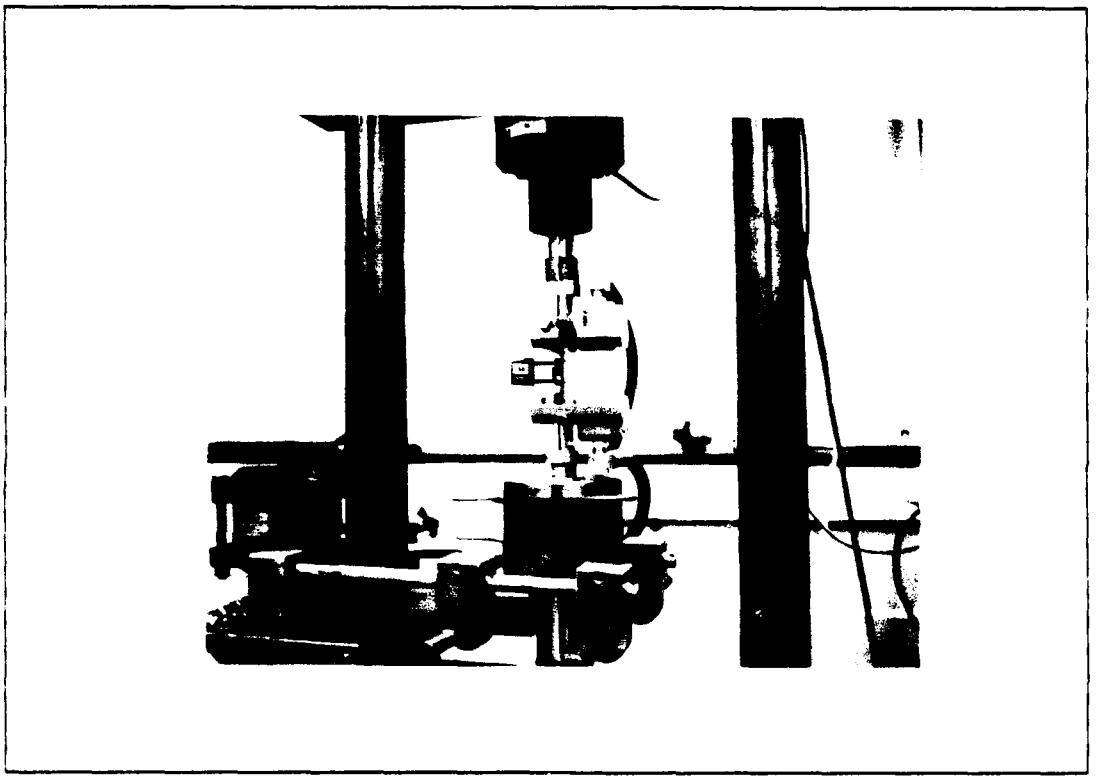

Figure 4 Specimen in Servo-hydraulic Grip System

This hydraulic pressure is supplied to a pair of hydraulic pistons, which acted upon a set of stainless steel grips via a system of hydraulic valves and hoses (Figure 5). The pump could pressurize the system to 10,000 Psi of hydraulic pressure, so all of the fittings, valves, and hoses were rated to that pressure. The system had a self-contained hydraulic return network and sump tank, as well as a separate

air filter and regulator. The pistons apply pressure upon the grips via a yoke assembly, and were positioned on the grips using a pair of dowels.

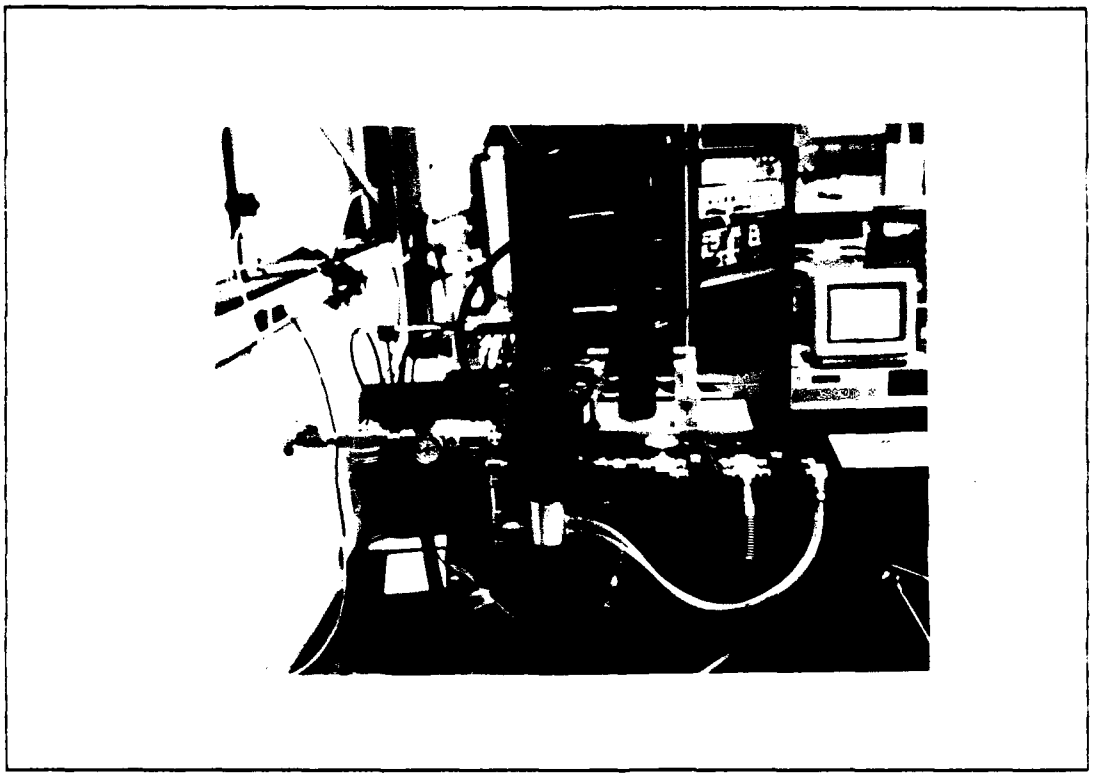

Figure 5 Air-Driven Hydraulic Pump, Filter, Regulator, Supply Valves and Hoses

The alignment device was an ingenious mechanism called a woods metal pot, that had a cylindrical stainless steel plug inserted into a cylindrical stainless steel cylinder of larger diameter (Figure 6). The space between the plug and the

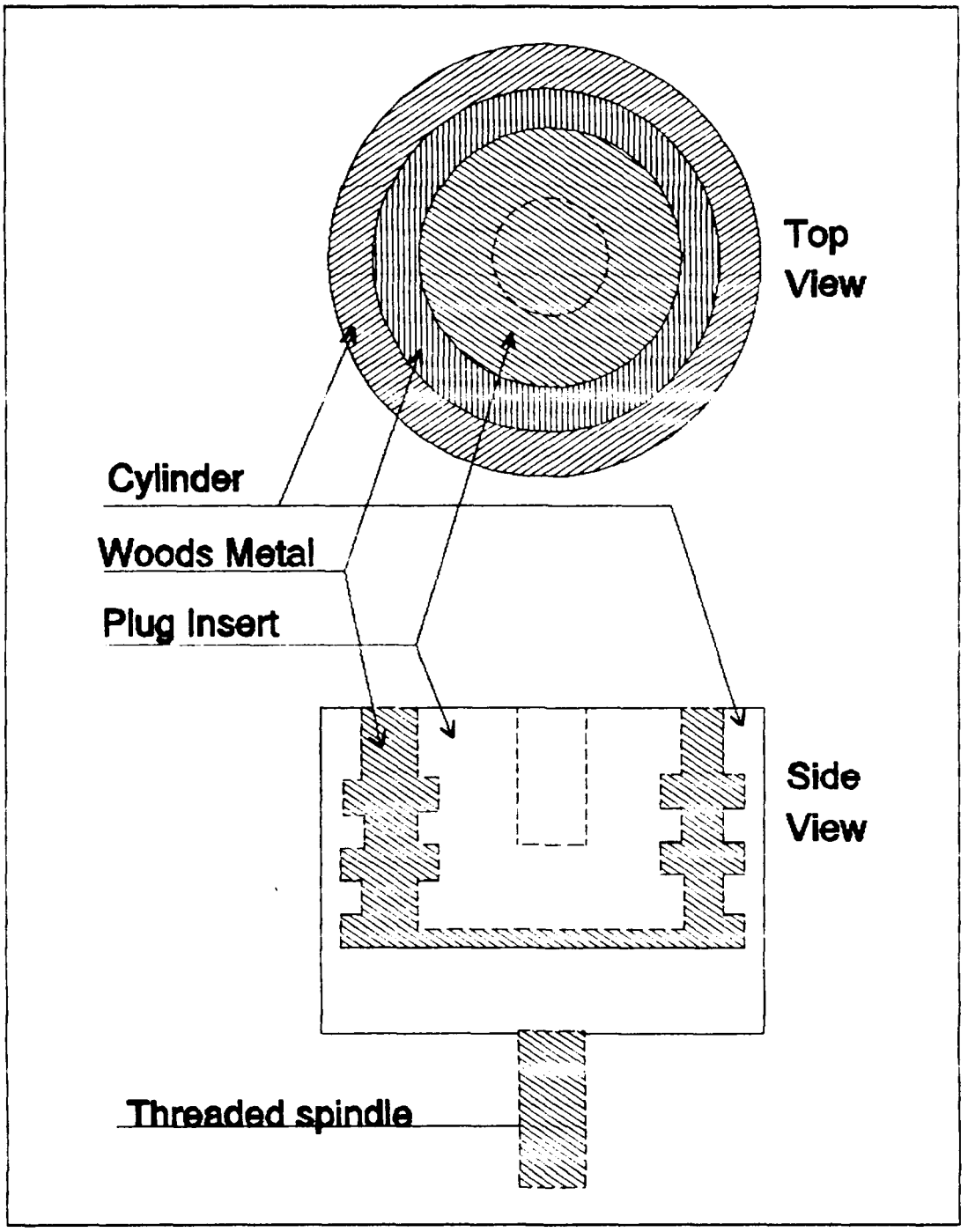

Figure 6 Woods Metal Alignment Assembly

cylinder was filled with Woods metal, an alloy of bismuth, tin, lead, and cadmium, which had a very low melting point. The upper grip was securely fixed to the MTS test stand load cell using adapters. The lower grip was attached to the plug of the woods metal assembly. The cylinder of the assembly was mounted onto the hydraulic actuator of the MTS test stand. The plug was then lowered into the cylinder, and molten woods metal was poured into the gap. While the Woods metal was still molten, a pair of alignment angles were clamped upon the reference surfaces of the grips. The Woods metal was allowed solidify, the insert plug was held rigidly in place by the woods metal, the angles were removed and near perfect alignment was attained.

The last piece of equipment that had to be built was an anti-rotation device to keep the hydraulic actuator of the MTS test stand from rotating with respect to frame of the stand. This piece of equipment featured a threaded aluminum collar that was screwed onto the actuator. A locking ring kept the collar from slipping. The aluminum collar had a 3/4th inch slot machined into the side of it. A stainless steel pin of 1/200th inch less diameter than the width of the slot was mounted into an aluminum block which was attached to a base plate on the frame of the test stand. The block was then positioned to allow for the pin to ride in the slot of the

collar. This device allowed the actuator to move freely in a vertical direction, but did not allow any rotation (Figure 1).

The MTS test stand was already in place in the AFIT Solid Mechanics Laboratory. It consisted of a test frame with a 5000 lb MTS Servoram Actuator, a 5500 lb MTS load cell, a MTS 436 Control Unit, a MTS 406 Controller, a MTS 408 Modular Testing Panel, a Wavetek 452 Filter, an MTS extensometer, a Measurements Group 2310 Amplifier, and a MTS 464.80 Data Display. An IBM PC-AT ran the MTS 406 controller using a fatigue cycling program (MATE233) that was created by George

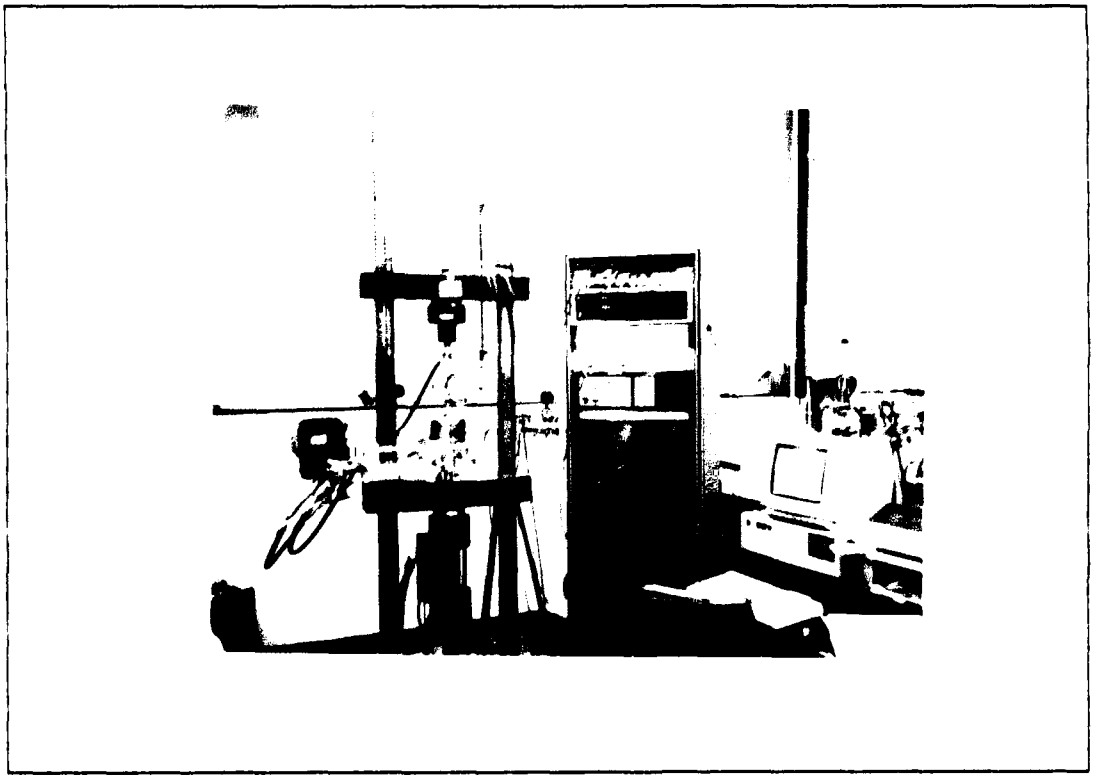

Figure 7 Experimental Test Stand

Hartman of University of Dayton Research Institute.

The center equipment rack holds all of the control, filtering, and data display units. The MTS frame with the Servoram actuator and grip assembly is shown in the left of Figure 7 and the IBM computer is on the right.

B. Specimen Preparation

The test specimens were cut from a single 4 inch by 6 inch plate (Figure 8). The width and thickness of the test specimens varied slightly from sample to sample due to changes in plate thickness and differences during cutting. The plate varied in thickness from .122 inches to .135 inches. The 3 inch specimen length was chosen to allow for twice as many samples to be made compared to a 6 inch length. The cutting of the material was done by a circular diamond blade mounted in a low speed Isomet saw.

After the specimens were cut from the plate, fiberglass tabs were epoxied onto the ends. The tabs were .75 inches long, .065 inches thick, tapered on one end at a 75 degree angle, and cut equal to the width of the sample to be mounted on. This allowed for a gage length of 1.5 inches. A schematic of the prepared specimen is shown in Figure 9. The dimensions of all specimens are given in Table 1.

The end surfaces of the samples were burnished with

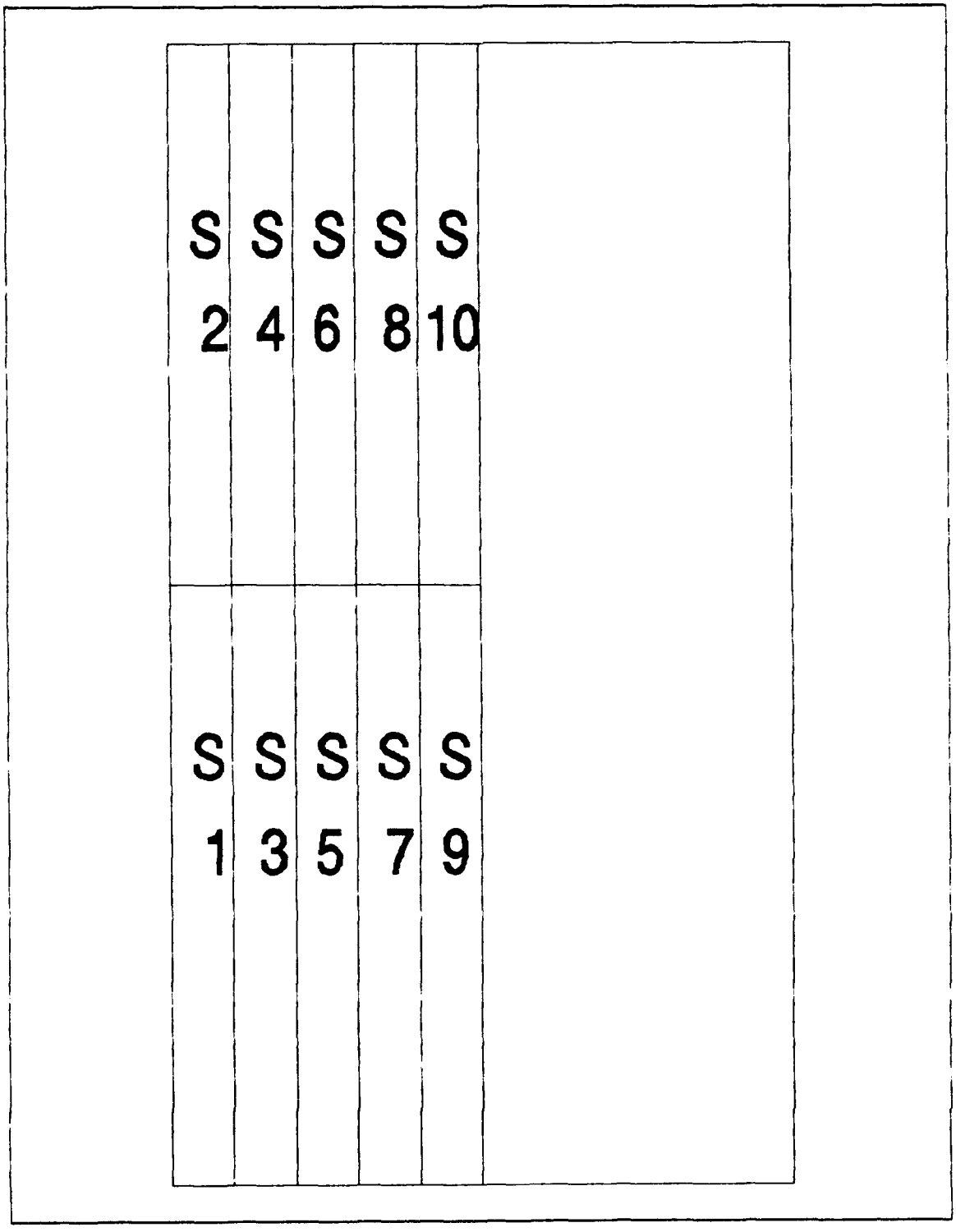

Figure 8 Location of Samples on Plate

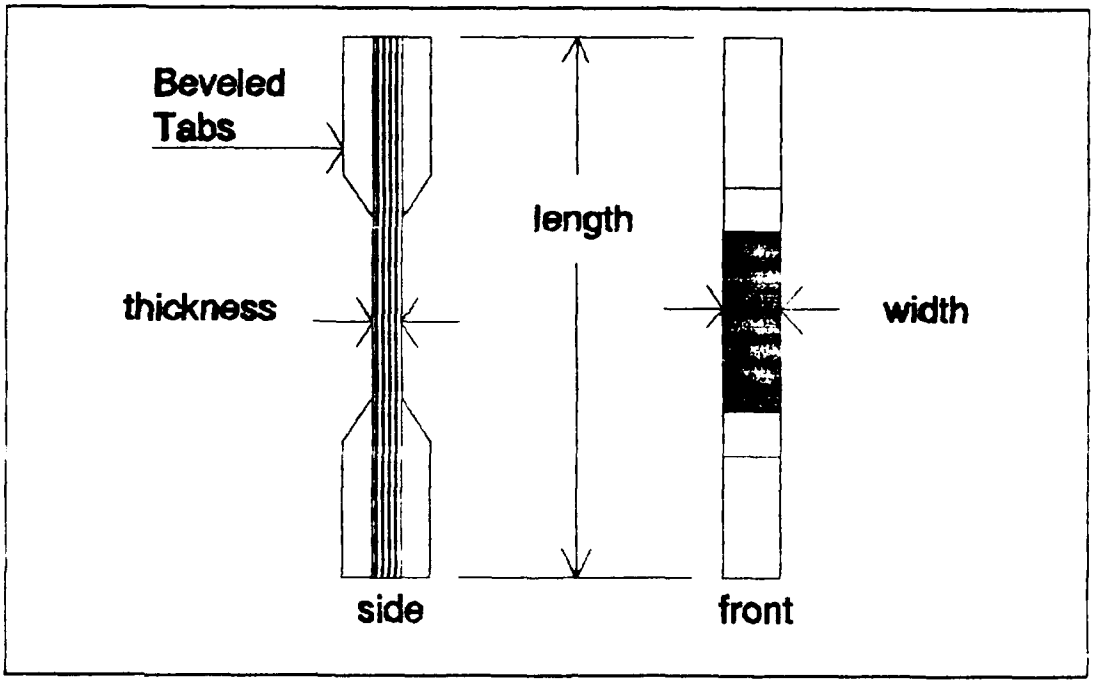

Figure 9 Sample Dimensions

Table 1 Specimen Dimensions

Sample Number	Average Thickness (inches)	Average Width (inches)	Sample Length (inches)
S1	.132	.235	3.0
S2	.131	.265	3.0
S3	.132	.314	3.0
S4	.130	.317	3.0
S5	.133	.301	3.0
S6	.130	.222	3.0
S7	.133	.236	3.0
S8	.129	.287	3.0
S9	.132	.315	3.0
S10	.128	.230	3.0

sandpaper, then Shell Epon two part epoxy was used to bond the tabs. The epoxy was cured for 2 hours at 200^0 F in a thermal oven.

After sitting 24 hours, the samples were then polished on one edge to obtain acetate replications. The polishing was done at the USAF Materials Laboratory specimen preparation branch. An aluminum holder was manufactured and used to hold two samples at one time for polishing. The polishing took place in several stages. Starting off with a 75 micron diamond polishing wheel, the polishing then progressed to a 45 micron polishing wheel, 800 grit silica sandpaper, 3 micron alumina paste, and finally, 1 micron alumina paste. The diamond wheels and the sandpaper were used to remove surface roughness and the alumina paste allowed for the proper amount of relief between the fiber and the matrix for replication. This procedure took approximately 2-3 hours. Visual confirmation of the polishing was performed using an inverted microscope. Test replications of the polished specimens were taken, and if they were deemed satisfactory, they were then ready to be tested.

C. Experimental Procedure

This portion of the chapter will consider the experimental procedures that were followed along with data acquisition and replication technique.

The MTS control unit was powered on and set for low hydraulic pressure. The controller was set for load cell feedback and the interlocks were disabled. The specimens were carefully mounted into the grip fixtures discussed above using a machined block to insure proper alignment.

The grip fixtures had the ability to accept a wide range of specimen widths by the use of a series of removable inserts, that could be made thicker or thinner according to the size of the sample (Figure 10). The specimen was aligned in the lower grip first, then the grip system hydraulic pressure was applied to the lower grip piston and yoke assembly. The MTS actuator was manually raised using the set point control until the sample was aligned in the upper grip, then the pressure to the upper grip yoke and piston assembly was applied.

The hydraulic pressure to the MTS actuator was then turned off and the feedback select was switched over to load control. The extensometer was put into position on the test article using stainless steel springs to hold it in place. The feedback control was nulled, and the interlock enabled.

The hydraulic pressure to the MTS actuator was set to high and allowed time to stabilize. The range control had been set for 10 percent, so the maximum allowable load available was 500 lbs. The sample was ready to be fatigue tested.

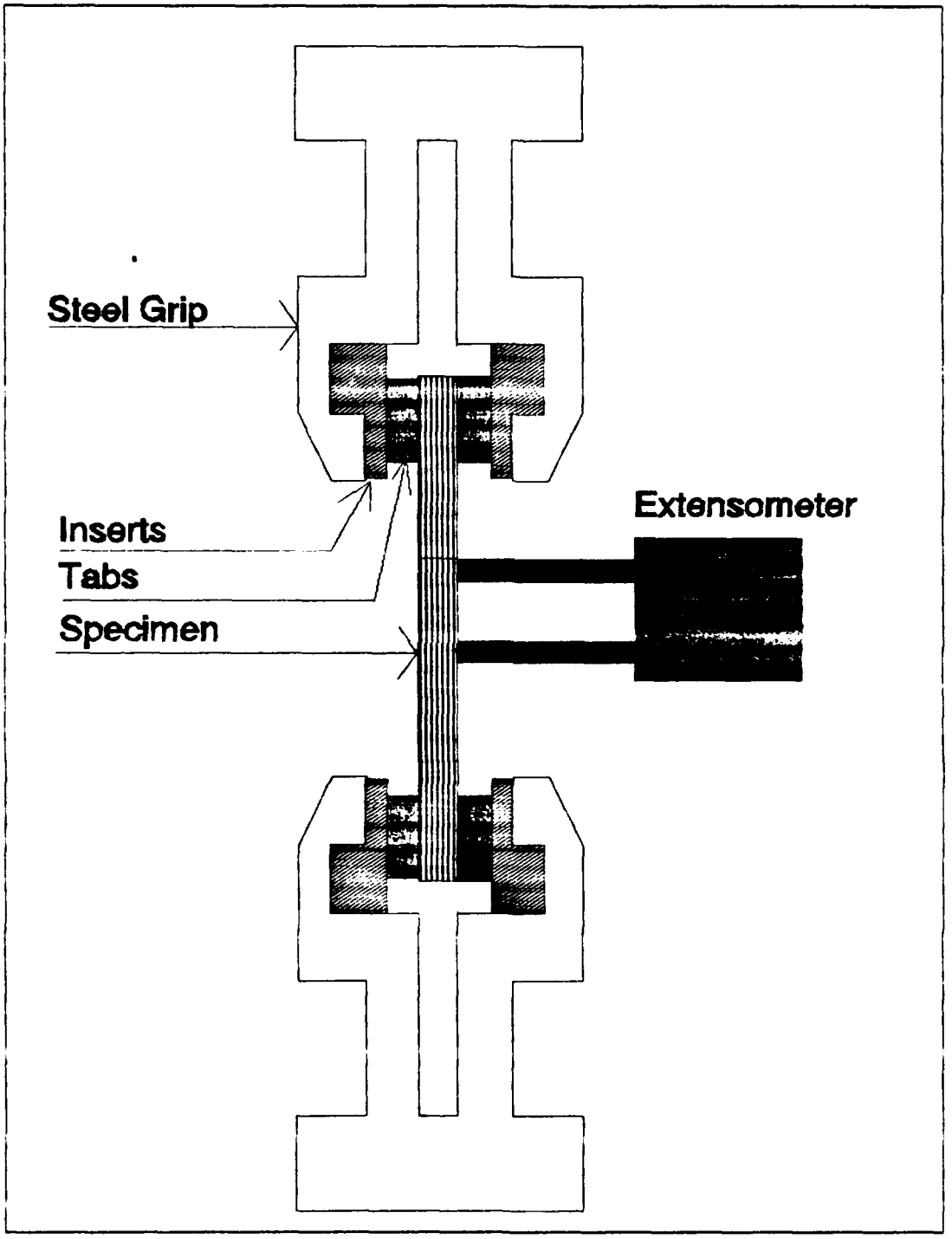

Figure 10 Detail Of Grips With Specimen In Place

The actual testing routine went as follows. First the initial elastic principal modulus of the sample was determined. This was accomplished by stressing the specimen to 1/2 of the first ply failure limit of the material, which had been previously experimentally determined by Mall and Kim (7) to be about 5.8 Ksi (40 MPa). Readings of the strain were taken from the data display and recorded at various points during the loading of the specimen. This data was entered into a graphing program (Grapher), and the slope of the line was numerically evaluated using a least squares curve fit method.

After this was accomplished, an acetate replication of the gage length of the sample was taken. The extensometer was left on the sample during this procedure to reduce the amount of testing time. A small piece of the acetate film was taped to the sample, and then acetone was sprayed on the area beneath the film. The film was quickly applied to the wetted sample, and slight pressure was applied to the film to force out any trapped air. After the film had set and the acetone completely evaporated, the film was lifted off of the sample and securely taped to a glass specimen slide.

After the replication procedure was complete, fatigue cycling could begin. Tension-tension fatigue testing was performed at room temperature. The tests were run at a cycling frequency of 10 hertz, (sinusiodal waveform) and stress ratio,

R ($\sigma_{min}/\sigma_{max}$) = 1/10. Each specimen would be stressed up to a designated maximum limit (Table 2).

Table 2 Maximum Stress For Each Sample Tested

Sample Number	S1	S2	S3	S4	S5	S6	S7	S8	S9	S10
Maximum Stress KSI (MPa)	5.8 (40)	13.0 (90)	8.7 (60)	10.1 (70)	11.6 (80)	13.8 (95)	14.5 (100)	12.3 (85)	14.5 (100)	5.8 (40)

These limits were selected on the basis of the static tests done by Mall and Kim (7) on the specimens from the same plate of material. Mall and Kim noted that the first decrease in stiffness occurred at 5.8 Ksi (40 MPa), which corresponded to the first ply failure stress. A further decrease in modulus was observed at 13.05 Ksi (90 MPa), correspondng to damage progression into the 45 degree plies. The other stress levels were chosen based on the results of the tests run at these initial levels.

Specimens that remained intact after fatigue cycling were tested for residual strength. This was done by applying a monotonically increasing static load to the specimen until failure occurred. The value of the load at the time of

fracture was recorded as the residual strength.

The first cycle was done by hand and the strain measurements at various stresses were manually recorded. The elastic modulus was recorded as noted above, and an acetate replication was taken to visually capture the damage initiation in the laminate. The extensometer was then reset to nullify any displacement induced during the replication procedure.

Elastic modulus data were acquired at various cycle intervals, depending upon maximum stress level. Zawada (6) found that damage seemed to ensue in a logarithmic fashion in ceramic composites, therefore elastic modulus data were collected at 0, 1, 2, 10, 50, 100, 200, 500, 1000, 2000, 5000, 10000, 20000, 50000, 100000, 200000, 500000, and 1000000 cycles. Replicas and full cycle stress-strain data collection took place less often due to time constraints. Full cycle data were collected on only four samples in order to save time. When running a sample above 13.05 Ksi (90 MPa), data collection was taken more frequently. The MATE233 program mentioned above was used to cycle the test stand between data collection points. The fatigue cycling was performed at a sinusoidal frequency of 10 cycles per second (10 Hz). The tests were conducted in laboratory conditions at ambient room air temperature, atmospheric pressure and humidity. The stress ratio R ($\sigma_{min}/\sigma_{max}$) was 1/10.

D. Data Reduction

The elastic modulus was the parameter used to monitor damage progression. The elastic stress-strain data were plotted on a computer graphing program and a least squares curve fit was used to find the elastic modulus for each cycle that data were collected for. A normalized modulus was produced for each cycle by dividing the modulus for that cycle by the initial modulus for the specimen. The damage parameter was generated by subtracting the normalized modulus from one.

$$Damage = 1 - E_x/E_{x_0} \qquad (24)$$

The use of the non-dimensional damage parameter permitted accurate comparisons of the test results. The resulting values of the damage parameter for each specimen were then plotted as a function of fatigue cycles.

The modulus for the unloading portion of the full cycle stress-strain curves was determined using the least squares program and plotted versus the elastic modulus to verify the elastic modulus as an appropriate modeling parameter.

Micrographs of the replicas were taken to systematically monitor the damage progression. This was done using an Olympus inverted photo-microscope at the USAF Materials Laboratory specimen preparation branch. This photo-microscope was also used for drawings that would show crack initiation and growth.

IV Results and Discussion

In this chapter the results of the experimental testing will be presented along with a discussion concerning these results and how they compare with current theoretical models.

In the first section of this chapter, details of the preparation of the material and the initial condition of each of the samples will be presented.

The second section of the chapter will discuss the factors of damage initiation, and progression in each of the tested samples. Factors to be considered include; (a) how did the cracks initiate in each sample, (b) where did they initiate, (c) did crack density increase as a function of the number of cycles, (d) did the cracks grow laterally or longitudinally during cycling, (e) how did the cracks propagate through the different plies and which plies failed first, (f) how did samples fail when they failed, (g) what did the fracture surfaces look like, (h) how did the modulus decrease as a function of the number of cycles and (h) how many cycles did each sample last?

The third section will take the test results and present conclusions based upon observations and comparisons with current theoretical and analytical models.

A. Material Preparation

As noted above, the material was received as a plate 4 inches wide, 6 inches long and approximately 1/8th inch thick. The material was a dark gray with whitish streaks on the front and back indicating concentrations of the glassy matrix material. One side was of a lighter shade than the other indicating a thicker coating of the matrix material on that side. There were some signs of stray fiber running across the face of the plate, but there were no signs of any serious flaws in the material visible to the human eye. After the individual samples had been cut from the plate and polished, microscopic inspection of the samples confirmed the integrity of the material. Fink (10) had noted that even when there were slight microscopic cracks in this material, it did not affect the properties of the material.

Few voids were observed during microscopic inspection of the polished specimens, indicating that the quality control in making the plate had been very good. There were areas of matrix concentration in the regions of ply interface of several samples.

There was some concern as to whether or not the cutting and polishing operations would damage the samples, but this was not the case. The initial elastic modulus (E_i) of the 10 samples averaged 17.314 Msi with a standard deviation of less

than 4.7 percent, indicating that none of the samples were damaged or weaker than the group as a whole. This averaged value compared favorably with the value of 16.45 Msi found by Mall and Kim for the same material (7).

Some specimens were trimmed to smaller widths in order to allow all of the testing to be conducted under one load range. At the 10 percent range setting, the maximum available load was 500 lbs., so for a sample to be subjected to a stress of 14.5 Ksi, (100 MPa) the area had to be less than .03333 square inches.

B. Damage Initiation and Progression

In this section, the damage initiation and progression for each specimen will be presented. The questions of how and why the cracks started, how did they grow, where did they grow, what did they look like, which plies where most affected, how did the crack density increase, how many cycles did the sample last, what did the fracture surfaces look like, and how did the elastic modulus (E_1), decrease as a function of the number of cycles, will be considered. Also, the question as to whether or not the elastic modulus (E_1) of the material was an appropriate parameter to use to model the damage progression in this material will be addressed.

As noted before, the stress levels were selected on the

basis of the static tests done by Mall and Kim (7) on the specimens from the same plate of material. Mall and Kim noted that the first decrease in stiffness occurred at 5.8 Ksi (40 MPa), which corresponded to the first ply failure (FPF) stress. A further decrease in modulus was observed at 13.05 Ksi (90 MPa), corresponding to failure of the 45 degree plies. The other stress levels were chosen after the results of the first two tests were evaluated.

1. 5.8 Ksi (40 MPa) Specimen

Two specimens were tested at this maximum stress level of 5.8 Ksi (40 MPa), the FPF stress of the material. The first sample (S1) was used as a demonstration and validation test of the new grip system and the data from that test was not analyzed. The data from the second test (sample S2) will be presented here. The test procedure followed the method given in section D of chapter II. The initial elastic modulus (E_I) was determined by stressing the sample up to 2.9 Ksi (20 MPa), which is 1/2 the FPF stress for the material, and was found to be 17.9 Msi (119 MPa). No damage occurred in the sample when it was stressed up to this level.

A replica of the gage length was obtained while the specimen was subjected to an applied load to document any pre-existing cracks or flaws in the virgin material. All replicas were acquired while the samples were subjected to 1/2 FPF

stress so that cracks in the material could be detected. The microphotograph in Figure 11 shows that there were no pre-existing cracks in this sample. Figure 11 also provides a representative example of how the undamaged material appeared for all cases. The 90 degree fibers appear as circles, the 45 degree fibers appear as ellipses and the 0 degree fibers appear as rods.

The first test cycle was run manually to the maximum stress of 5.8 Ksi. The elastic modulus E_1 was acquired after the first cycle, with a resulting decrease in modulus of about 4.7 percent to 16.1 Msi. The specimen was tested to 1,000,000 cycles. The elastic modulus and damage parameter data collected during the test were listed in Table 3 in the appendix.

Some stress-strain curves from which these modulus data were determined have been for various fatigue cycle counts in Figure 12. This gives a visual representation of the decrease in stiffness as a function of cycle count. The stress-strain curves do not include any residual strain, that is, each curve starts at zero strain regardless of the residual strain at that particular cycle count. Figure 13 shows how the damage parameter increased as a function of cycle count. Note that the majority of the damage occurred in the first cycle and that the slope of the damage curve decreased as cycle count increased.

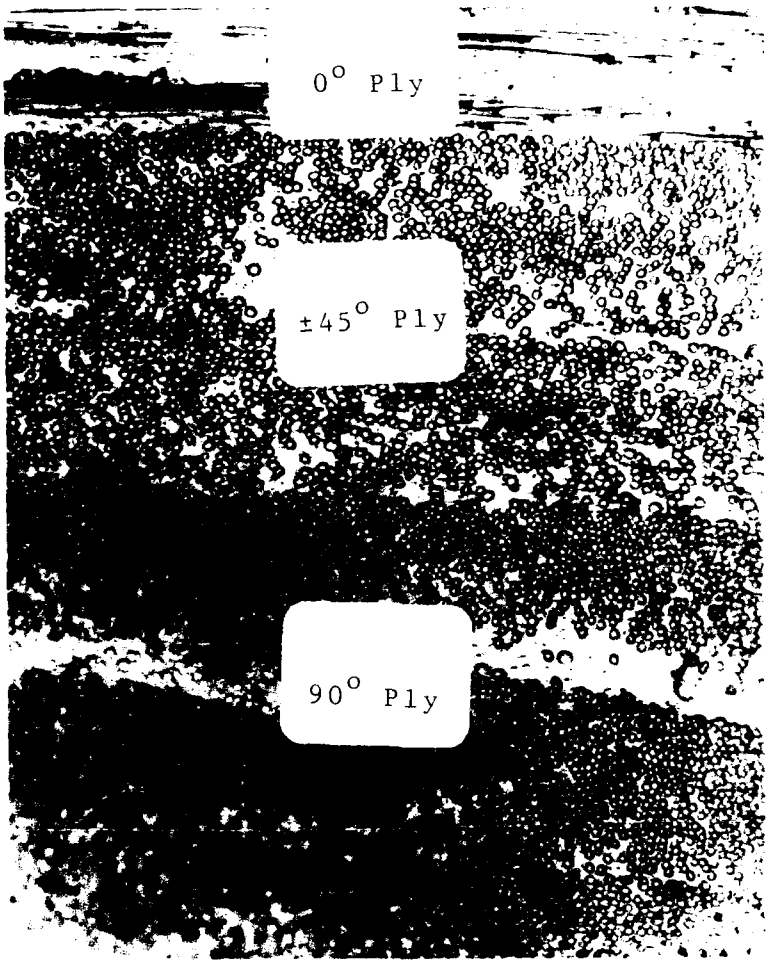

Figure 11 Micrograph of Undamaged Polished Material

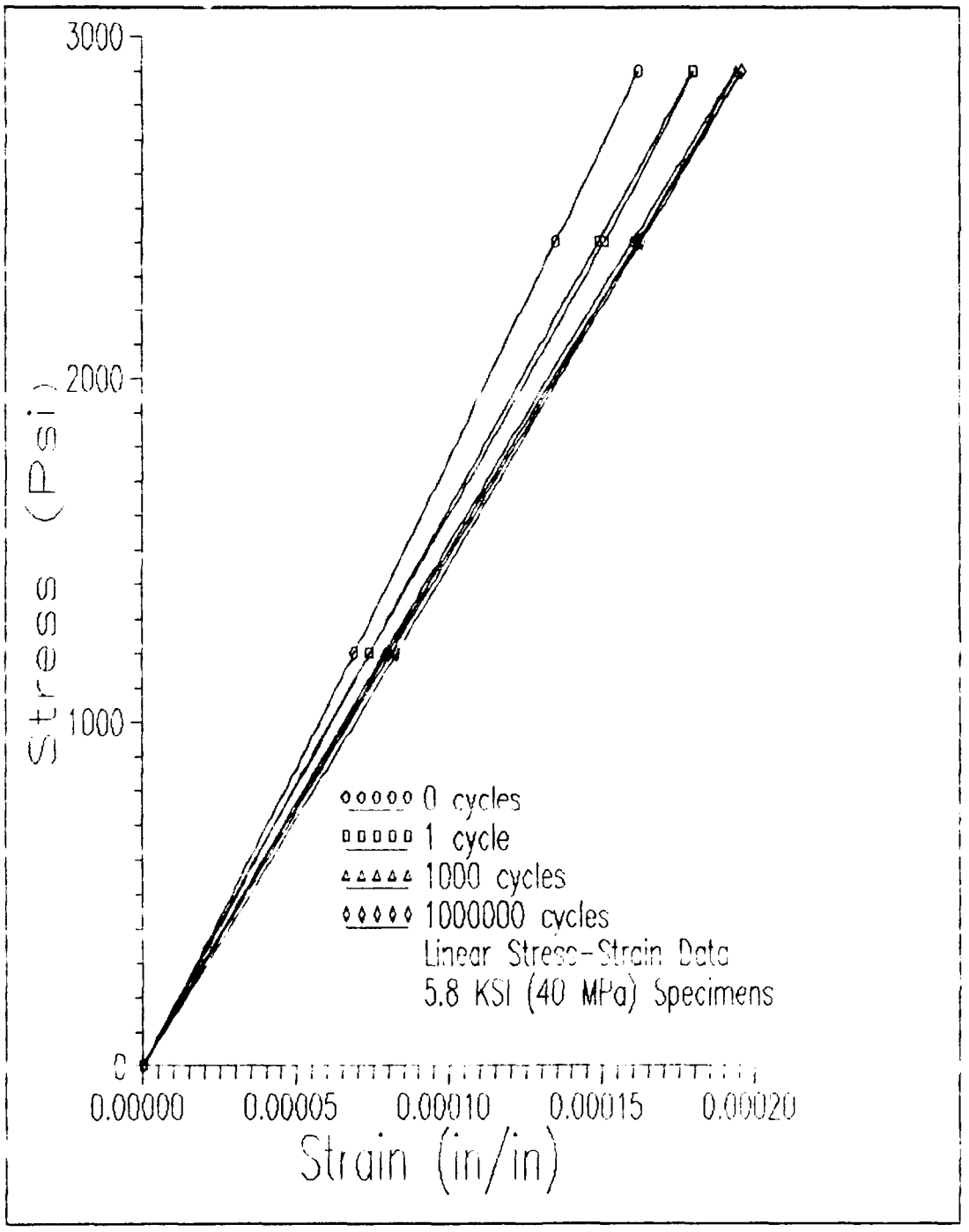

Figure 12 Stress-Strain Data
8.5 KSI (40 MPa) Specimen

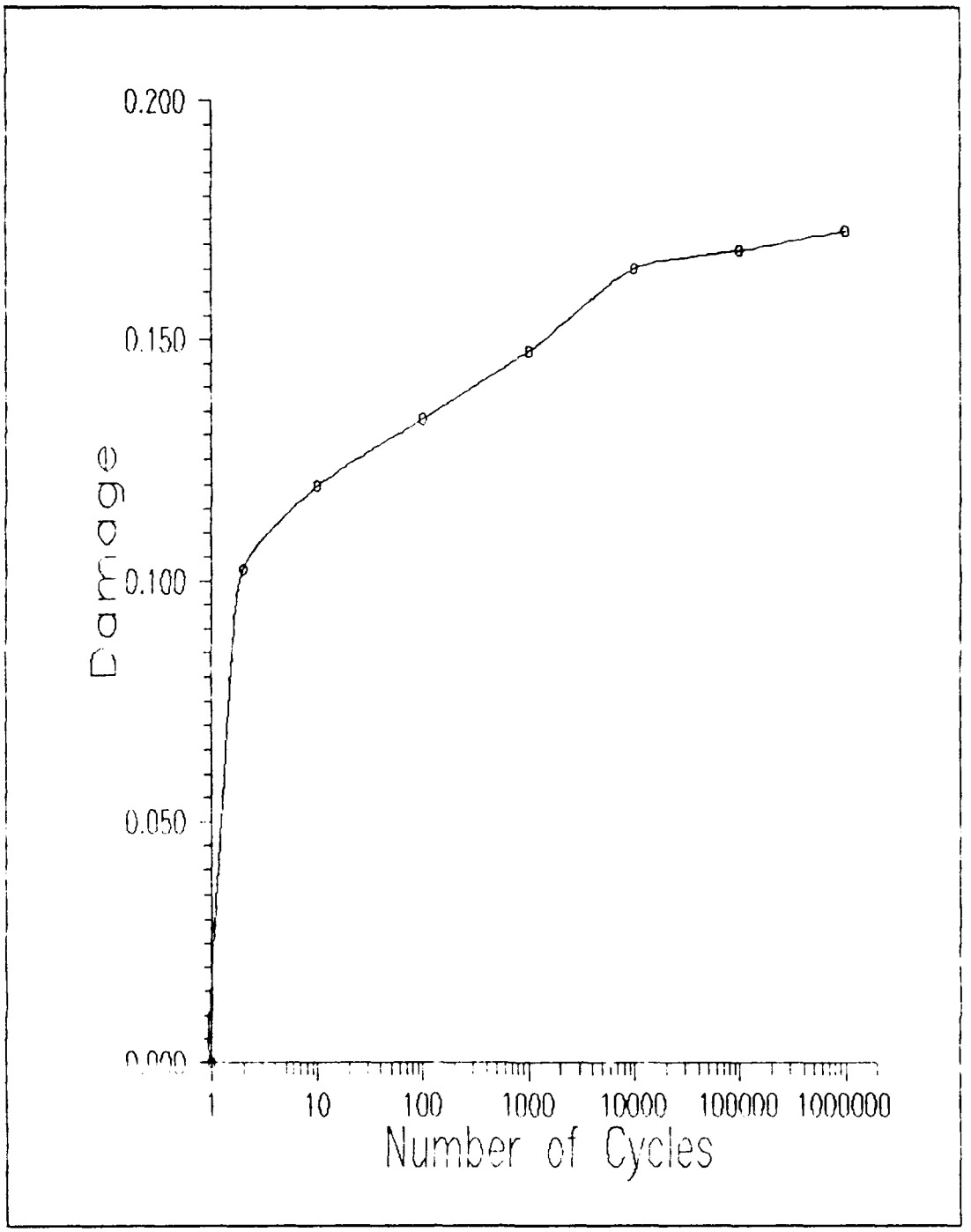

Figure 13 Damage Versus Cycle Count
5.8 KSI (40 MPa) Specimen

From the modulus data, the stress-strain curves, and the damage vs. cycle count curve, it was observed that over 90 percent of the decrease in modulus occurred in the first 100 cycles. At the end of the test run of 1,000,000 cycles, the modulus approached 14.8 Msi, which gave an overall decrease in stiffness over the entire test of 3.1 Msi, less than an 18 percent decrease from the initial measurement.

From microscopic examination of the replicas, several observations can be made. First, cracks initiated at the $90^0/45^0$, and $45^0/45^0$ ply boundaries and then grew in a transverse fashion into the plies. Second, the most damage occured in the 90 degree ply, due to the weakness of the fiber-matrix bond which lead to an inability to withstand the longitudinal strain as shown in the replicas. Third, as cracks extended laterally in the material, they passed around the fibers, through the matrix. This phenomenon had been previously observed by Daniel, et al (3).

In this specimen, the majority of the observed cracking took place in the $90^0/45^0$ and $45^0/45^0$ ply boundaries. Figure 14 shows how cracks originated in the $90^0/45^0$ ply interface. This same phenomena also occurred at the $45^0/45^0$ ply interface. At this stress level, the $0^0/45^0$ ply interface was not affected and was left undamaged through out the test.

Figure 15 depicts how a transverse crack had completely

Figure 14 Crack Initiation At Ply Boundary

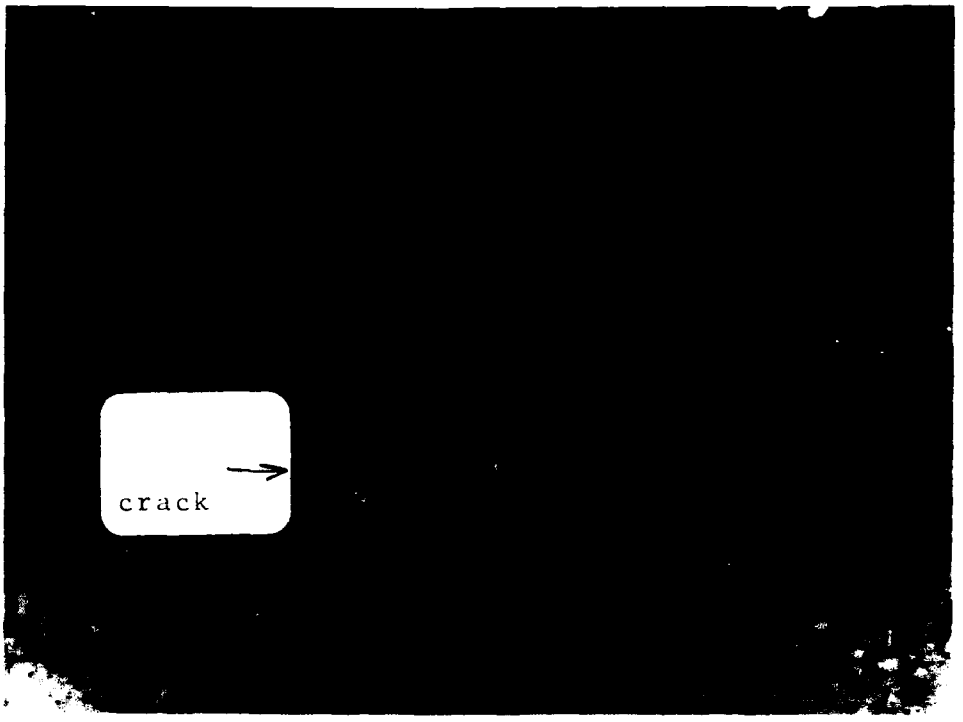

Figure 15 Crack Growth Through 90^0 and 45^0 Plies

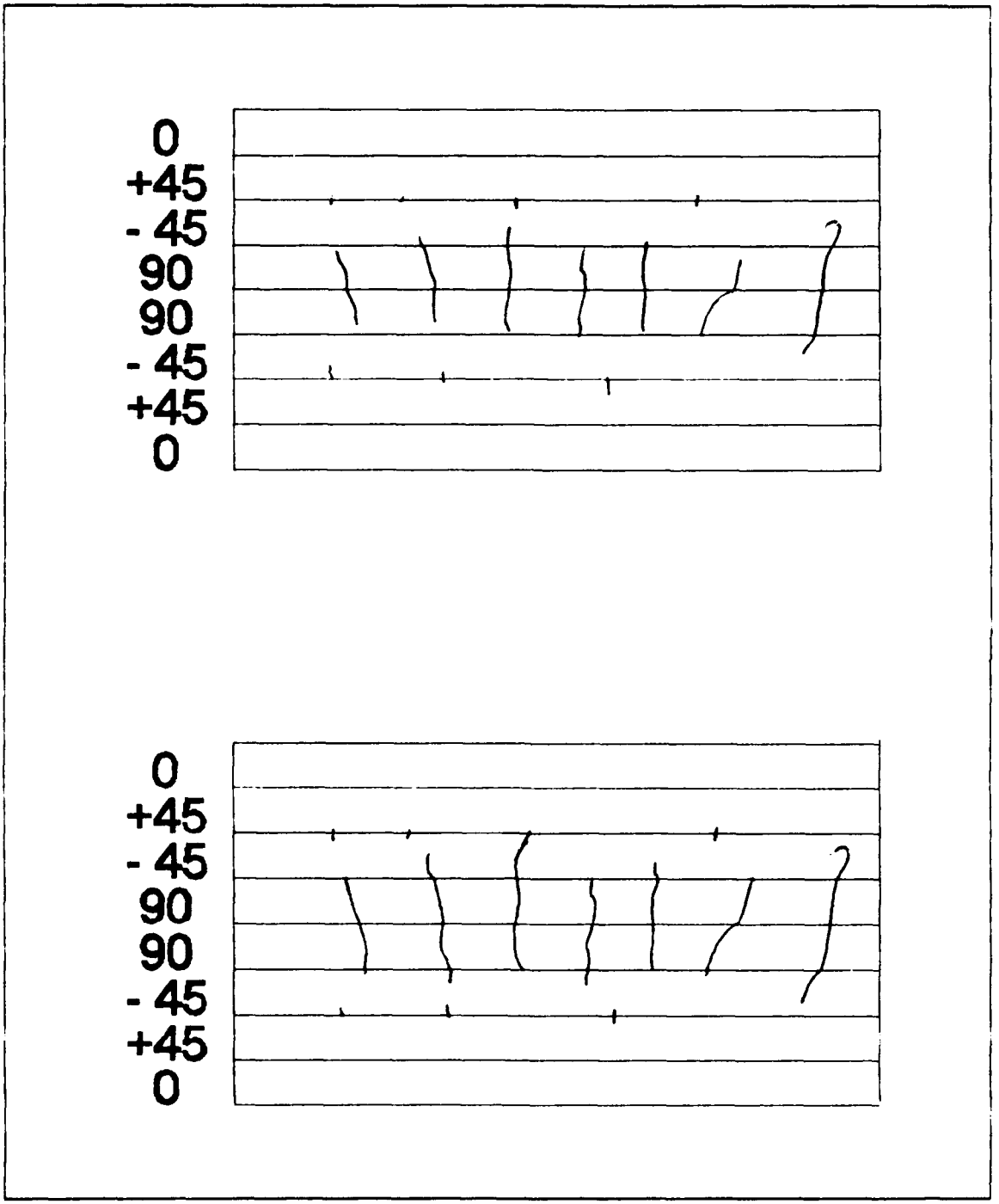

Figure 16 Damage Progression In 5.8 KSI Specimen
At 1 Cycle (top) and 1,000,000 Cycles (bottom)

driven through the 90^0 plies after it had started at the boundaries. Most of the damage occurred in the 90^0 plies, but there were a few instances of cracks extending into the 45^0 ply next to the 90^0 ply. The cracks that penetrated through the entire 90^0 ply tended to run in a straight line perpendicular to the ply boundary while the cracks that entered the 45^0 ply ran diagonally through the ply at an angle to the ply boundary, but penetrated no further than the $45^0/45^0$ boundary.

Figure 16 gives a schematic representation of the crack pattern in the gage length area after 1 cycle and 1,000,000 cycles. The increase in crack size without an increase in crack density is shown. The cracking occurred mainly in the first cycle. After that, no new cracks were seen to develop, but as cycling continued, these existing transverse cracks grew longer and wider. So, at this stress level, the crack density did not grow appreciably during the testing, but the crack length did.

2. 8.7 Ksi (60 MPA) Specimen

Sample S3 was tested at this stress level, which was a 50 percent increase over the prior test. The results of the testing are presented in table form in the appendix (Table 4). Figure 17 shows representative stress-strain curves from which the elastic modulus data were developed. The damage and normalized modulus were then calculated and the damage

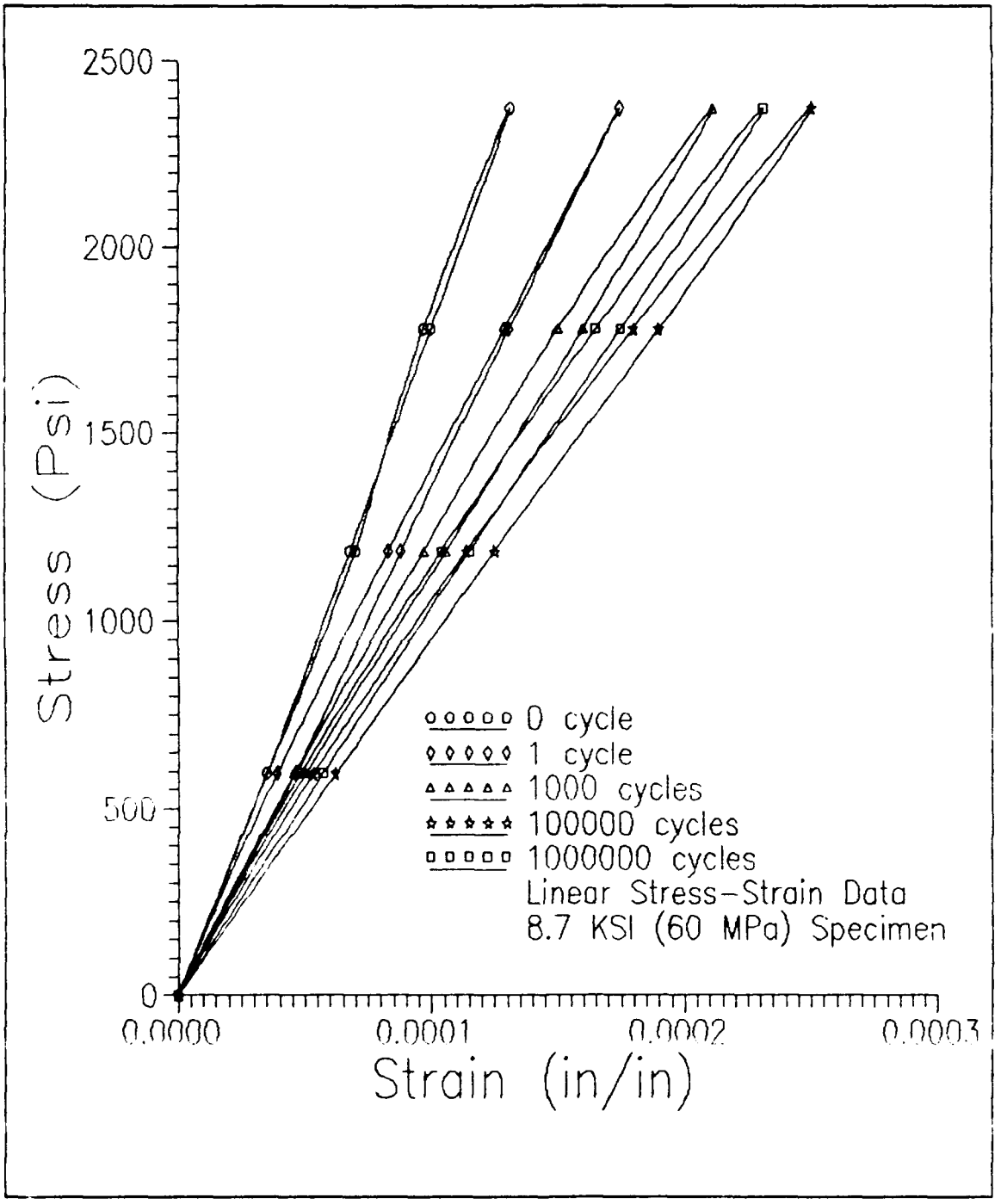

Figure 17 **Stress-Strain Data**
8.7 KSI (60 MPa) Specimen

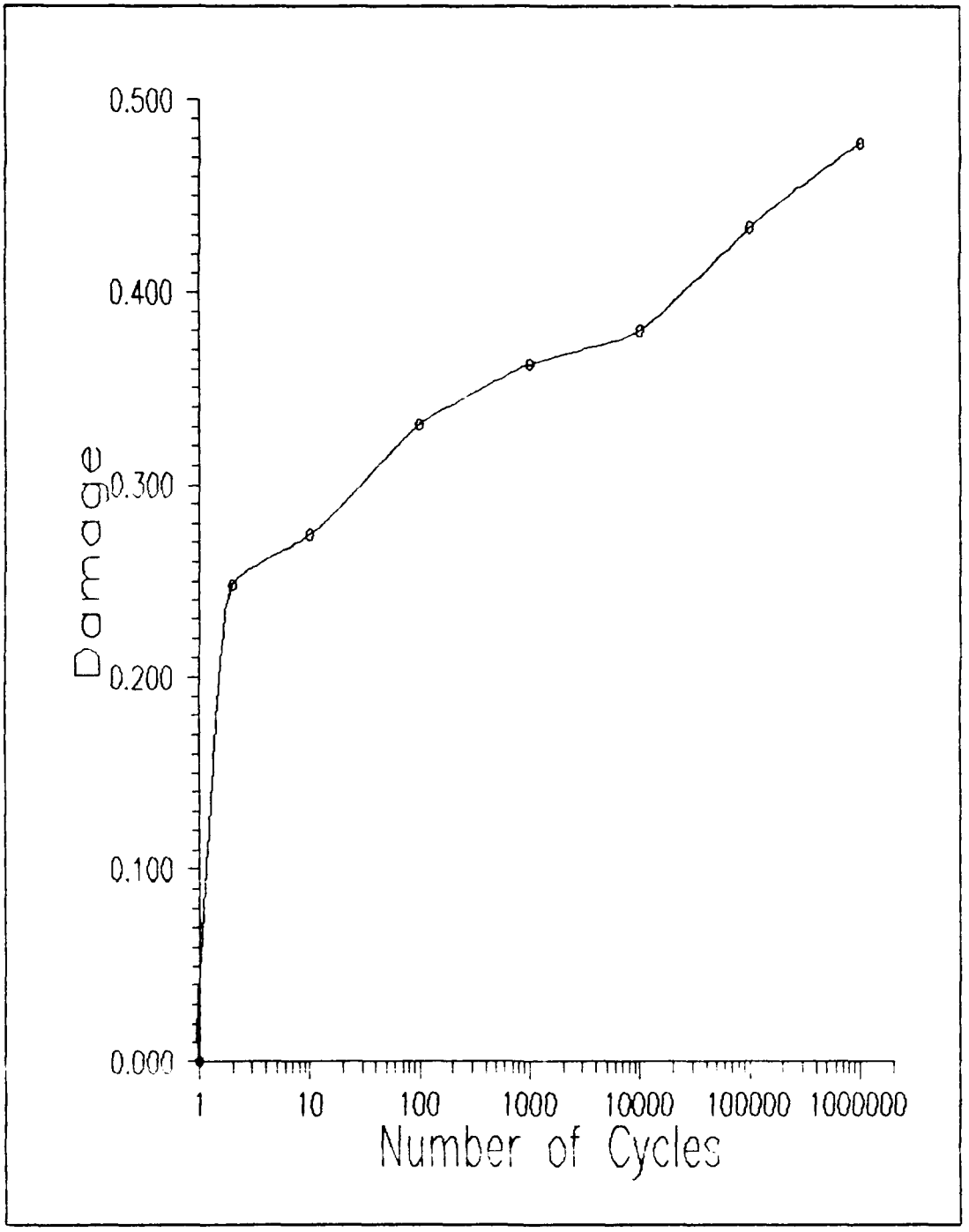

Figure 18 Damage Vs Cycle Count
8.7 KSI (60 MPa) Specimen

parameter was plotted against cycle count (Figure 18).

From the data table and the figures, the observed decrease in modulus after the first cycle of 3.5 Msi was almost twice the decrease observed after the first cycle of the 5.8 Ksi test. The decrease after the first cycle of this test was greater than the decrease over the entire 1,000,000 cycles of the 5.8 Ksi test. The decrease in modulus as a function of cycle count for this sample occurred at a faster rate, and the slope of the damage parameter curve was greater. The modulus of the specimen approached 9.5 Msi after 1,000,000 cycles had been run, which was approximately 47 percent of the initial modulus value of 18.15 Msi.

As in the 5.8 Ksi specimen, the cracking started in the ply boundaries, but at this stress level, not only had the cracks extended transversly from the $90^0/45^0$ ply interfaces, and the $45^0/45^0$ ply interfaces, but from the $0^0/45^0$ ply interfaces as well (Figure 19) The 0^0 ply was not affected during the test, but cracks had penetrated all of the 45 and 90 degree plies. The initial crack density had increased slightly when compared to the first test, but did not change during the testing. There was no secondary cracking, crack coupling or delamination taking place.

An interesting feature in this specimen was that a crack started at a void in the material at the $45^0/90^0$ ply boundary

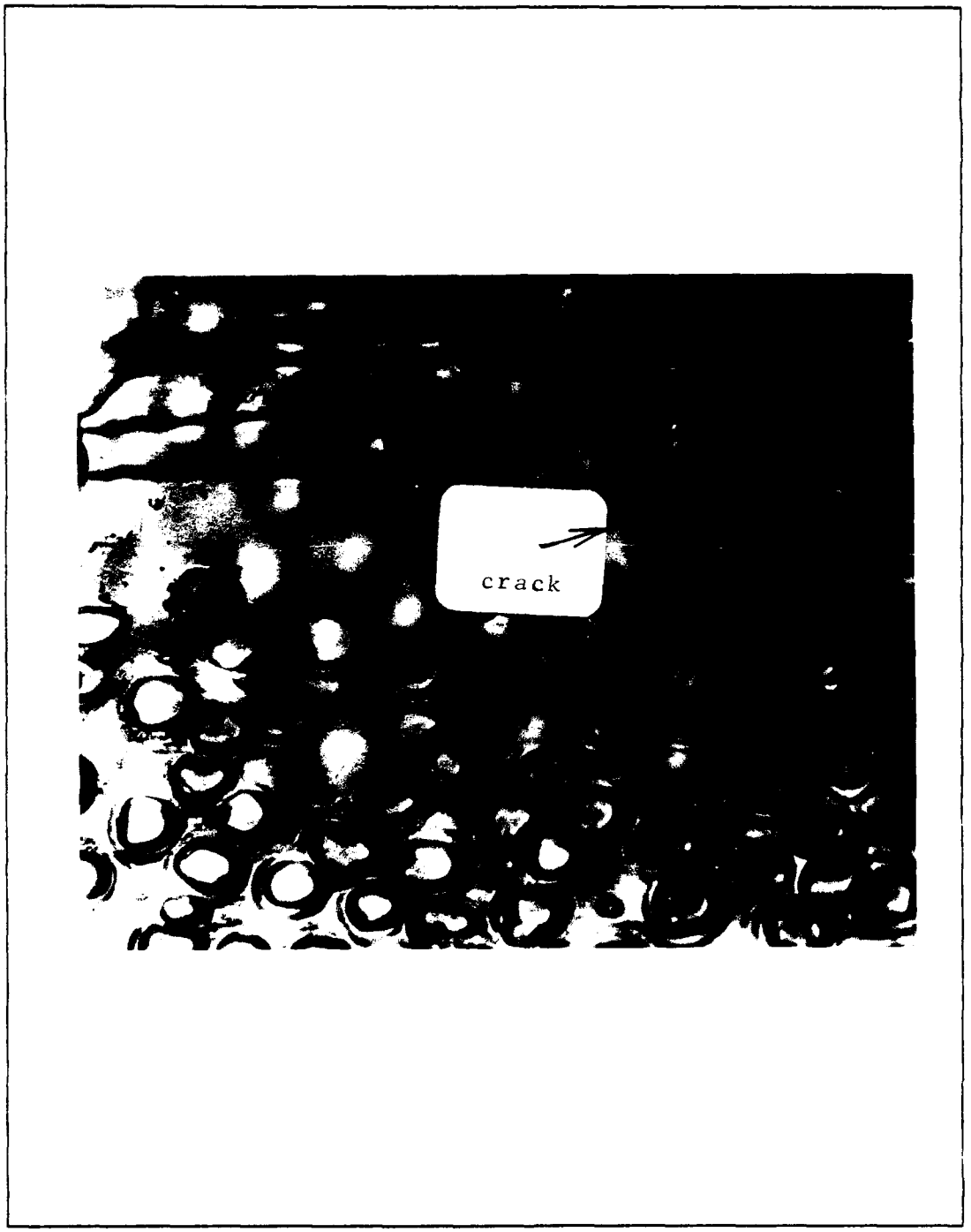

Figure 19 Crack Initiation at $0^0/45^0$ Boundary
8.7 KSI (60 MPa) Specimen

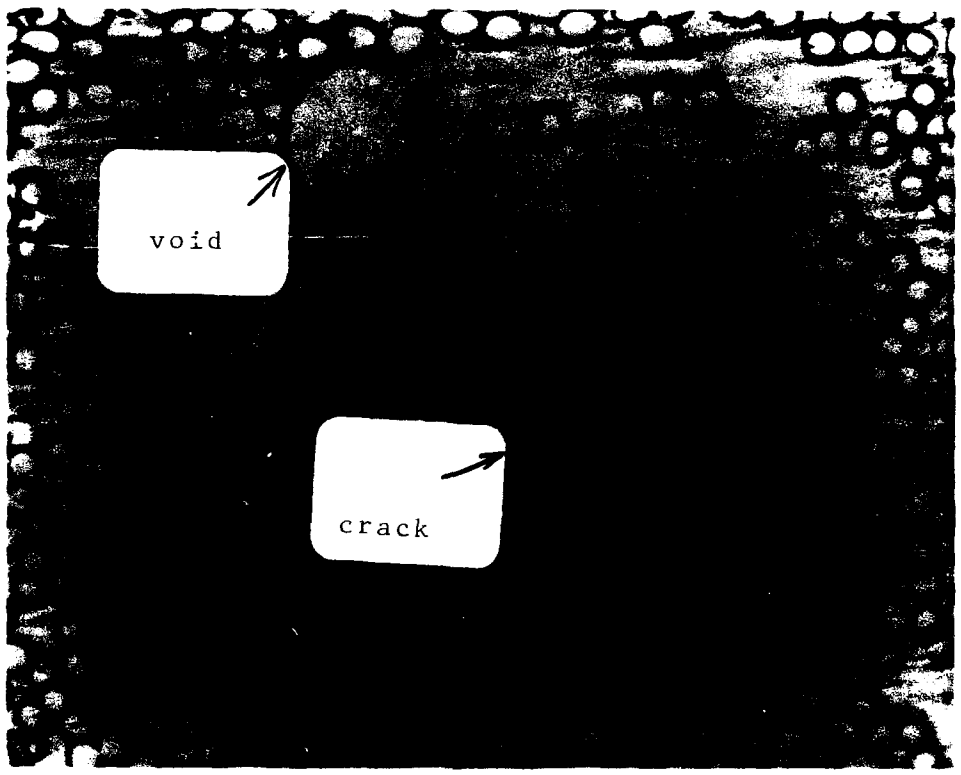

Figure 20 Crack Initiation from Void at $90^0/45^0$ Boundary

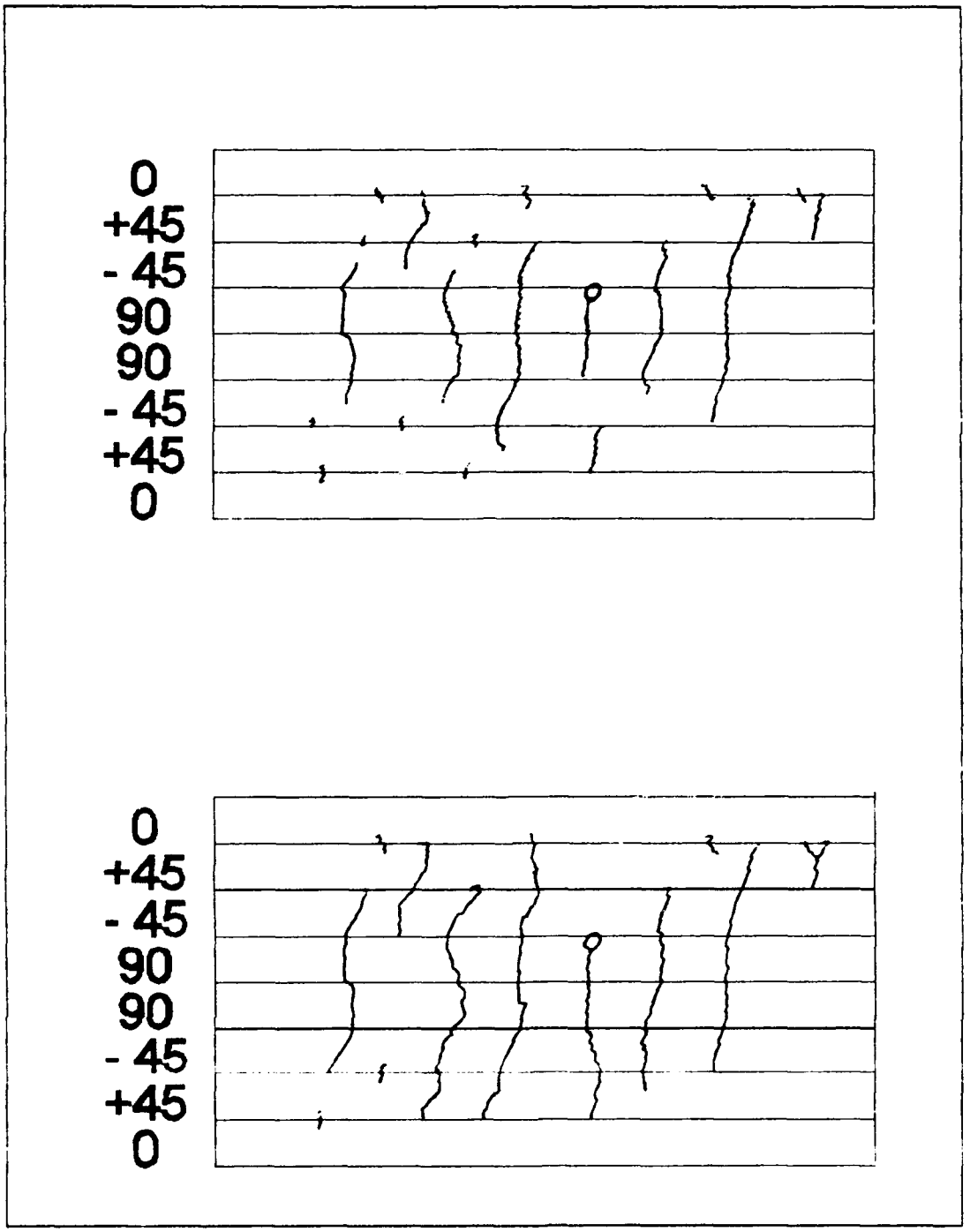

Figure 21 Damage Progression In 8.7 KSI Specimen
1 Cycle (top), 1,000,000 Cycles (bottom)

(Figure 20). The void was located in a matrix rich area and was probably a point of stress concentration. The crack extended transversly into the 90^0 ply, but not into the adjacent 45^0 ply. The void did not affect the strength of the specimen.

Figure 21 gives a graphic representation of crack initiation in the gage length after the first cycle and the final crack configuration after 1,000,000 cycles. Once again, there was no increase in crack density, only in crack length, which was the main factor for the decrease i.. stiffness.

3. 10.15 Ksi (70 MPa) Specimen

The crack initiation and growth for this specimen (S4) was very similar to that of the 8.7 Ksi (60 MPa) specimen, except that the decrease in modulus after the first cycle (5.01 Msi) was greater and the final modulus (8.52 Msi) was less. The elastic modulus data table is located in the appendix (Table 5). The elastic stress-strain curves and damage parameter curves are shown in Figures 22 and 23 respectively. The slope of the damage curve is very similar to that of the 8.7 Ksi specimen, but the damage done on the first cycle was greater and this carried through for the rest of the cycling. This led to the lower final modulus value of 8.52 Msi, which was more than a 53 percent drop in modulus.

The only difference in crack growth pattern in this

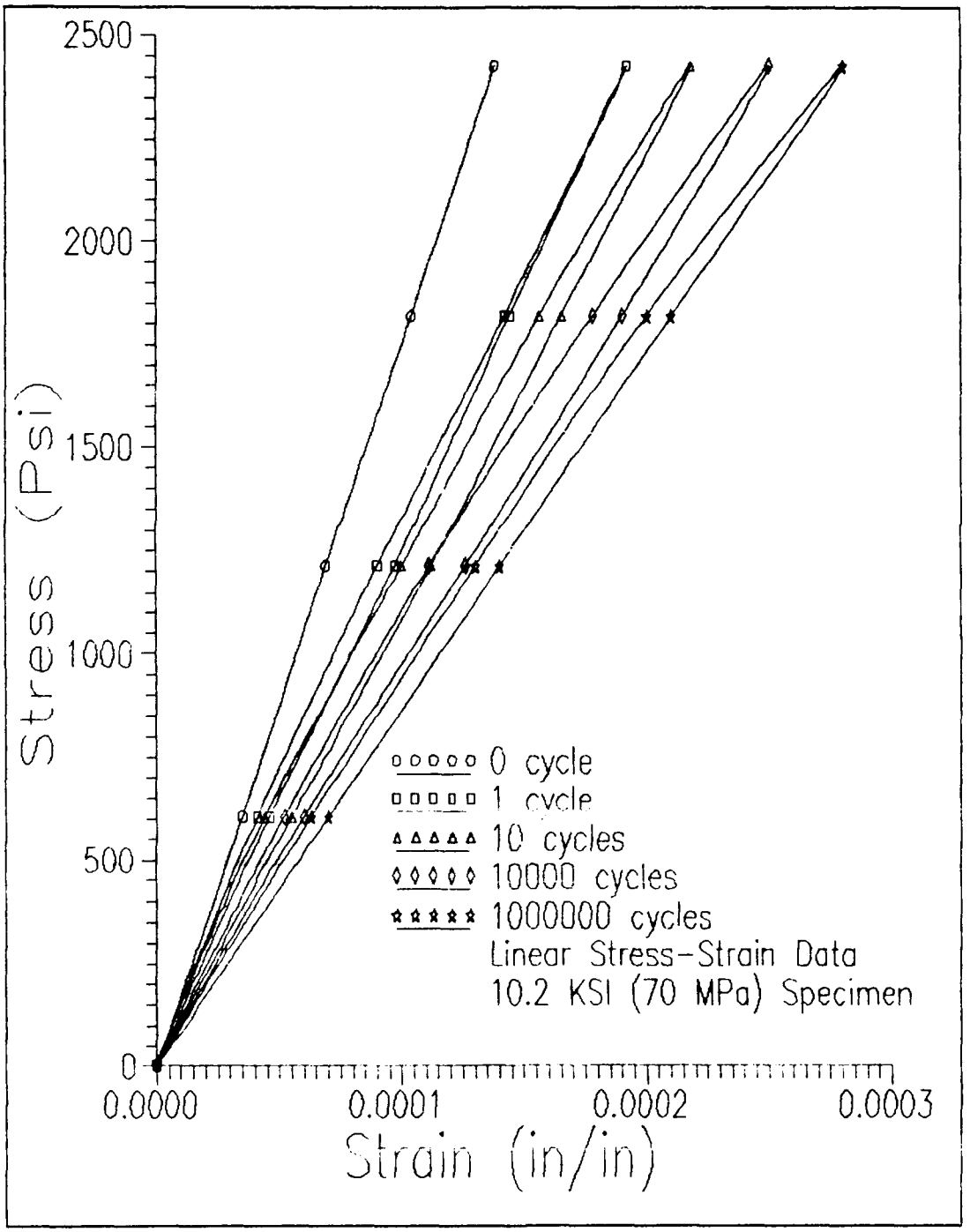

Figure 22 **Stress-Strain Data**
10.15 KSI (70 MPa) Specimen

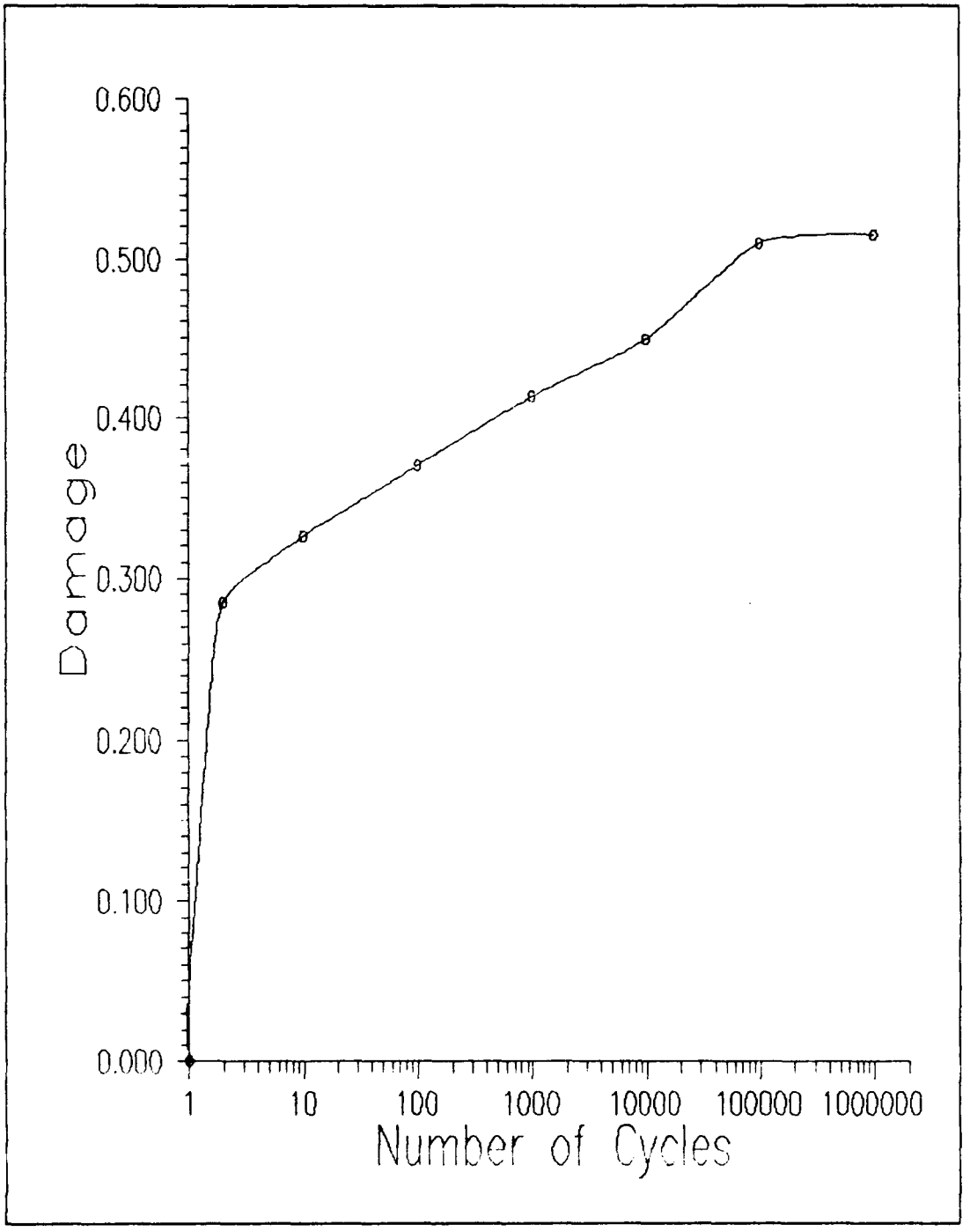

Figure 23 Damage Vs Cycle Count
10.15 KSI (70 MPa) Specimen

Figure 24 Surface Crack in 0^0 Ply
10.15 KSI (70 MPa) Specimen

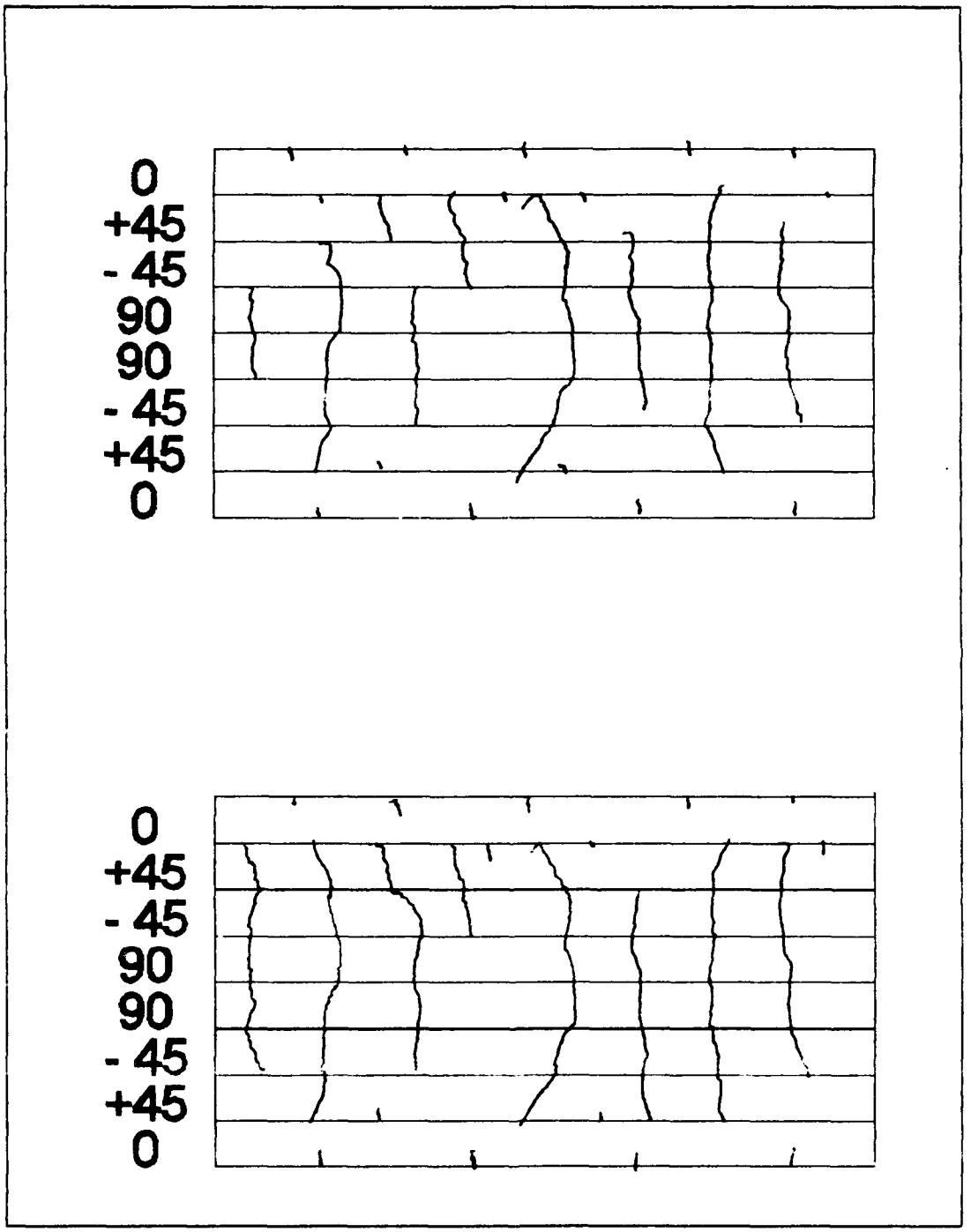

Figure 25 Damage Progression in 10.15 KSI Specimen
1 Cycle (top), 1,000,000 Cycles (bottom)

specimen compared to the 8.7 Ksi specimen is that there was a very limited amount of damage in the 0^0 ply. Small transverse cracks in the surface of the 0^0 ply appeared after the first cycle (Figure 24), but did not make any progress through this ply as cycling continued. This feature can be seen in the crack initiation and growth schematics in Figure 25.

4. 11.6 Ksi (80 MPa) Specimen

The elastic modulus data is given in Table 8 in the appendix. The elastic stress-strain curves and the damage parameter curve for this sample (S5) are shown in Figures 26 and 27. The distribution of the modulus decrease was displayed in Figure 26. The decrease in modulus after the first cycle was almost the same as the preceeding test but the modulus decreased more rapidly as cycle count increased. The slope of the damage curve was greater in the earlier cycling than in any of the previous samples, but after 10,000 cycles the curve flattened. After 1,000,000 cycles, the final elastic modulus had decreased to 7.2 Msi, more than 57 percent less than the initial measurement of 16.73 Msi.

The crack pattern initiation followed the same pattern as the previous tests. The cracks started at the ply boundaries and then spread laterally into the 45 and 90 degree plies with the 0 degree ply still largely unaffected. But as cycling continued secondary cracking and crack coupling could

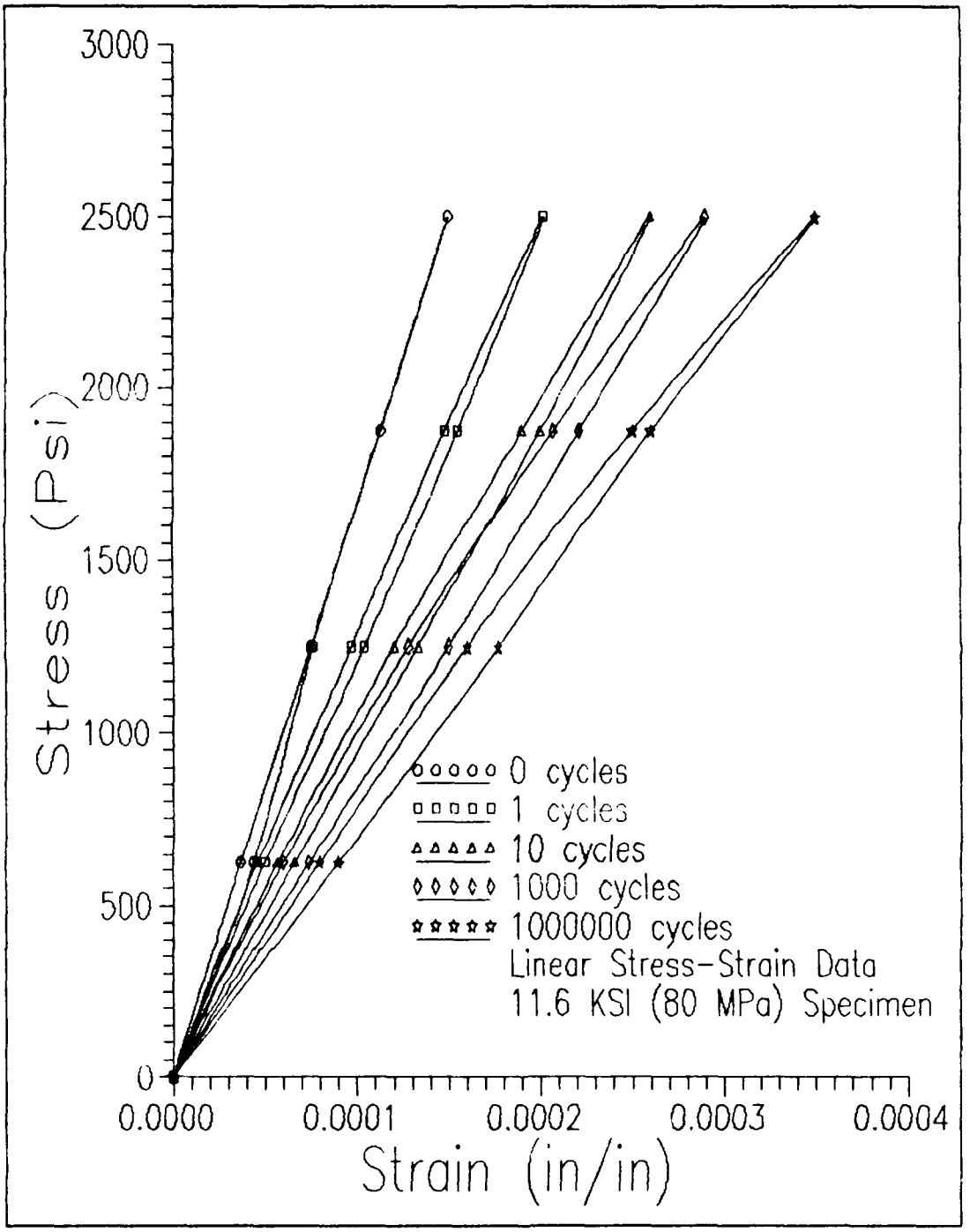

Figure 26 **Stress-Strain Data**
11.6 KSI (80 MPa) Specimen

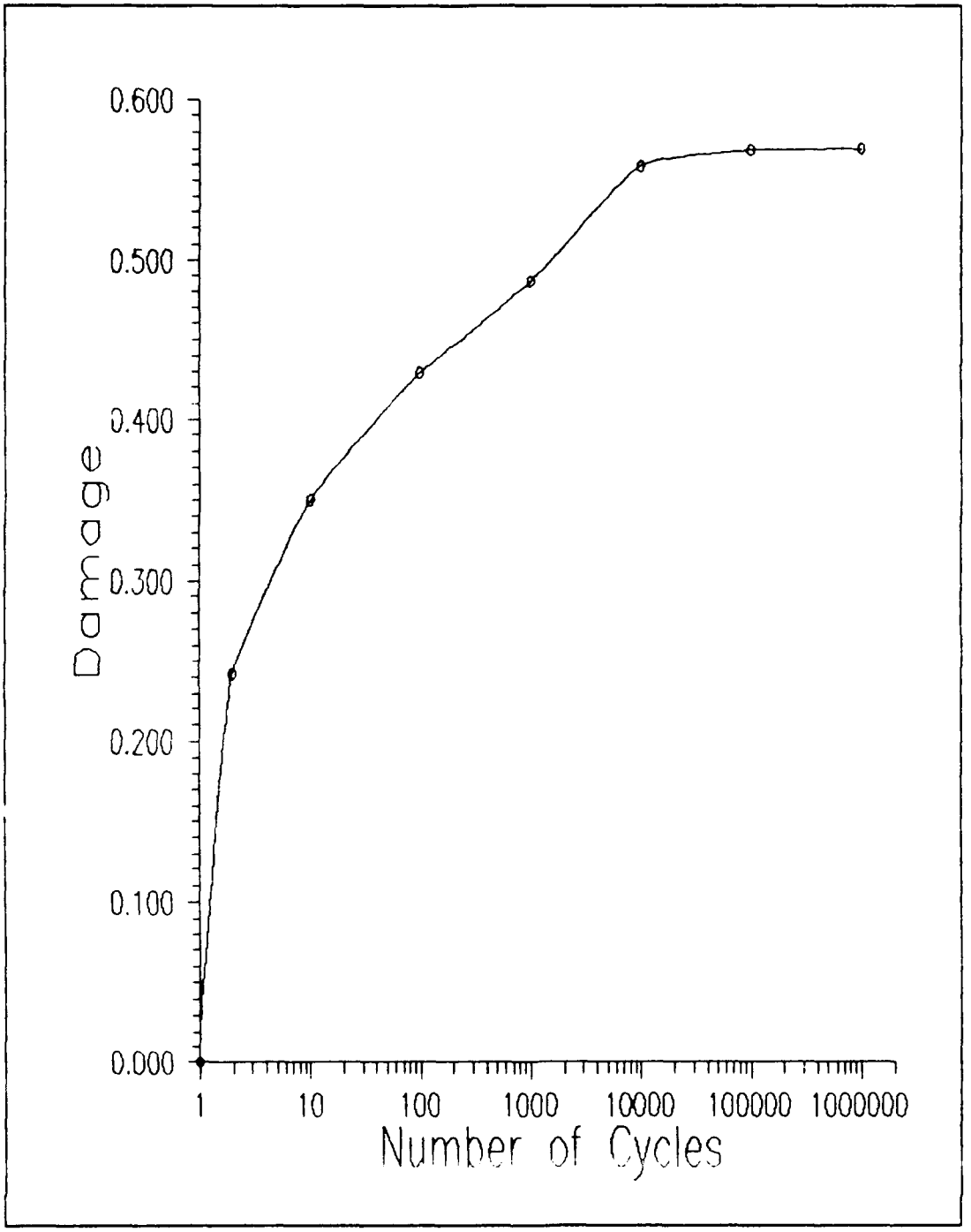

Figure 27 Damage Vs. Cycle Count
11.5 KSI (80 MPa) Specimen

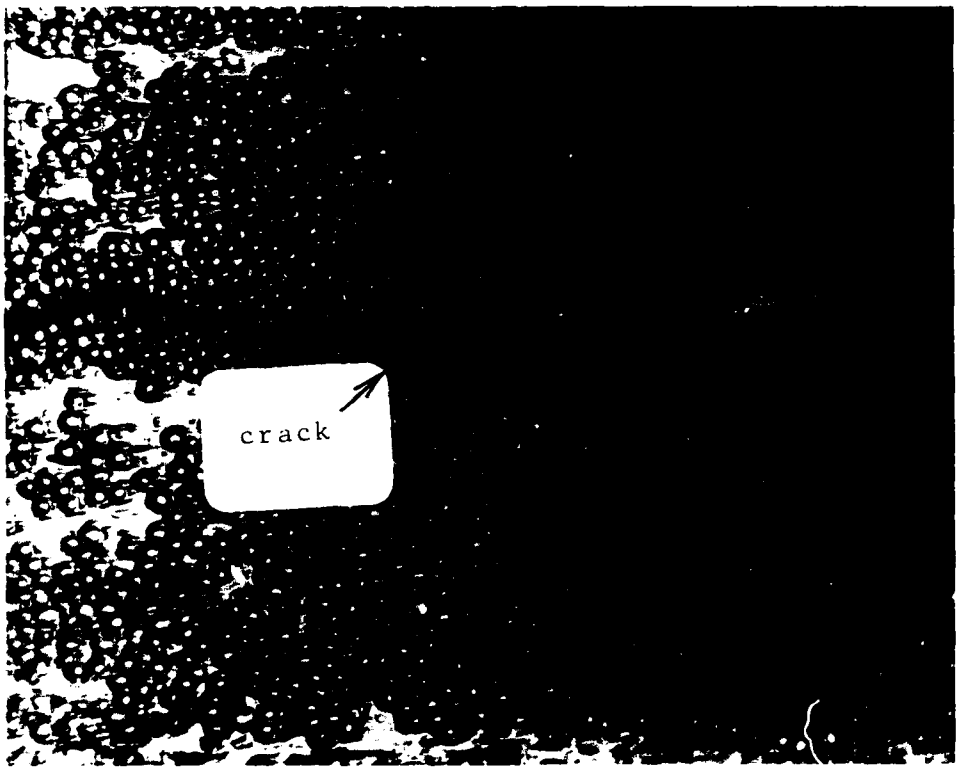

Figure 28 Longitudinal Crack Near $90^0/45^0$ Ply Boundary 11.6 KSI (80 MPa) Specimen

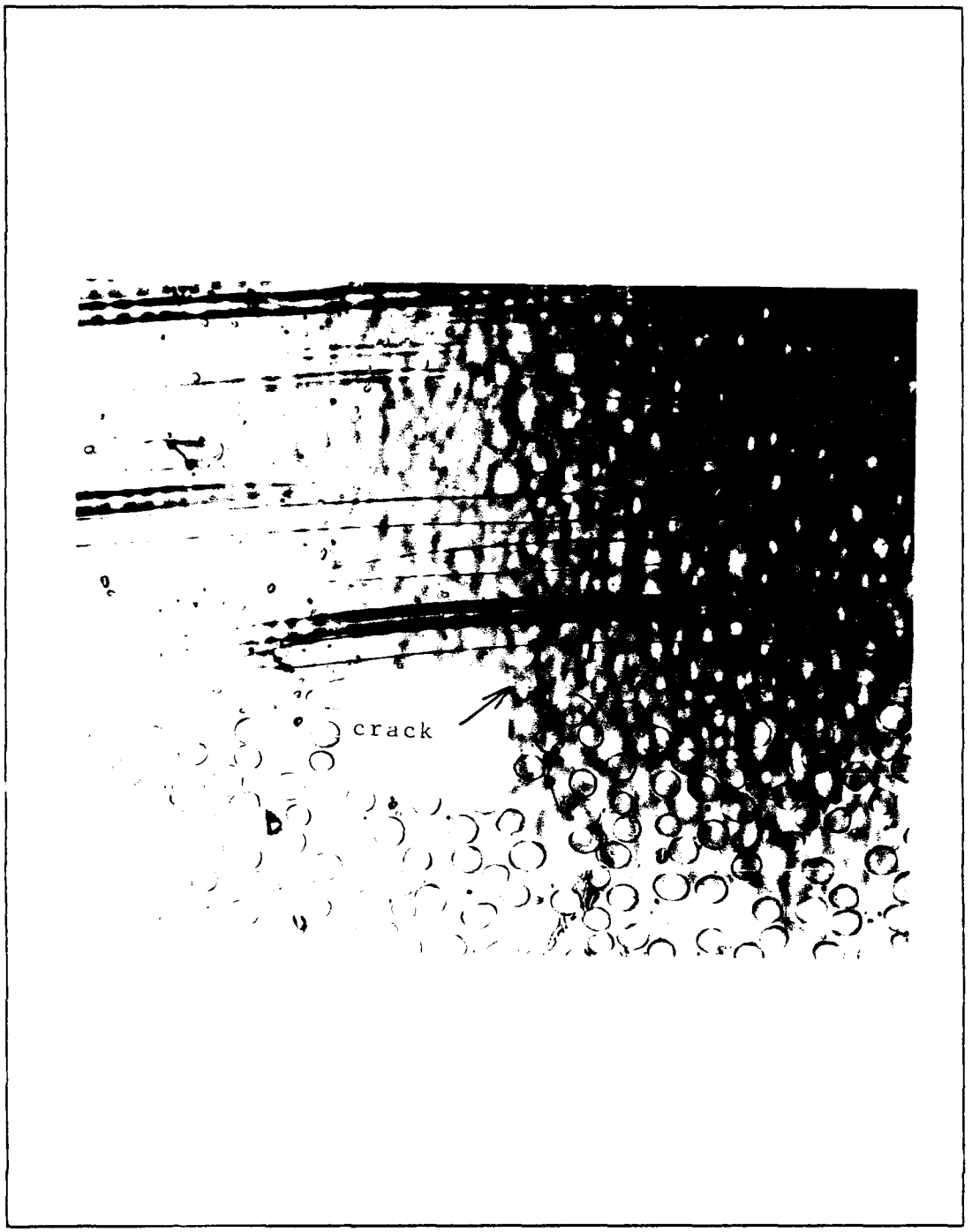

Figure 29 Transverse Matrix Damage in 0^0 Ply 11.6 KSI (80 MPa) Specimen

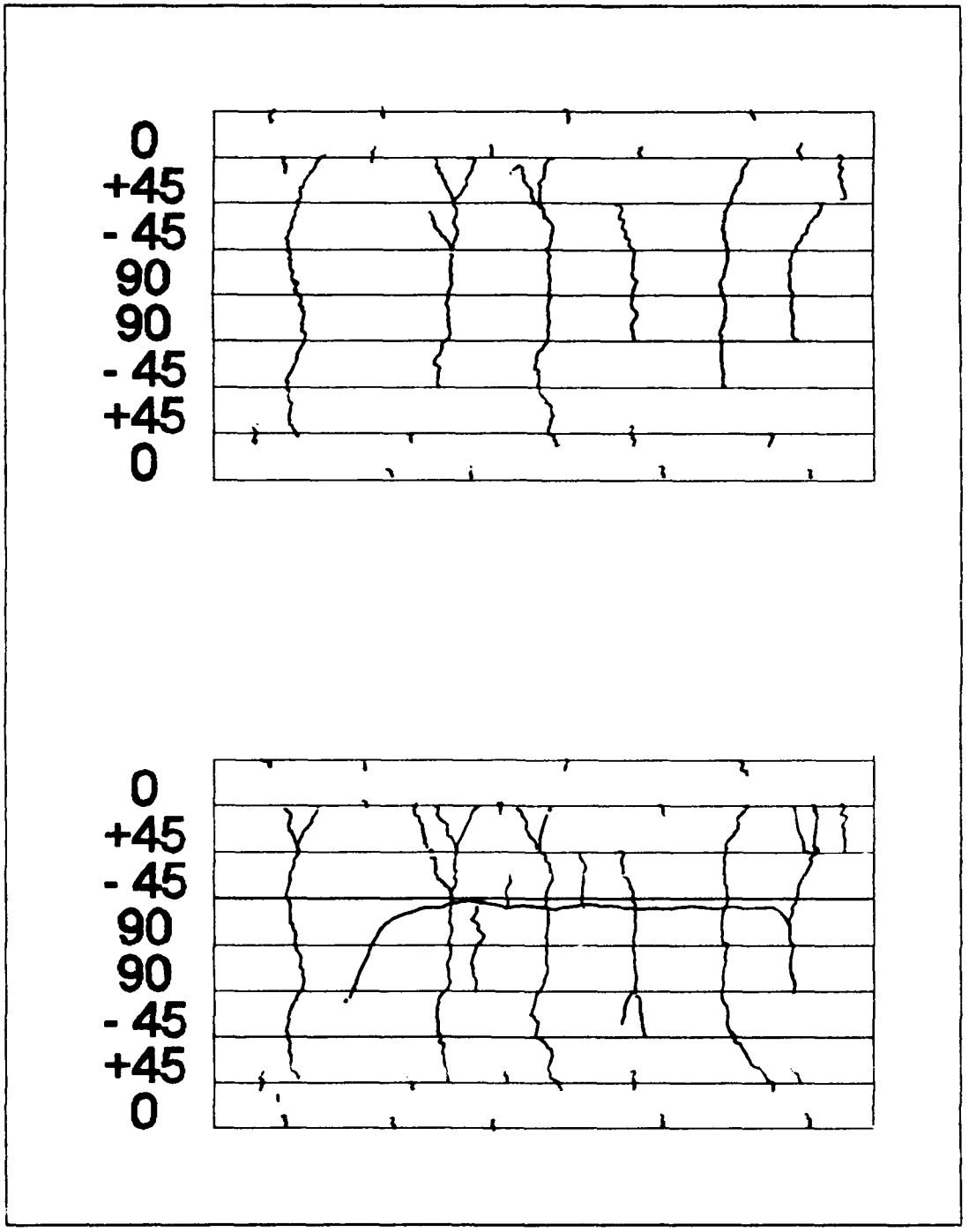

Figure 30 Damage Progression in 11.6 KSI Specimen
1 Cycle (top), 1,000,000 Cycles (bottom)

be observed. After 50 cycles, a longitudinal crack started to develop in the 90 degree ply near the mid-plane of the specimen (Figure 28). This was the first time any type of delamination effects had been observed. At the same time, small transverse cracks started to appear between the fibers in the 0^0 plies of the laminate (Figure 29).

The longitudinal crack in the 90 degree ply grew in length as cycling progressed. The matrix damage in the 0 degree ply increased slightly during testing, but did not penetrate very far into the plies (Figure 30). Secondary cracking and crack coupling increased as a function of cycle count as depicted in Figure 30. At the end of the 1,000,000 cycles the 90 and 45 degree plies were heavily fractured, but the 0 degree ply was still largely intact.

5. 12.33 Ksi (85 MPa) Specimen

The modulus decrease and damage progression patterns for this specimen (S8) were very similar to that of the 11.6 Ksi (80 MPa) specimen. The elastic modulus data table is listed in the appendix (Table 7). The elastic stress-strain curves and the damage curve are shown in Figures 31 and 32. The final modulus decreased to 6.0 Msi, a 63 percent drop from the initial modulus of 16.27 Msi. This was the lowest modulus observed for any unbroken specimen.

The damage curve shows that the damage progressed very

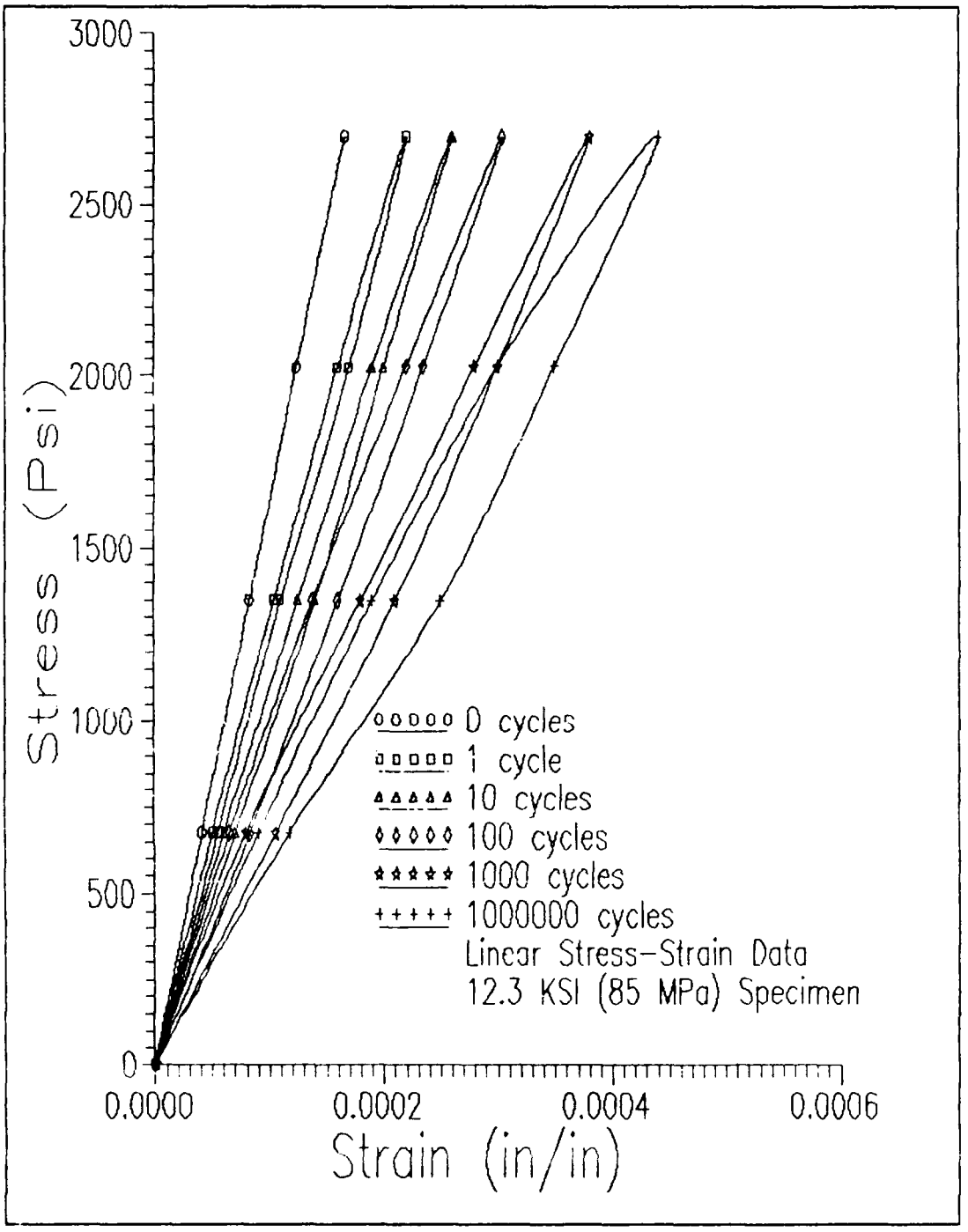

Figure 31 **Stress-Strain Curves**
12.3 KSI (85 MPa) Specimen

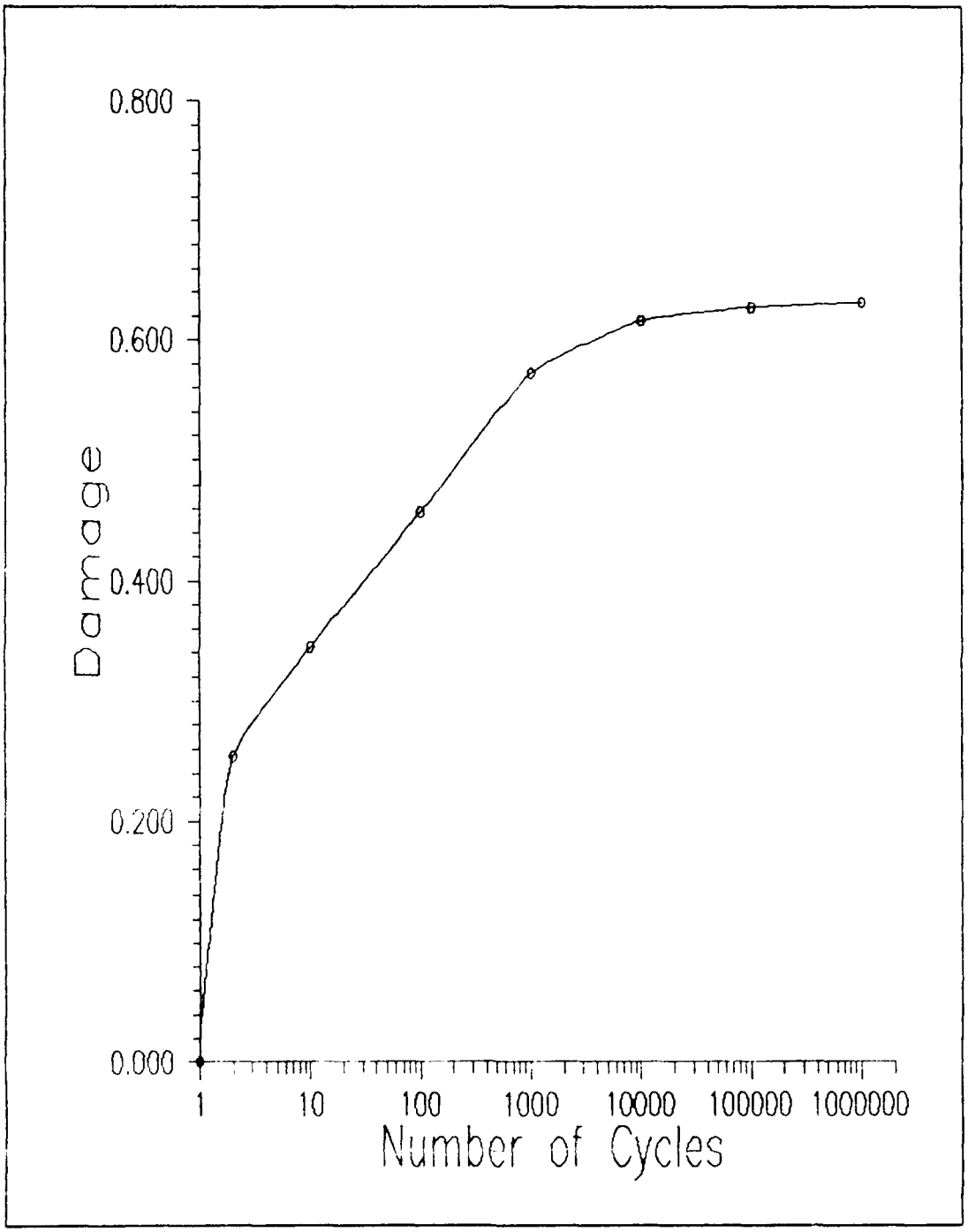

Figure 32 Damage Vs. Cycle Count
12.3 KSI (85 MPa) Specimen

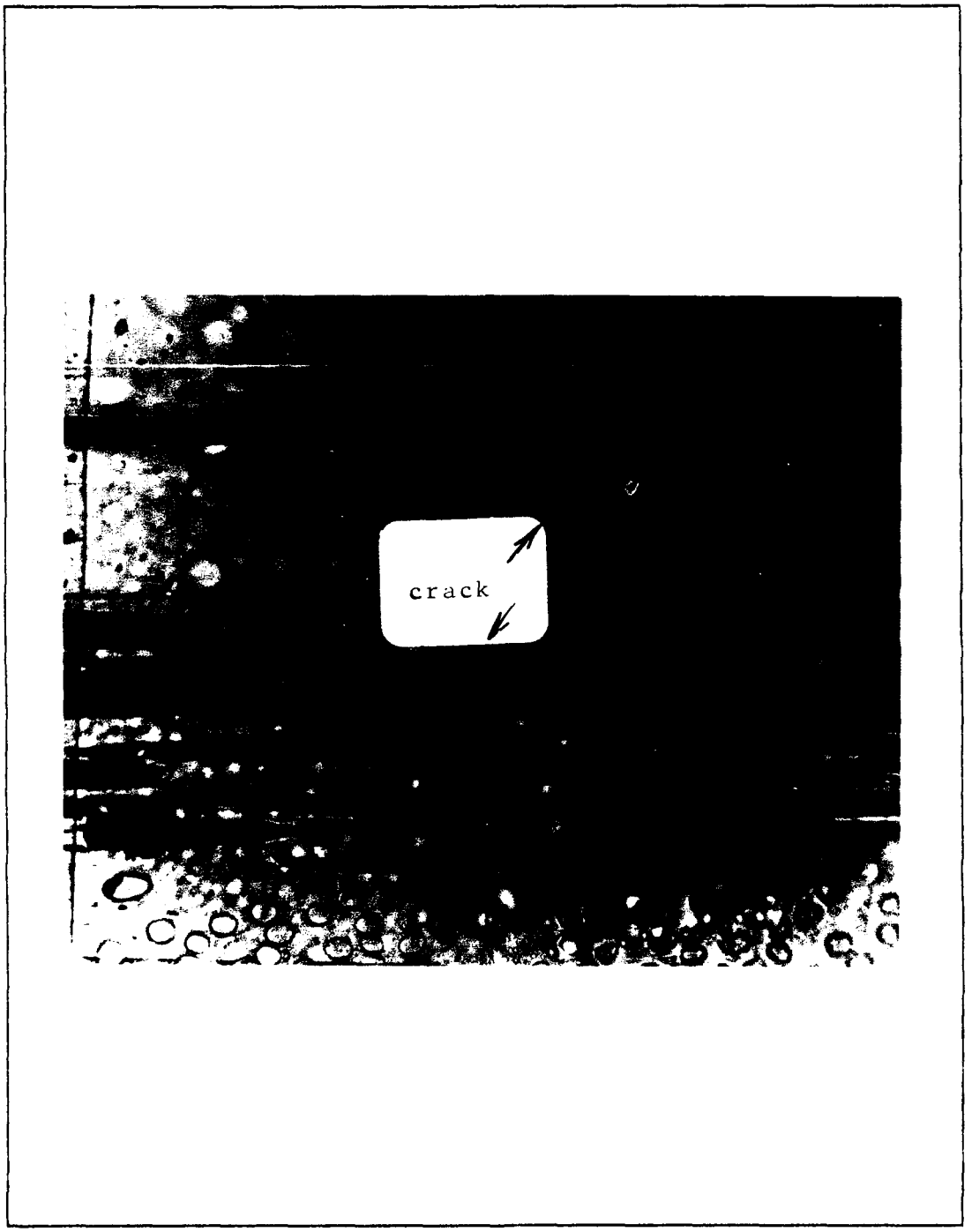

Figure 33 Crack Penetration Into 0^0 Ply
12.3 KSI (85 MPa) Specimen

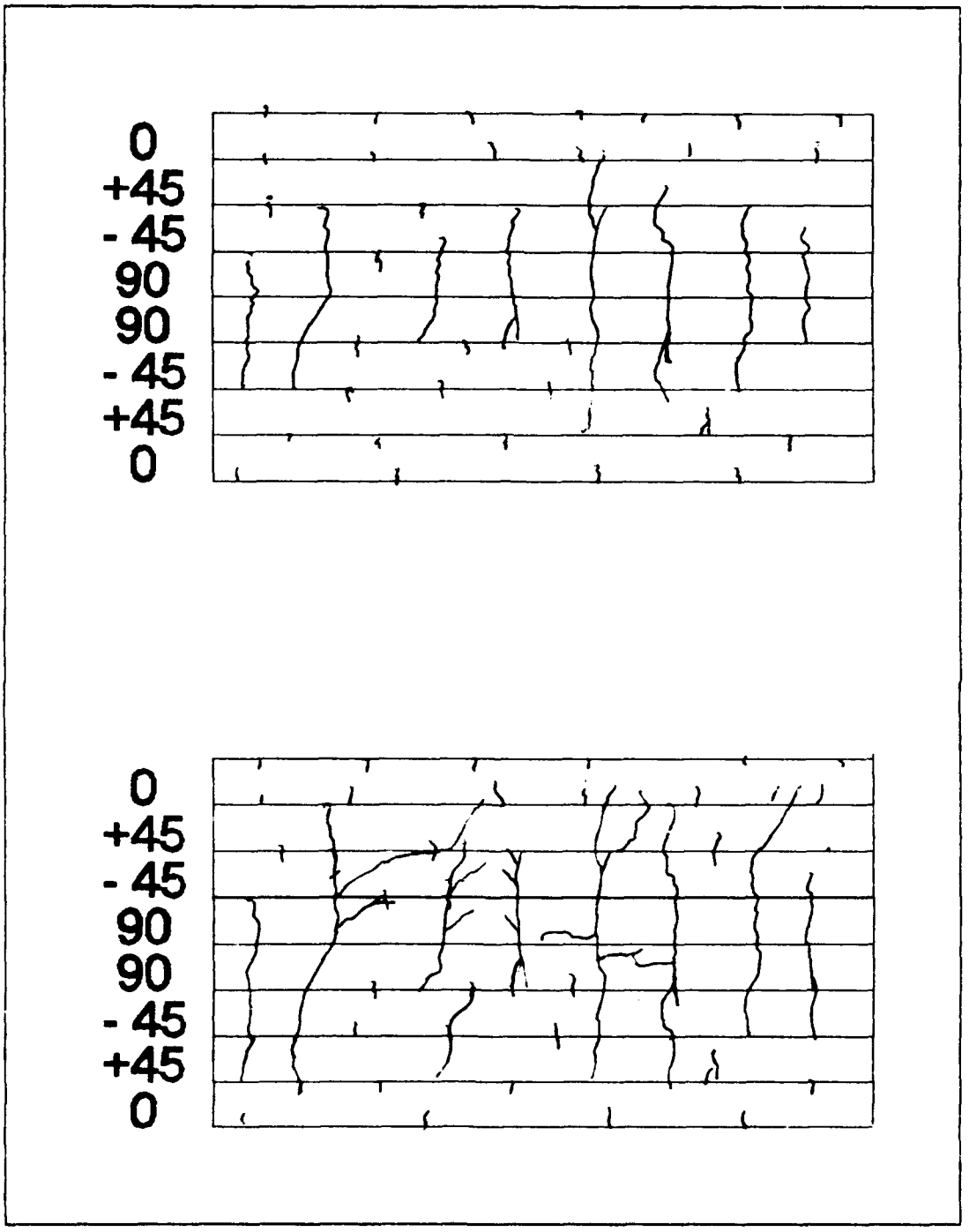

Figure 34 Damage Progression in 12.3 KSI Specimen
1 Cycle (top), 1,000,000 Cycles (bottom)

rapidly until it reached a plateau at 10,000 cycles. After that the curve flattened and the damage stabilized.

The crack initiation and progression was also very similar to that of the 11.6 Ksi specimen. The dissimilarities were, (1) the damage progressed more rapidly as a function of cycle count with extensive secondary cracking and crack coupling, and (2) the crack penetration of the 0 degree ply was more extensive (Figure 33). Longitudinal delamination cracks branched off of existing transverse cracks between the 45^0 and 90^0 plies after 10 cycles. The transverse matrix cracks at the 0/45 degree ply interfaces had extended well into the 0^0 plies between the fibers, but none of the cracks had completely extended across the 0 degree plies (Figure 34).

6. 13.0 Ksi (90 MPa) Specimen

This specimen (S2) broke after 687 cycles. The elastic modulus data is contained in Table 8 in the appendix. The elastic stress-strain curves and the damage parameter curve are shown in Tables 35 and 36. The modulus decrease was similar to the 85 Ksi specimen until the 100 cycle point. After that point, the modulus decreased rapidly leading to failure.

Figure 36 gives a representation of the damage progression. First, there was a steep rise in damage as initial cracking occurred. Then there was a period of relative

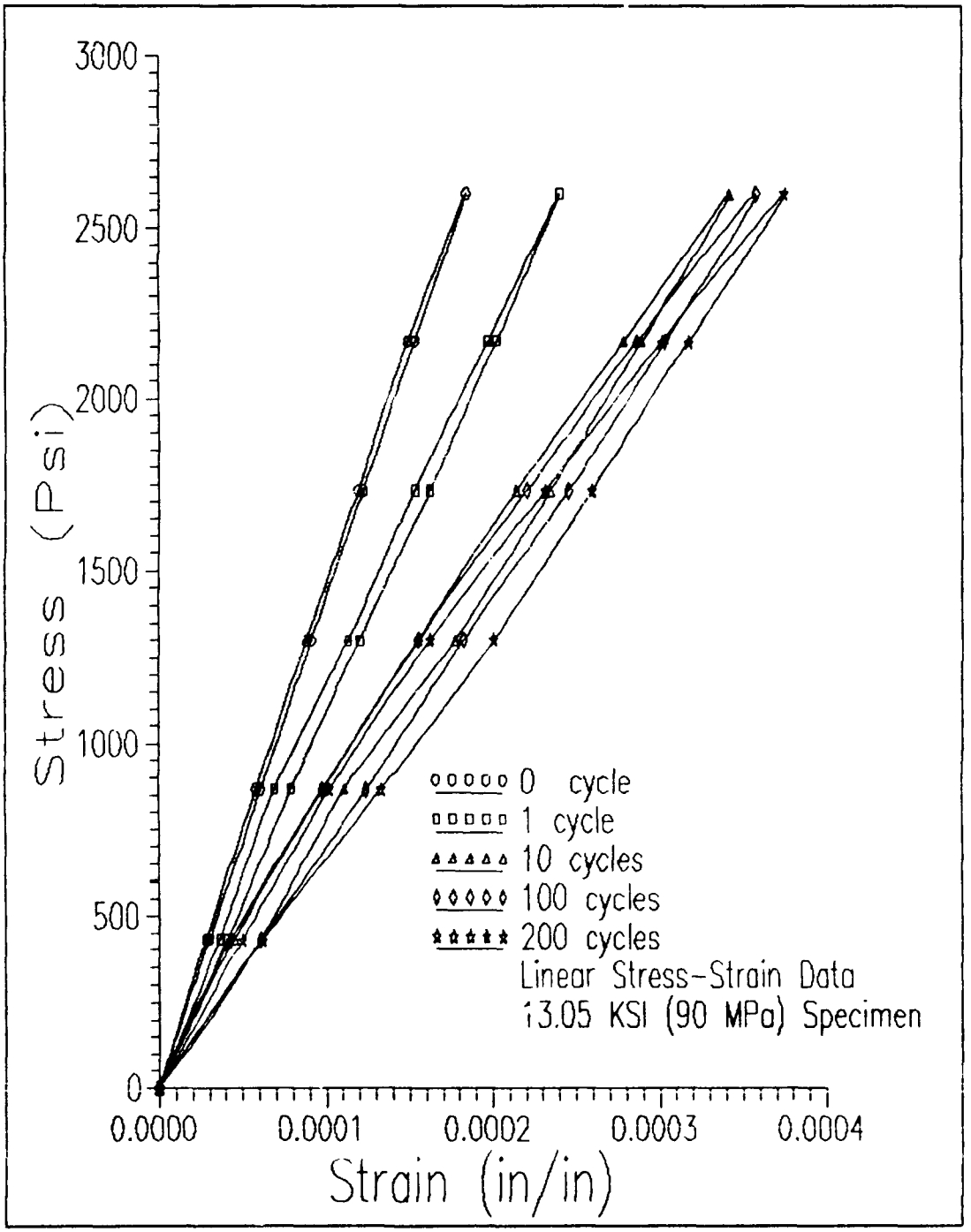

Figure 35 Stress-Strain Data
13.0 KSI (90 MPa) Specimen

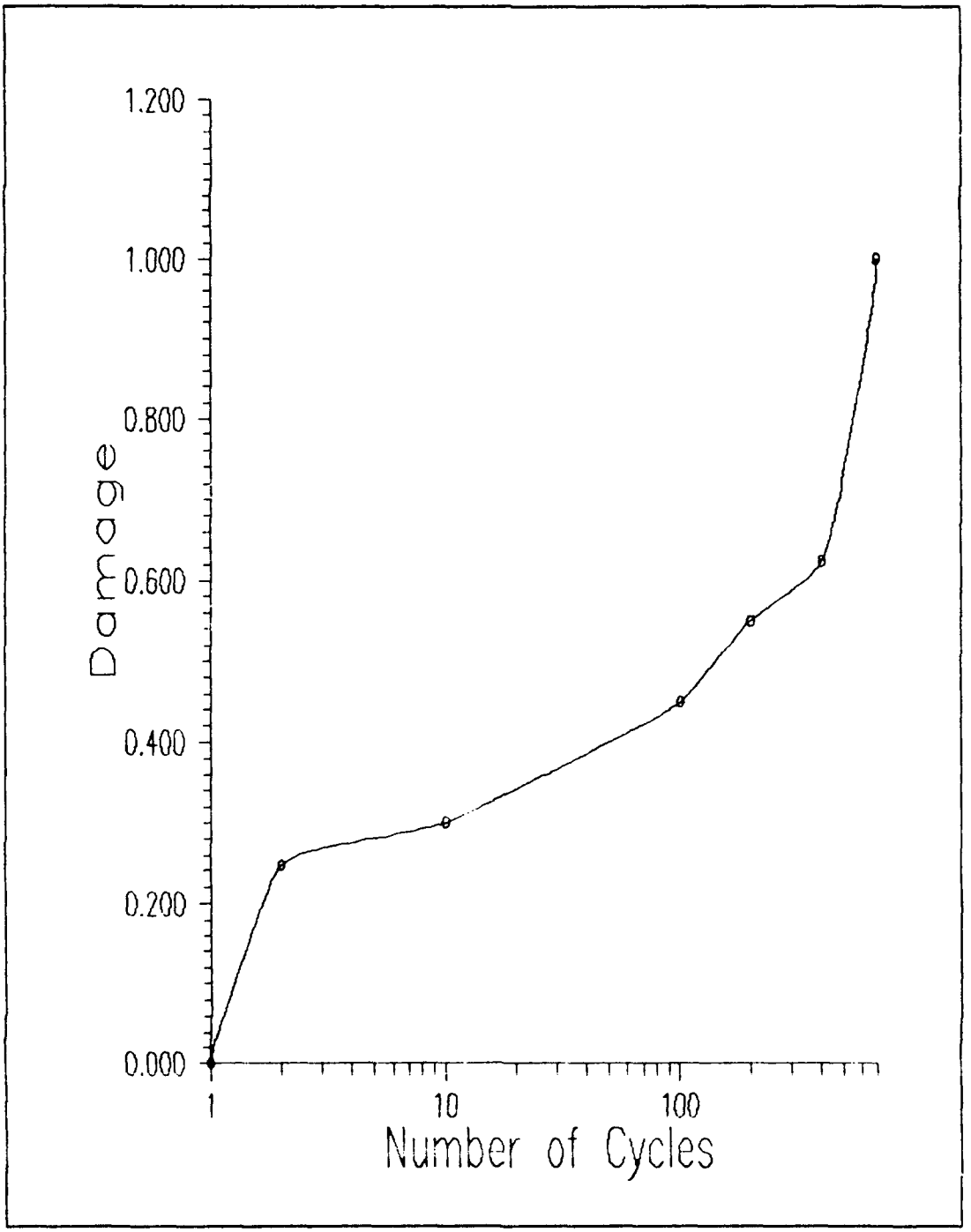

Figure 36 Damage Vs. Cycle Count
13.0 KSI (90 MPa)

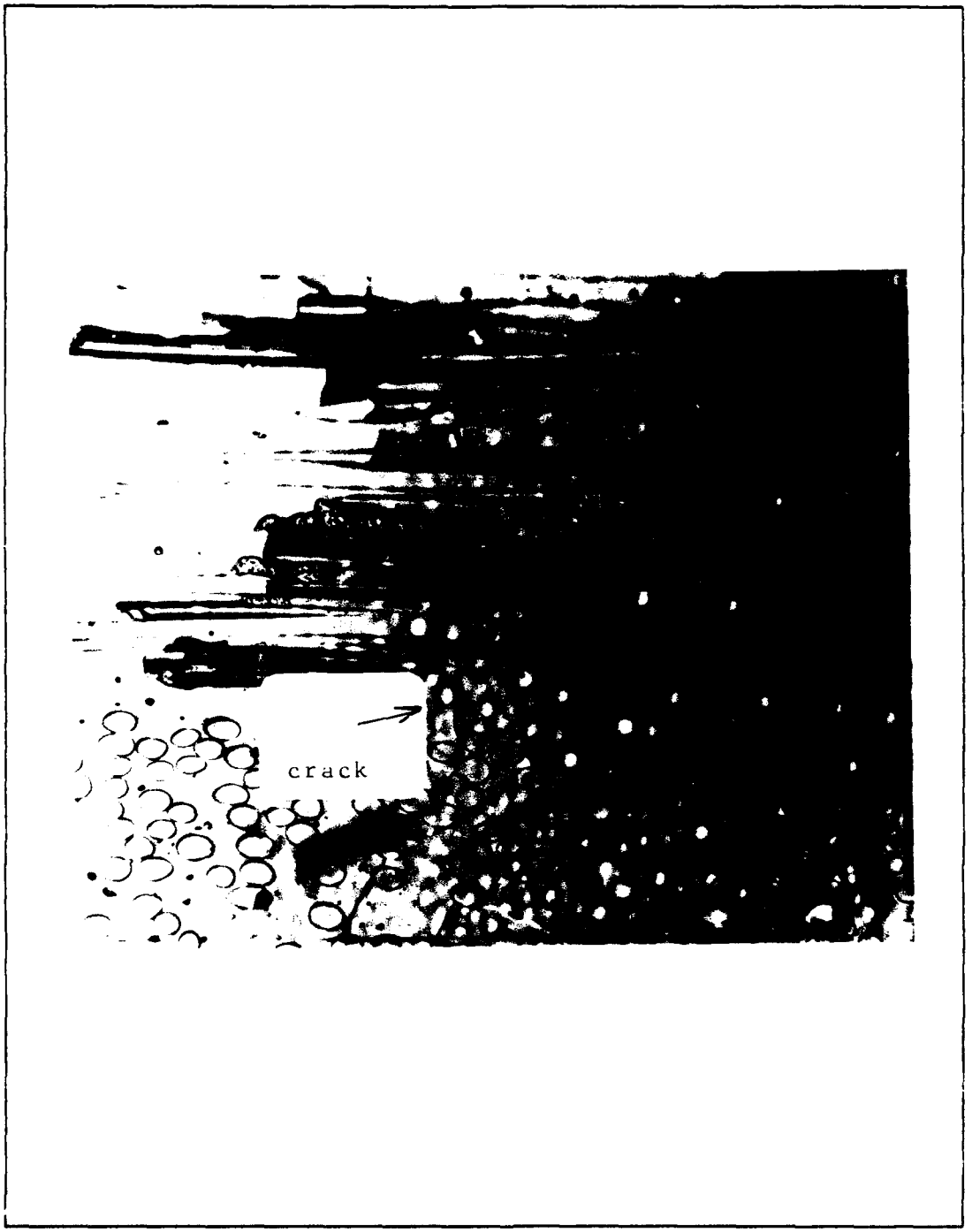

Figure 37 Matrix Cracking In 0^0 Ply After 100 Cycles 13.0 KSI (90 MPa) Specimen

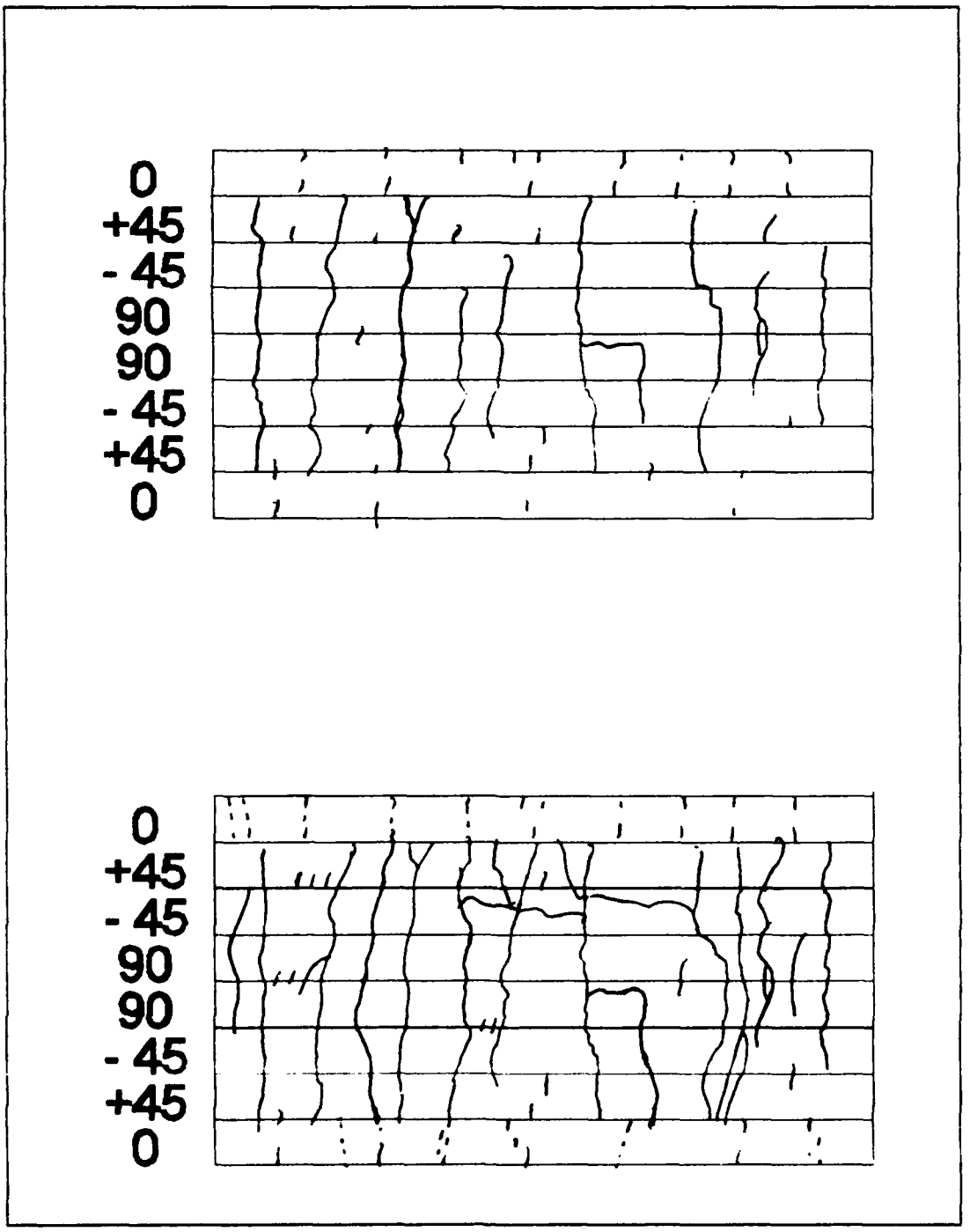

Figure 38 Damage Progression in 13.0 KSI Specimen 1 Cycle (top), 200 Cycles (bottom)

stablility as secondary cracks formed and connected. Finally, there was a rapid increase in the slope of the curve after 300 cycles, as the fibers in the 0^0 plies started to break, on the way to 100 percent damage, or failure, at 687 cycles.

The main reason the specimen failed was the extensive damage done to the fibers in the 0^0 plies. The damage in the other plies was extensive and complex, having started in the first cycle, but in none of the other tests had the 0^0 plies been damaged to such an extent. There was little damage in the 0^0 plies after the first cycle, but within 50 cycles, matrix cracks had extended transversly well into the 0^0 plies (Figure 37). As cycling continued, the damage became even more acute in all plies, as secondary cracking and crack coupling occurred. There was evidence of fiber breakage in the 0^0 plies within 100 cycles.

Finally, after the matrix material in the 0^0 plies had been sufficiently fractured, the fibers in the plies could no longer sustain the load and broke (Figure 38). Unfortunately, the failure occurred within the tabbed area of the specimen, so the test was considered marginally successful.

7. 13.8 Ksi (95 MPa) Specimen

This specimen (S6) failed after only 383 cycles. The modulus decrease and crack growth patterns were very similar to that of the 13.0 Ksi (90 MPa) specimen. The modulus data

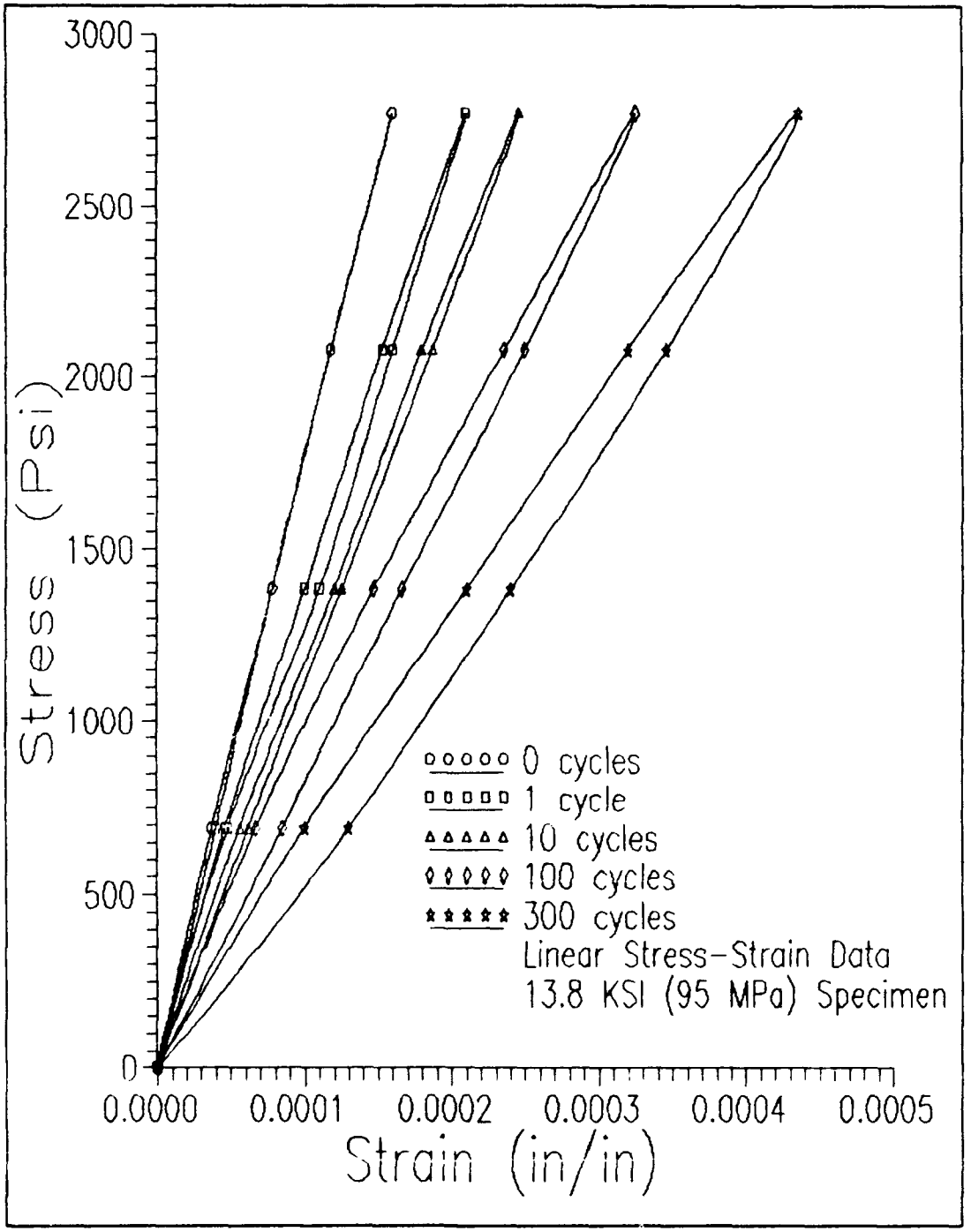

Figure 39 **Stress-Strain Curves**
13.8 KSI (95 MPa) Specimen

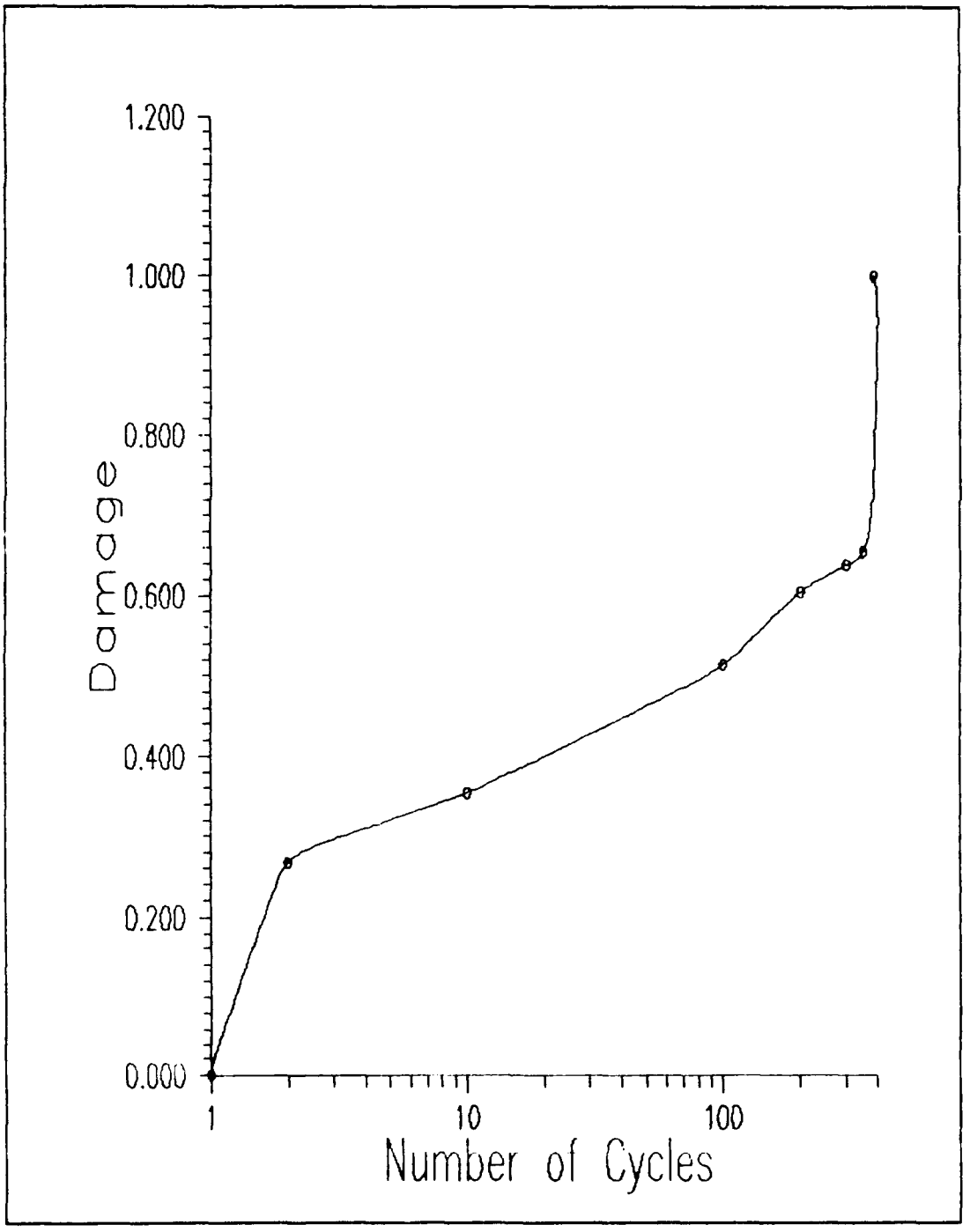

Figure 40 Damage Vs. Cycle Count
13.8 KSI (95 MPa) Specimen

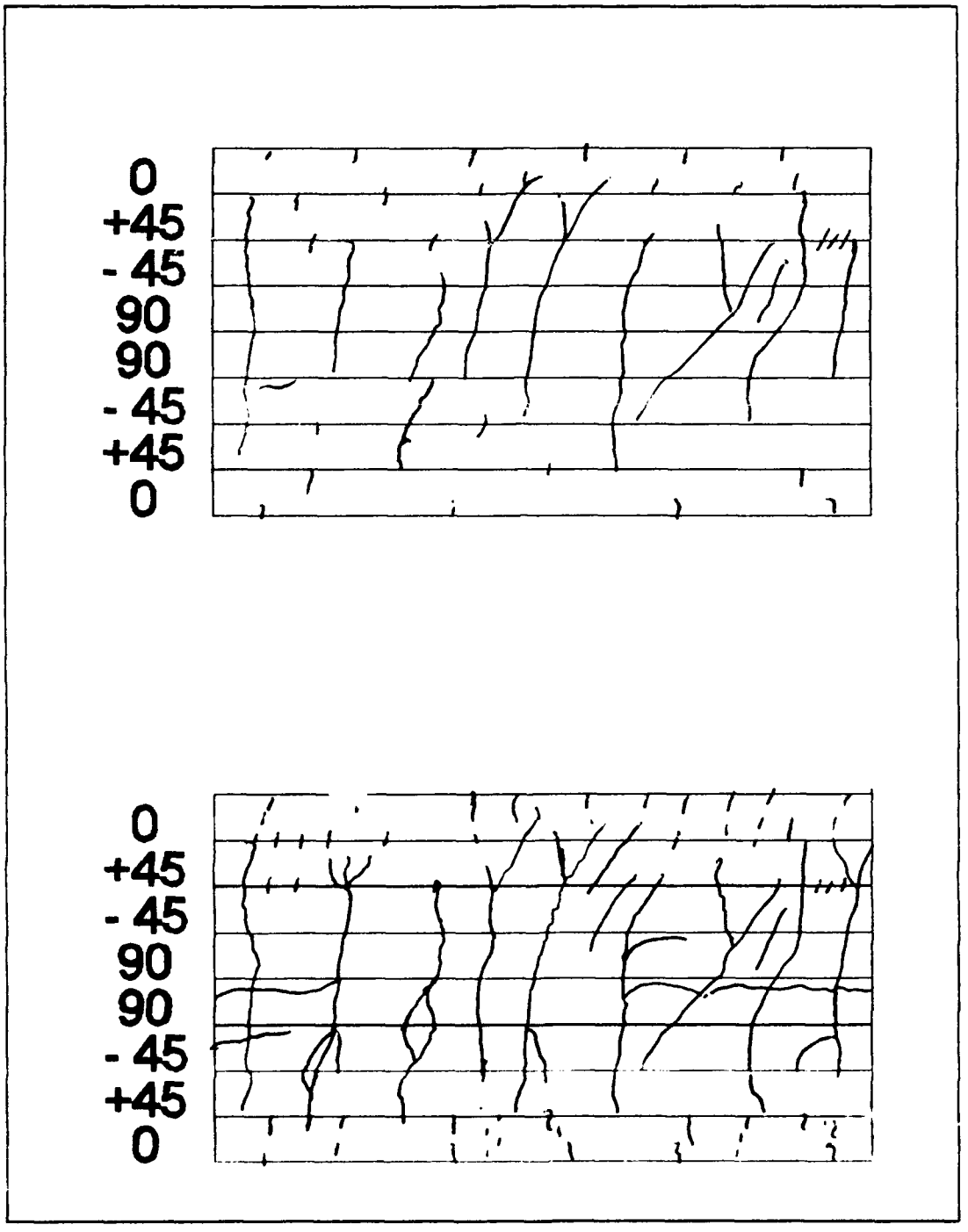

Figure 41 Damage Progression in 13.8 KSI Specimen
1 Cycle (top), 200 cycles (bottom)

table (Table 9) located in the appendix, the elastic stress-strain curve (Figure 39) , and the damage parameter curve (Figure 40) illustrate that the results of this test were nearly identical to the results of the previous test. The damage curve was again divided into 3 distinct slopes. The only difference was that this sample failed 300 cycles sooner. The crack initiation, propagation and density patterns were virtually identical. Substantial damage occurred in the 90 and 45 degree plies within the first cycle. Matrix cracking started in the 0 degree plies immediately. There were numerous longitudinal delamination and secondary transverse cracks in the off-axis plies (Figure 41) as cycling continued. The longitudinal delamination cracks appeared to have originated from existing transverse cracks. The final failure took place above the tabbed area, with the individual plies easily seen in the fracture surface.

8. 14.5 Ksi (100 MPa) Specimen

This specimen (S10) failed after 376 cycles. This is only 6 cycles less than the 13.8 Ksi specimen even though there was a 5 percent increase in stress. The elastic modulus data table in the appendix (Table 10), the elastic stress-strain curves (Figure 42) and the damage parameter curve (Figure 43) show that this specimen failed in the same fashion as the 13.8 Ksi (95 MPa) specimen above. The damage curves

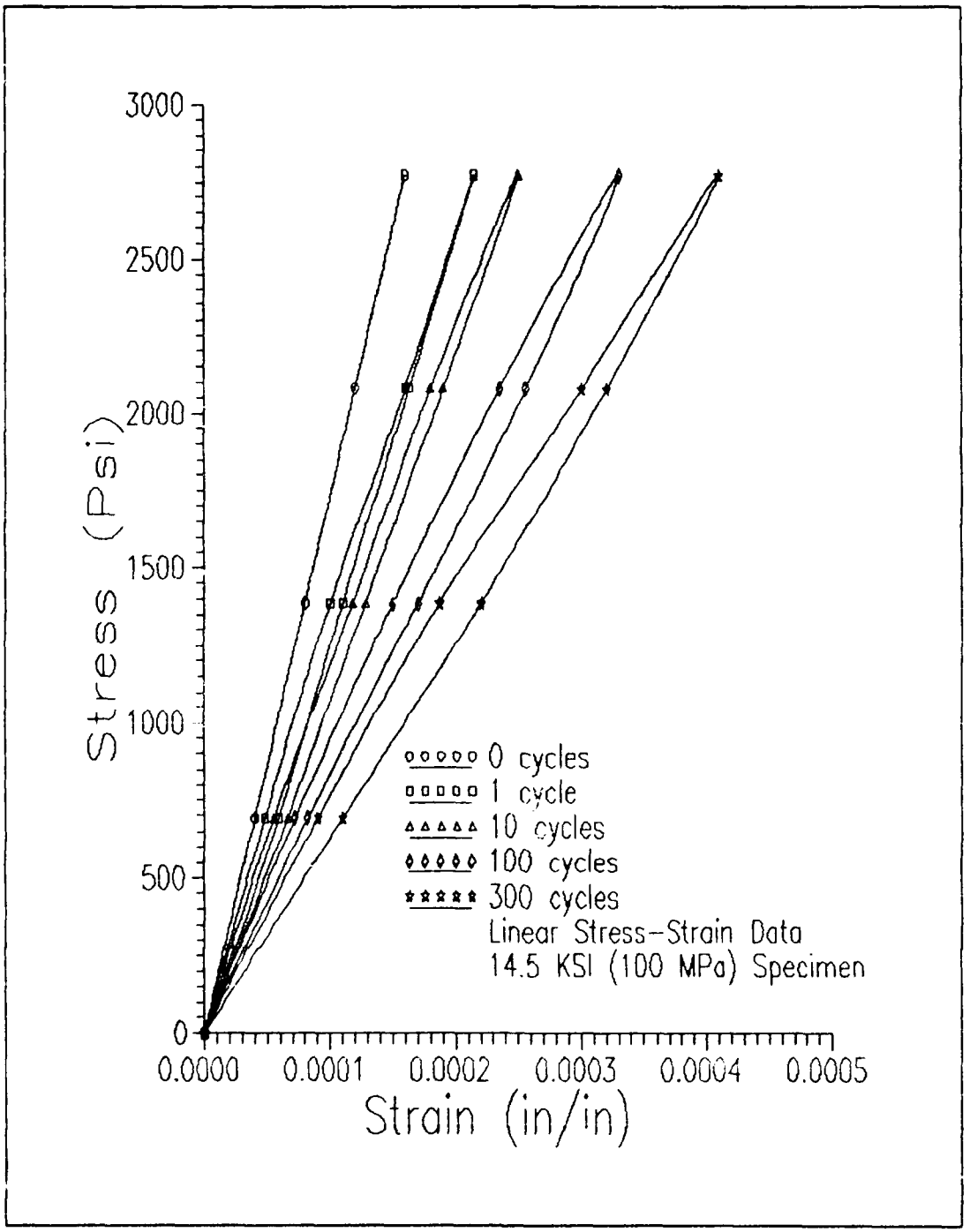

Figure 42 **Stress-Strain Curves**
14.5 KSI (100 MPa) Specimen

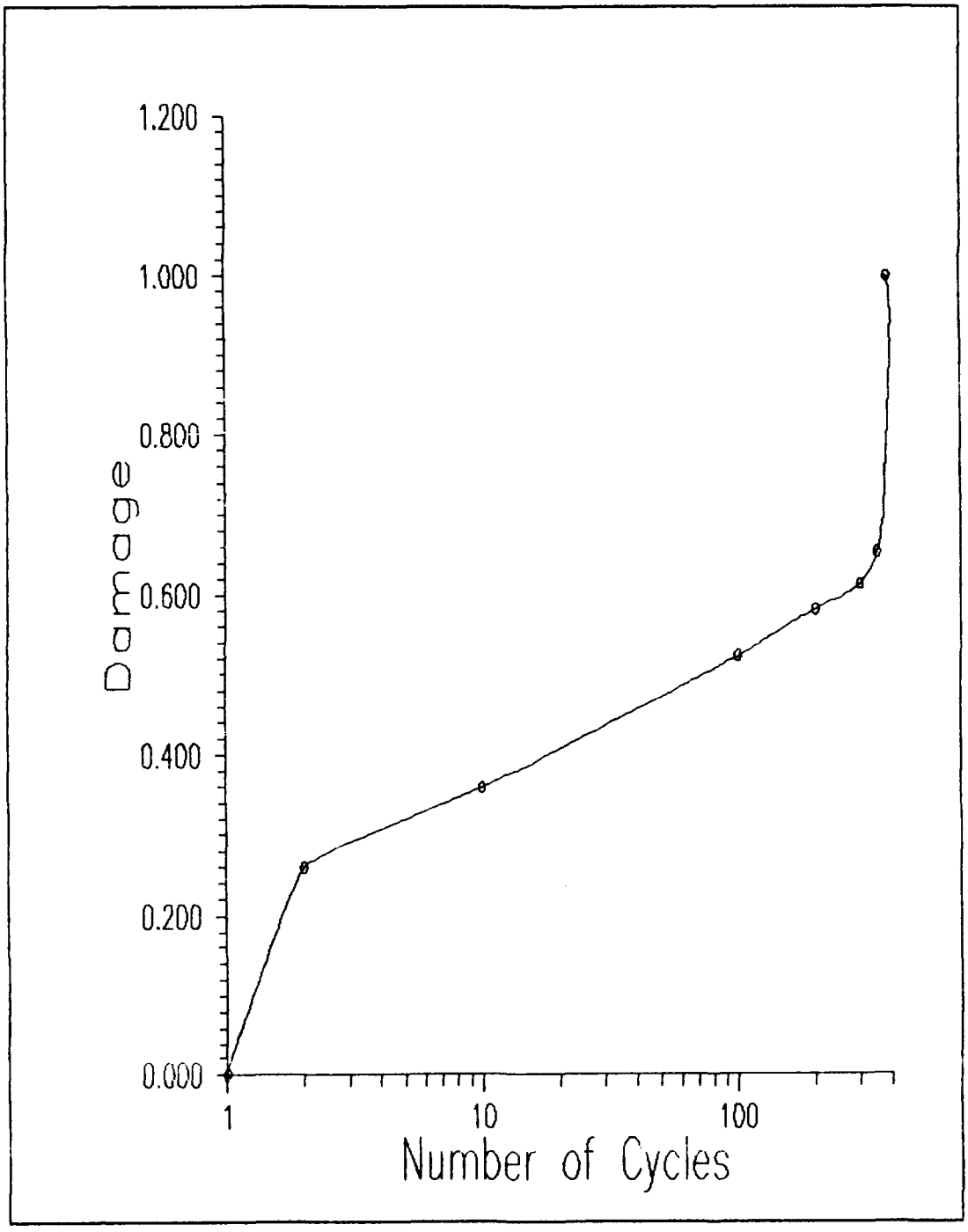

Figure 43 Damage Vs. Cycle Count
14.5 KSI (100 MPa) Specimen

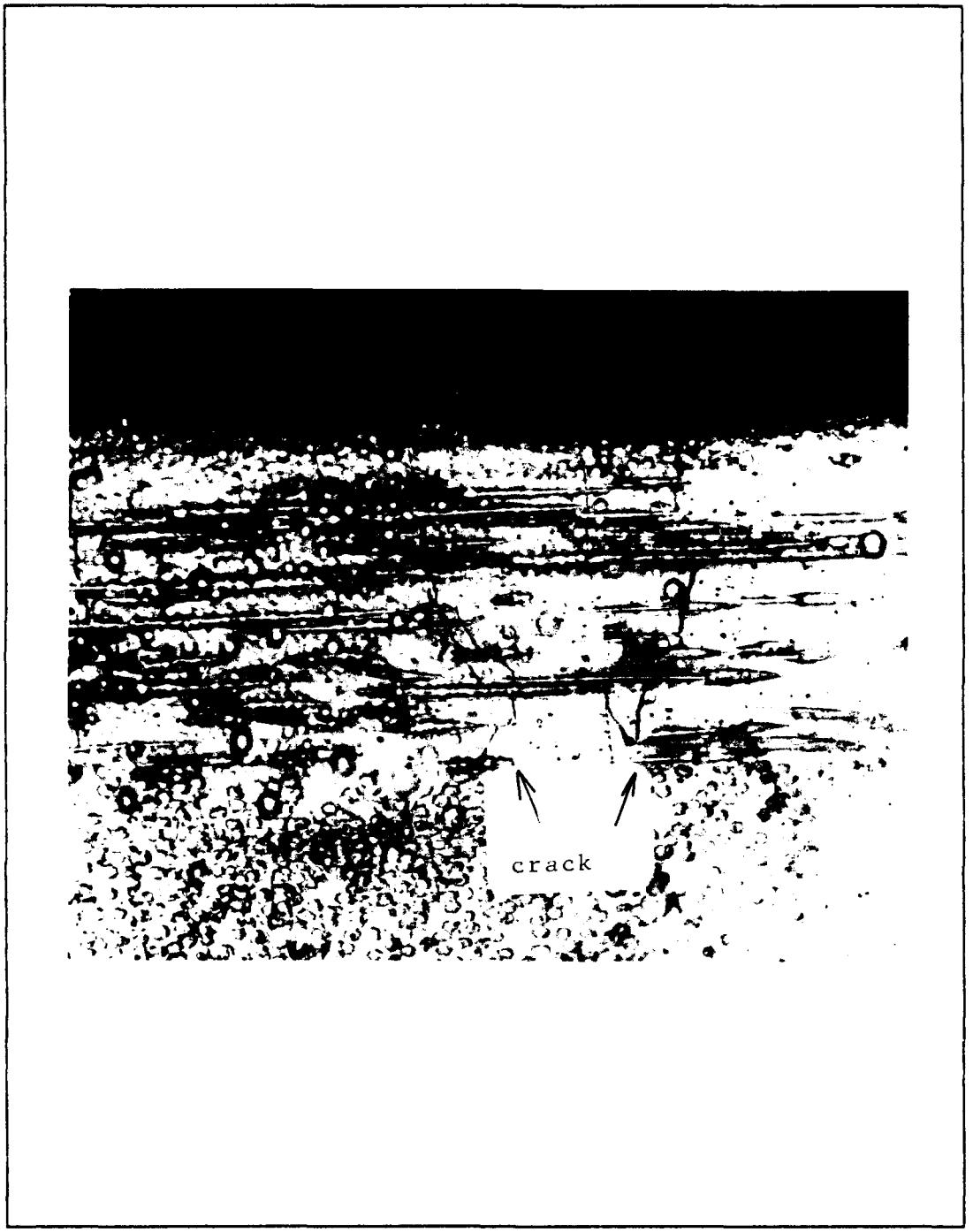

Figure 44 Micrograph Of 0^0 Ply At 300 Cycles 14.5 KSI (100 MPa) Specimen

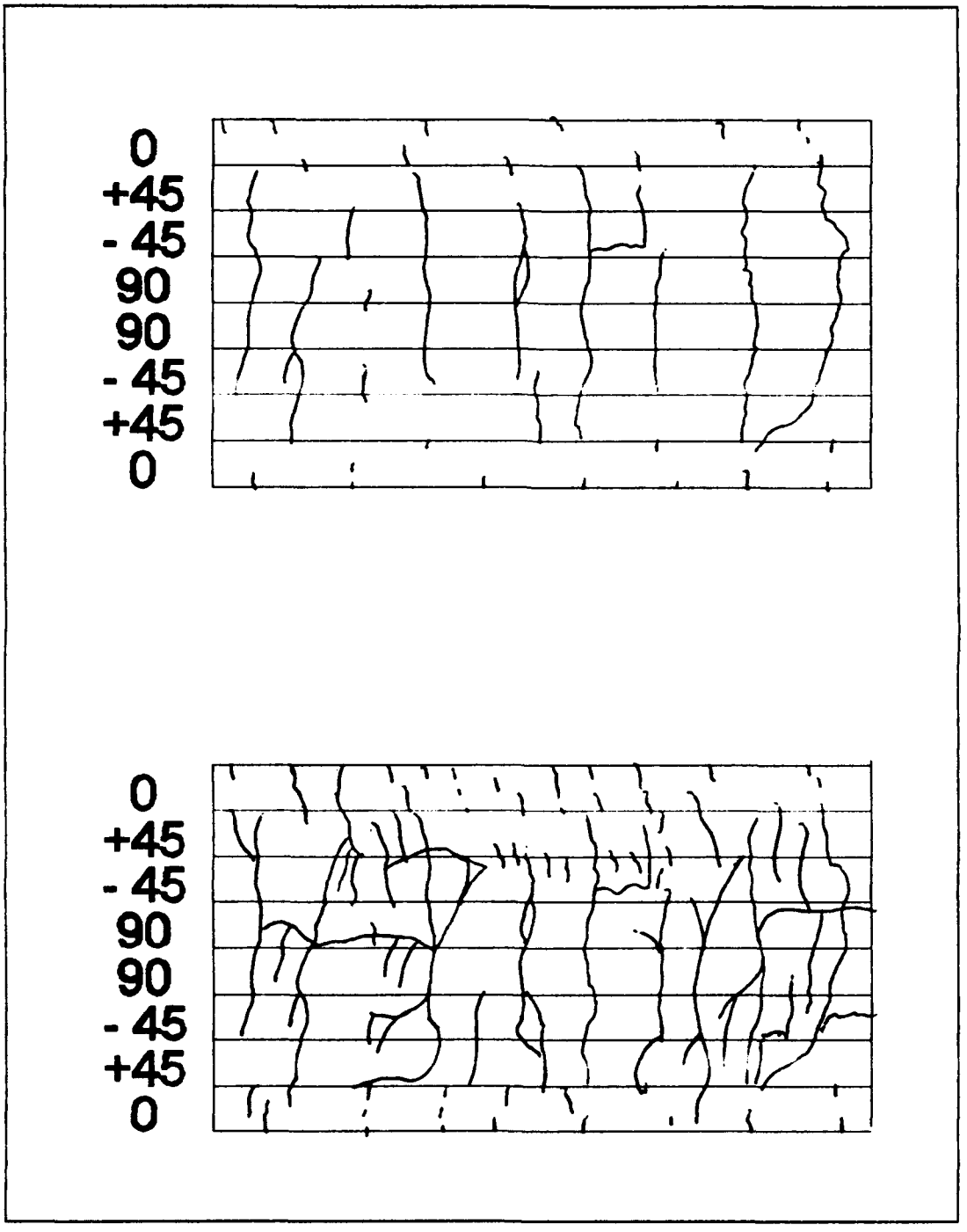

Figure 45 Damage Progression in 14.5 KSI Specimen
1 cycle (top), 300 cycles (bottom)

were nearly identical, having three distinct slopes.

Crack initiation was immediate and substantial in the off-axis 90 and 45 degree plies, with substantial amounts of transverse and longitudinal damage. There was immediate matrix cracking in the 0 degree plies after the first cycle, but there was no substantial damage until the tenth cycle. At 300 cycles all plies were heavily fractured. Figure 44 is a micrograph of the region in which the final failure took place. The fracture occurred in the middle of the gage length. Figure 45 shows crack initiation and progression at 1 cycle and 300 cycles. The pattern was identical to that of the 13.8 Ksi sample shown above.

9. Overall Observations

The tests can be grouped into three catagories. The first catagory would consist of the 5.8 Ksi (40 MPa) test, in which most of the decrease in modulus took place in the first 10 cycles, with little decrease thereafter. The second catagory would include the 8.7 Ksi (60 MPa), 10.2 Ksi (70 MPa), 11.6 (80 MPa), and 12.3 Ksi (85 MPa) tests, where there was a large drop in stiffness after the first cycle, and then a reduced, but sustained decrease over the rest of the cycling, with no failure. The third category, includes the 13.0 Ksi (90 MPa), 13.8 Ksi (95 MPa), and the 14.5 Ksi (100 MPa) tests, all of which failed in less than 1000 cycles.

After fatigue testing was completed, the residual strengths of the intact specimens were determined by statically loading the specimens until they failed. The residual strength values were recorded in the appendix in Table 14.

Was the elastic (linear) stress-strain modulus the appropriate parameter to use to monitor damage initiation and progression? The full cycle (non-linear) stress-strain curves were plotted as a function of cycle count for the 5.8 Ksi (40 MPa), 8.7 Ksi (60 MPa) 10.2 Ksi (70 MPa), and 13 Ksi (90 MPa) in Figures 46, 47, 48, and 49. These curves do not display residual strain. In theory, the modulus values of the unloading portion of these curves should have been equal to the corresponding elastic stress-strain modulus values.

The modulus values of the unloading portions of these stress-strain curves were generated by computer using a least squares curve fit (Tbl 11). The resulting values were compared to the elastic modulus data as a function of cycle count. Figures 50, 51, 52, and 53 present the comparisons. These modulus comparisons show that full cycle unloading modulus curves and the elastic modulus curves follow the same trends.

C. Theoretical and Analytical Models

This section will compare the test results with the theoretical and analytical models.

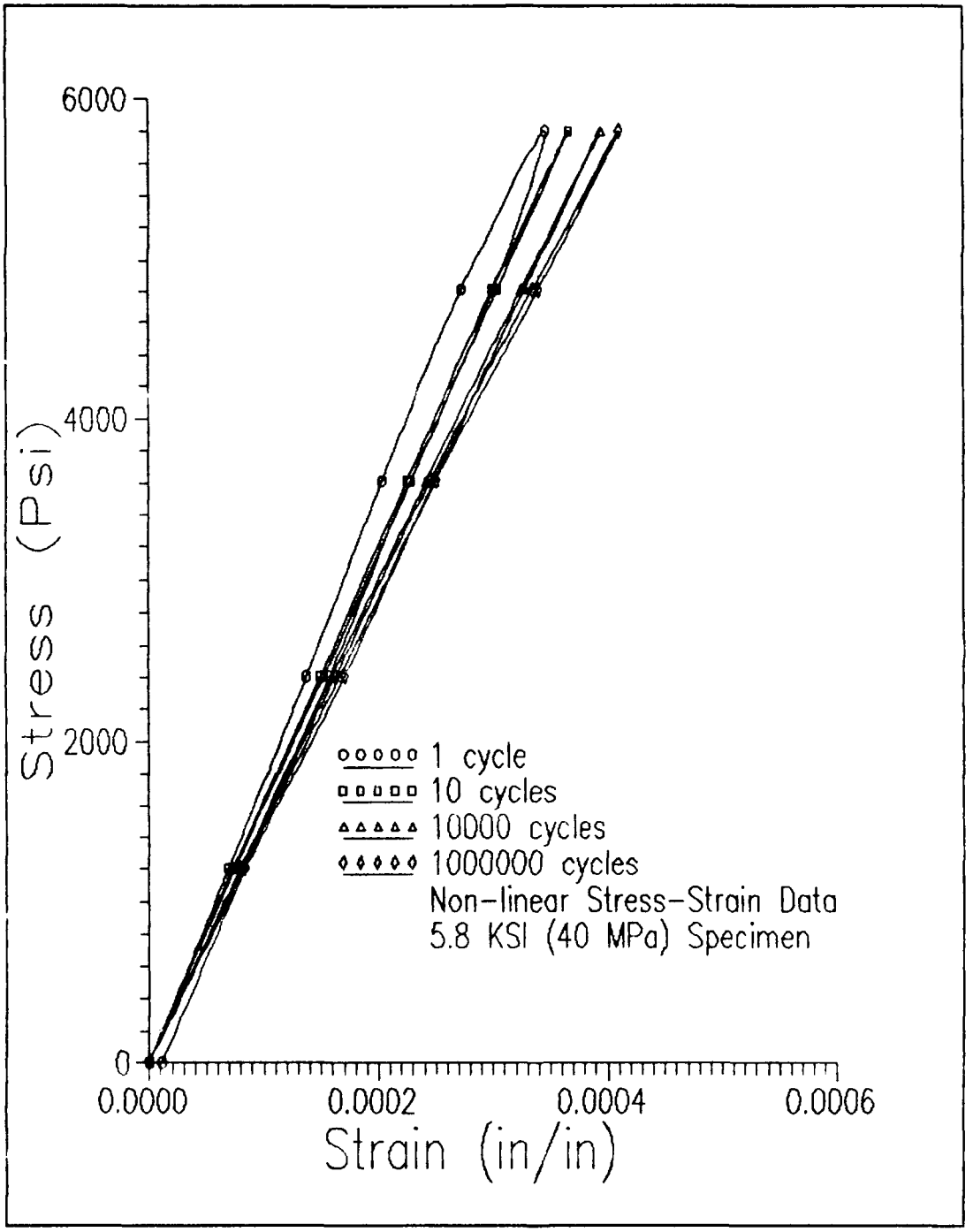

Figure 46 **Full Cycle Stress-Strain Data**
5.8 KSI (40 MPa) Specimen

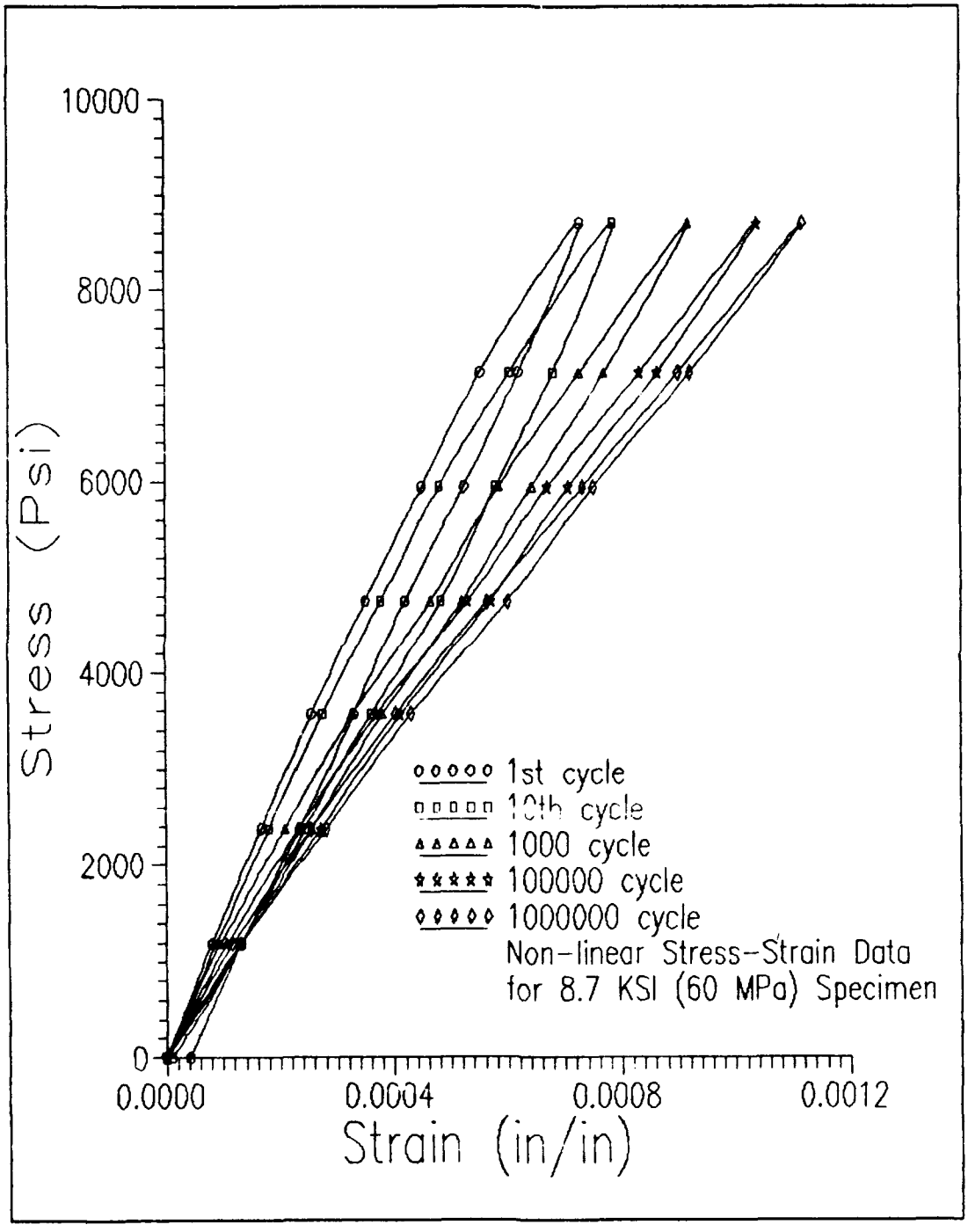

Figure 47 **Full Cycle Stress-Strain Data 8.7 KSI (60 MPa) Specimen**

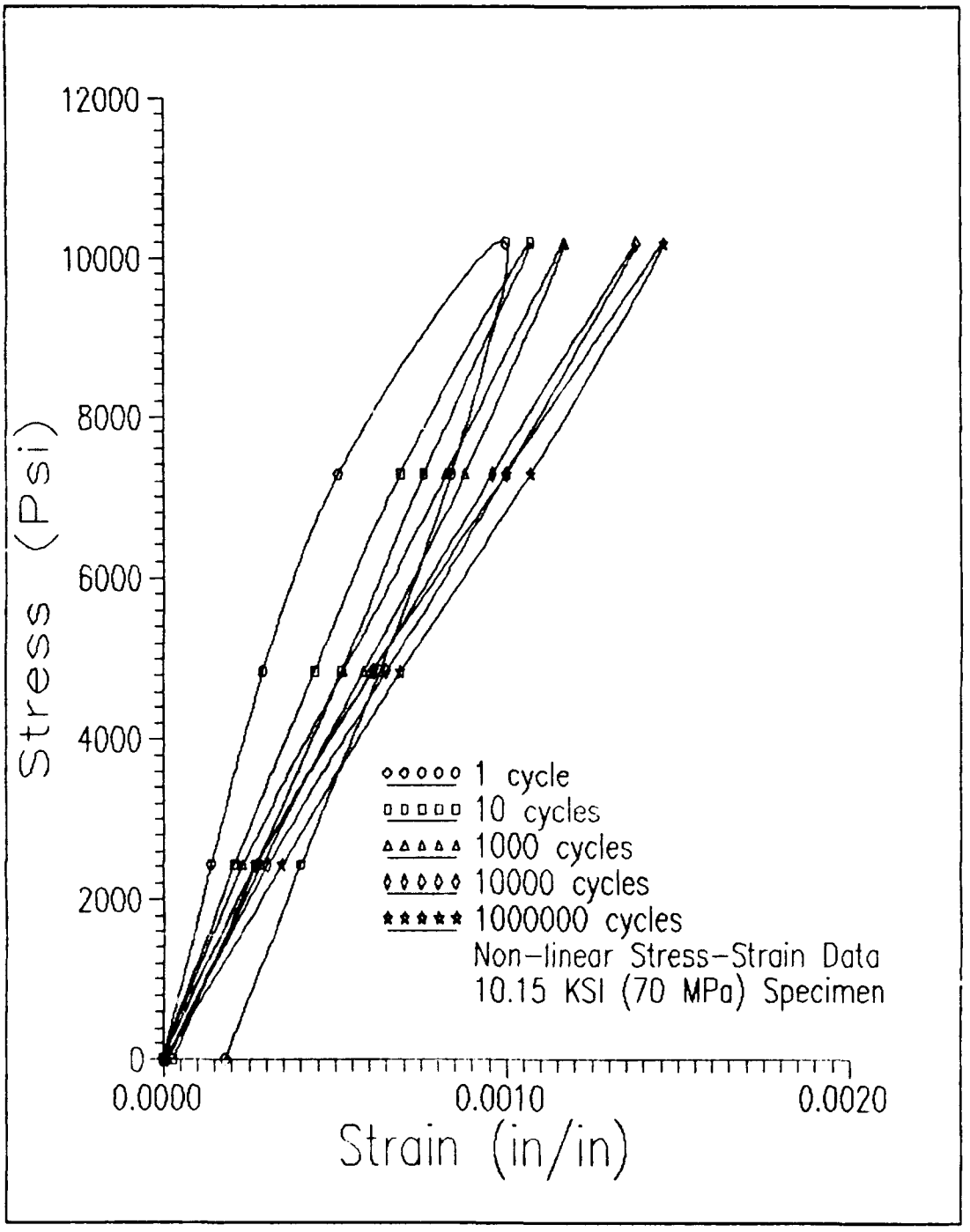

Figure 48 **Full Cycle Stress-Strain Data 10.15 KSI (70 MPa) Specimen**

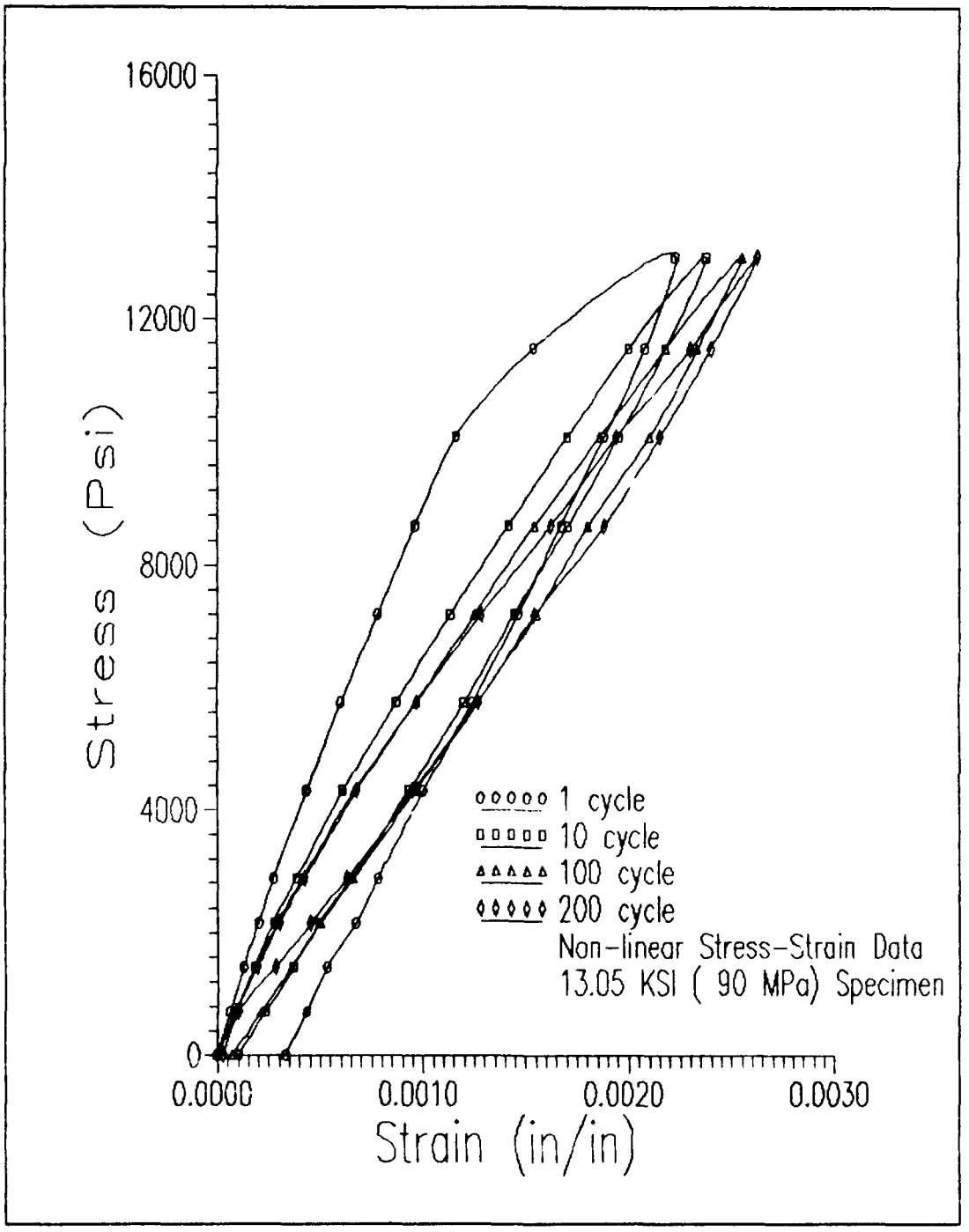

Figure 49 **Full Cycle Stress-Strain Data**
13.0 KSI (90 MPa) Specimen

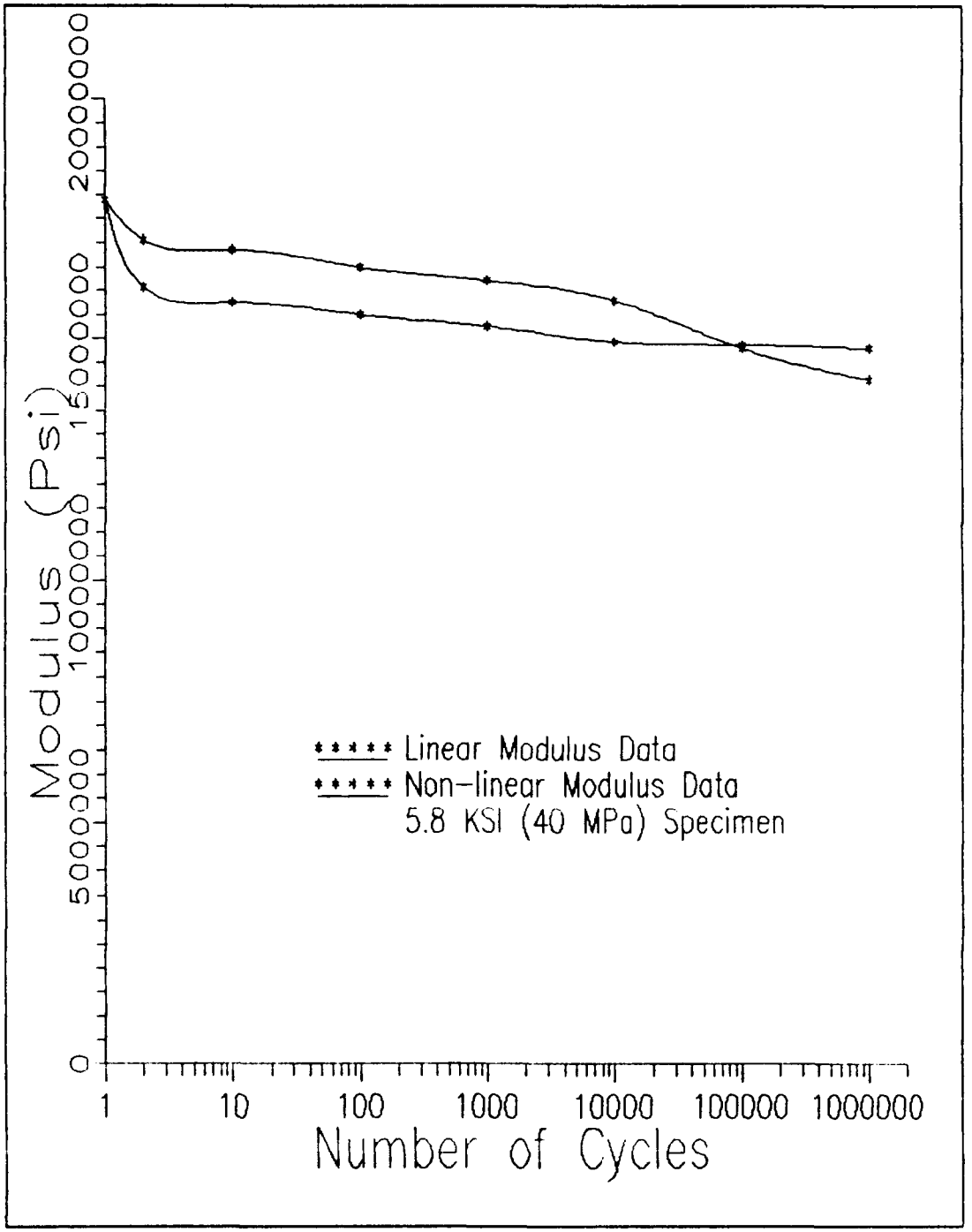

Figure 50 Modulus Comparison
5.8 KSI (40 MPa) Specimen

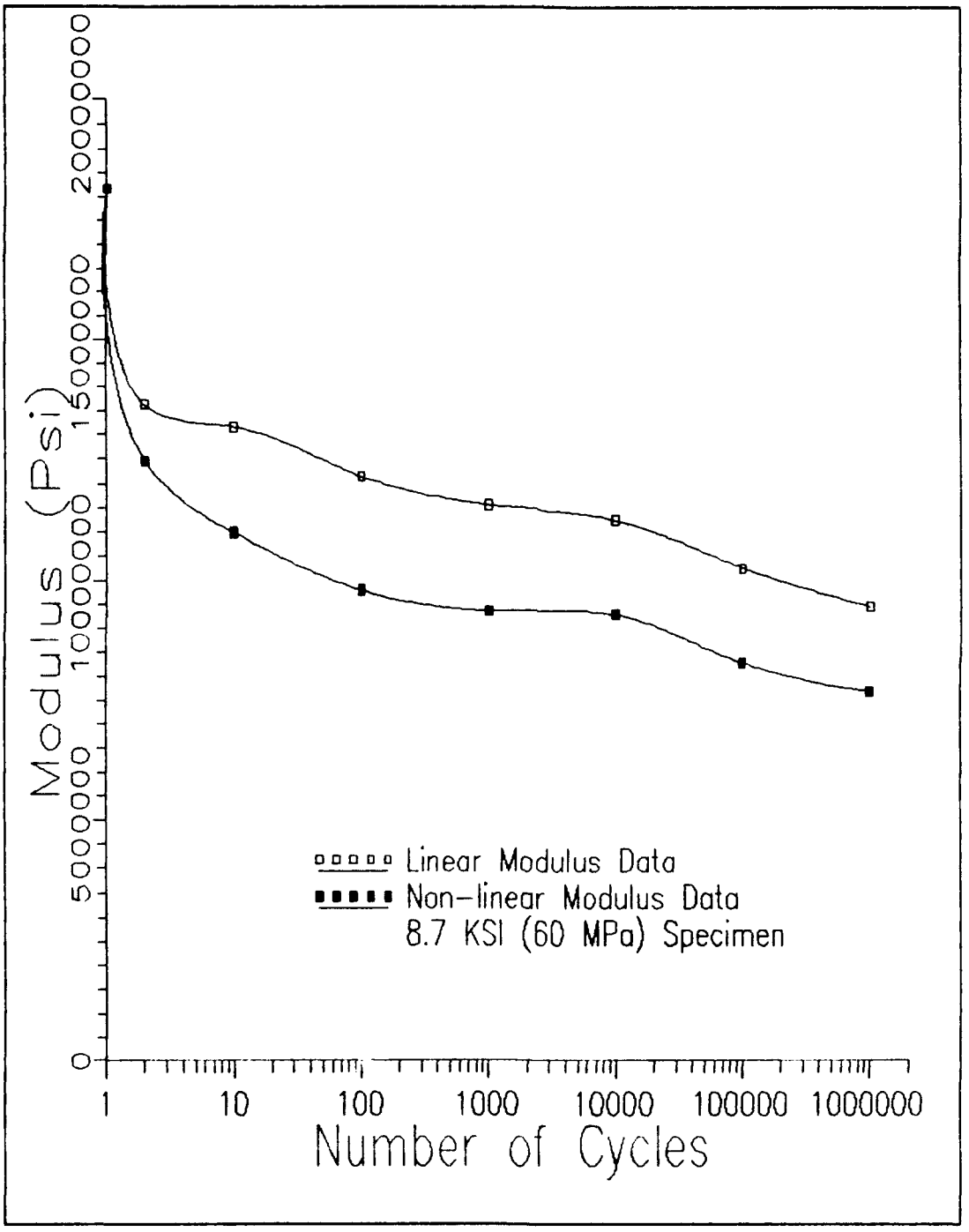

Figure 51 **Modulus Comparison**
8.7 KSI (60 MPa) Specimen

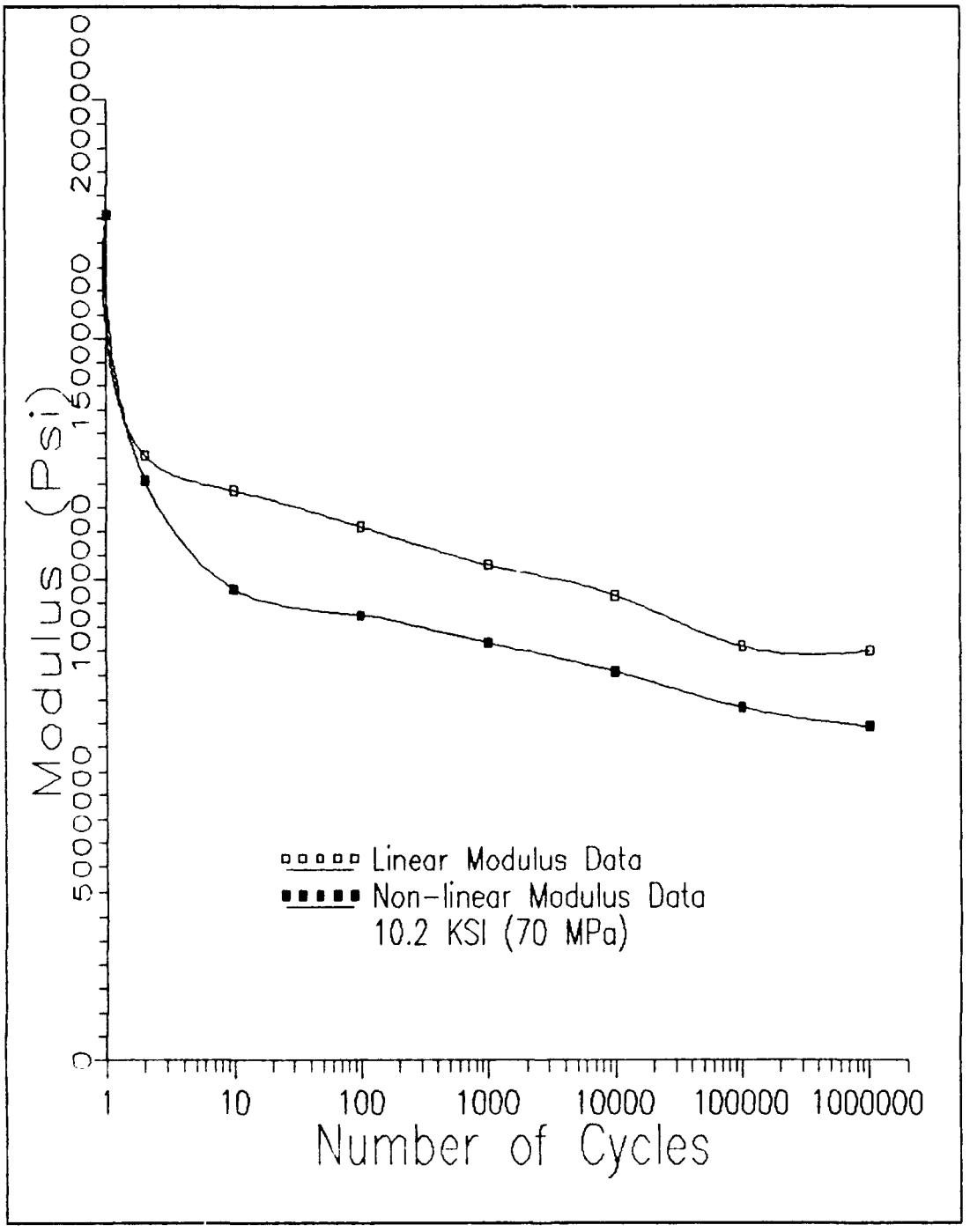

Figure 52 **Modulus Comparison**
10.2 KSI (70 MPa) Specimen

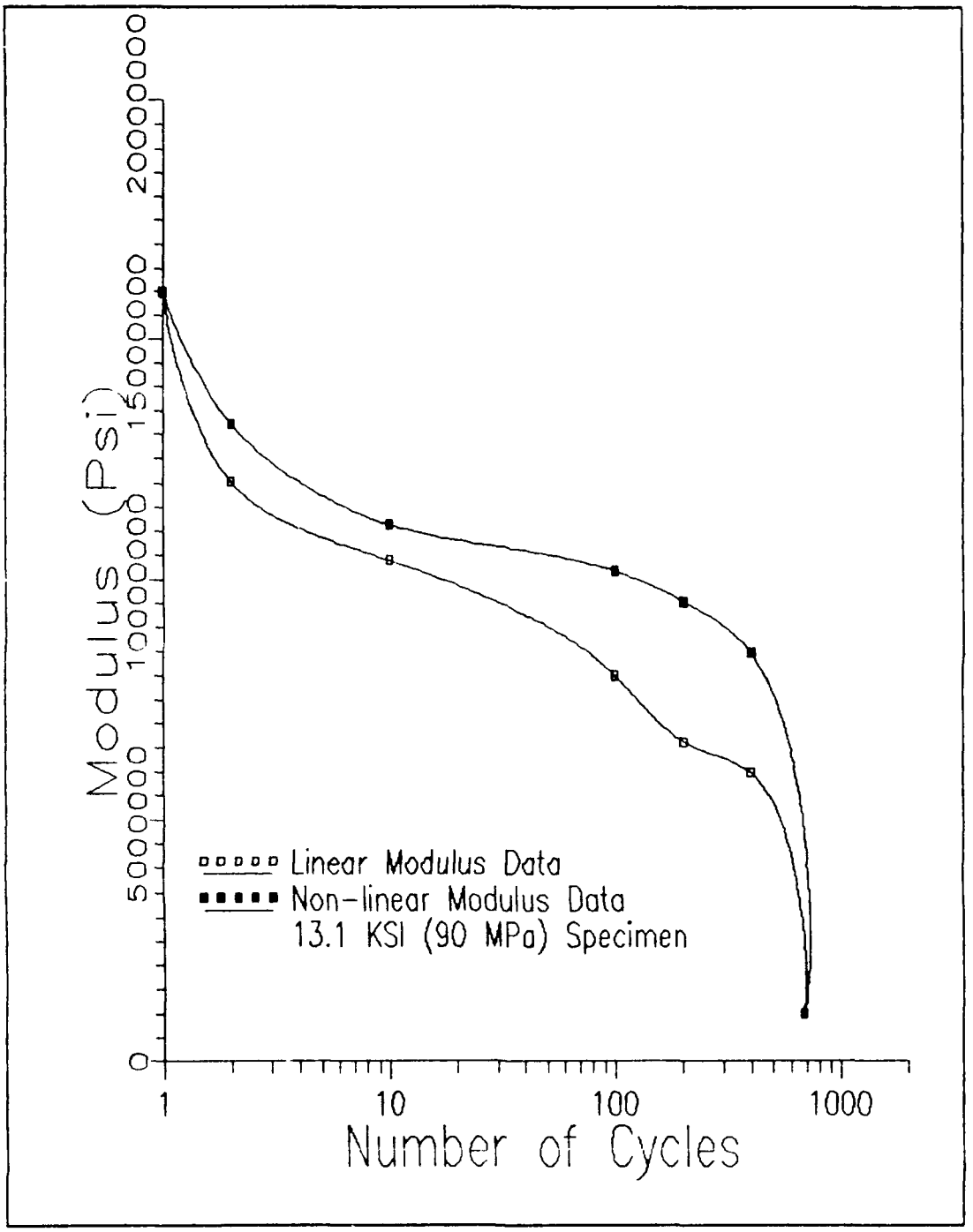

Figure 53 **Modulus Comparison**
13.0 KSI (90 MPa) Specimen

As discussed in Chapter II, classical laminated plate theory was intended for static problems, but prior studies have shown that the theory can be used as a tool to predict residual fatigue life. The values for principal longitudinal and transverse modulii (E_1 and E_2), principal Poisson's ratio (ν_{12}), and principal shear modulus (G_{12}), that Fink (10) had determined for the unidirectional lamina of this material were used to find the principal modulii (E_x) for the laminate. Fink found the following properties for the lamina.

$$E_1 = 20.16\ MSI\ (139\ GPa)$$

$$E_2 = 14.025\ MSI\ (96.7\ GPa)$$

$$\nu_{12} = .247$$

$$G_{12} = 6.381\ MSI\ (44\ GPa)$$

When these values were inserted into equations 5-12 in Chapter II and the rest of the calculations performed using a measured average thickness, t = .131 inches, the laminate stiffness matrices produced a value for the longitudinal stiffness of E_x = 17.616 Msi (121.46 GPa). This value was within 2 percent of the experimentally determined value for the average initial stiffness of 17.413 Msi (119.38 GPa) for the tested specimens, and within 5 percent of the elastic

modulus value of 116.5 Ksi (114.9 GPa) that Mall and Kim (7) had experimentally determined for the same material.

Next, the modulus was found when the 90 degree plies were discounted, the following material properties for the 90 degree plies were set equal to zero.

$$\bar{Q}_{11} = \bar{Q}_{12} = \bar{Q}_{16} = \bar{Q}_{22} = \bar{Q}_{26} = \bar{Q}_{66} = 0$$

The laminate stiffness matrices now produce a value for the longitudinal stiffness of the material, E_x = 13.93 Msi (96.05 GPa). This value of laminate material stiffness reflects the theoretical elastic modulus of the material for complete 90 degree ply failure.

The next step was to find the value of the longitudinal stiffness for total off-axis ply failure. In order to determine the stiffness for the 45 and 90 degree ply discount, the same values that were set to zero for the 90 degree ply discount were now set to zero for the 90^0 and 45^0 degree plies. The laminated plate equations produced a longitudinal stiffness matrix that set E_x = 5.304 Msi (36.57 GPa).

When the values of E_x for the three cases above were plotted along with the modulus versus cycle count curves of the eight tested specimens, as seen in Figure 54, several observations became apparent.

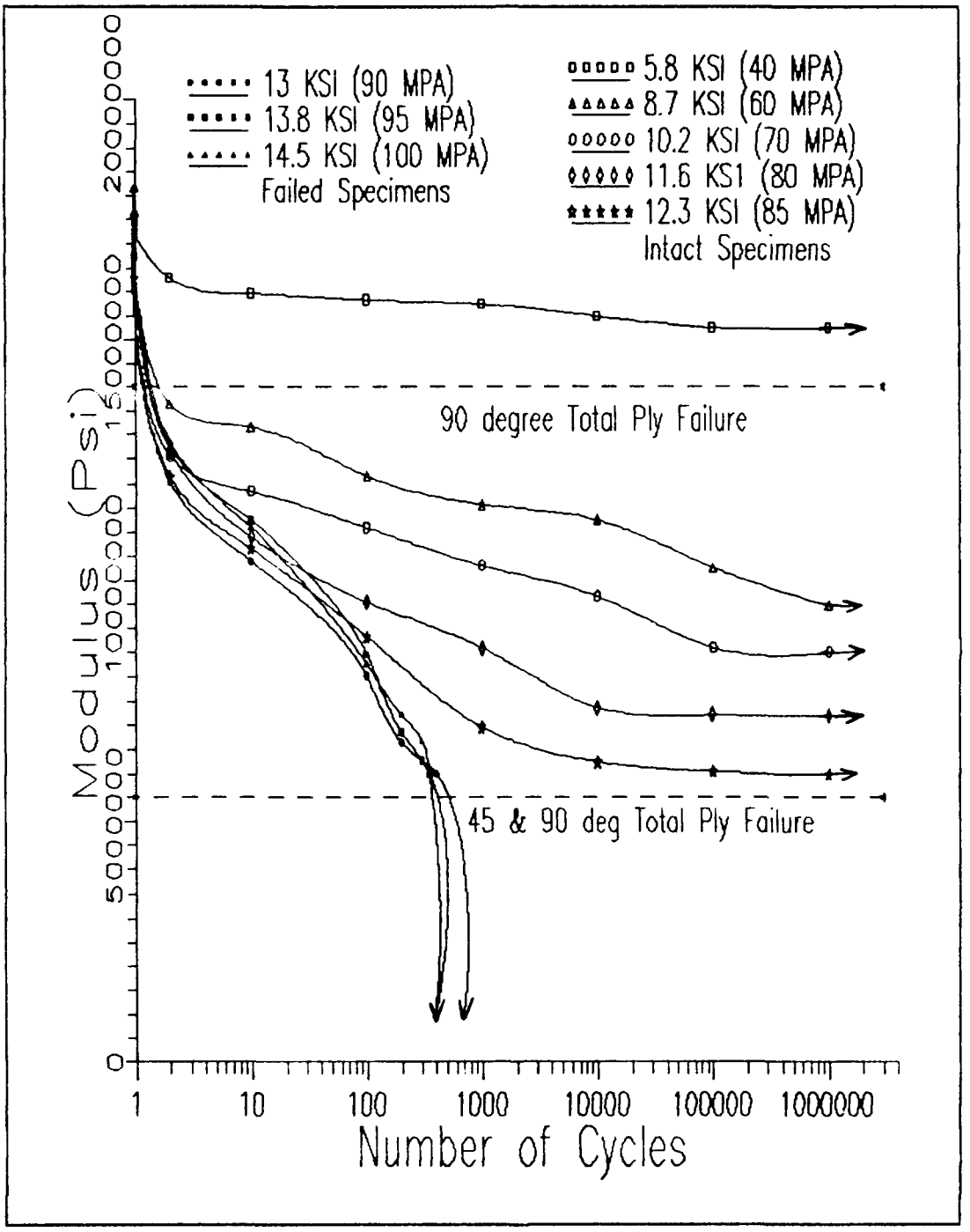

Figure 54 **Modulus Vs. Cycle Count For All Specimens With Lines of Total Ply Discount**

First, the separation of the three different categories of damage in the test specimens could be based on the ply discount method. The first category, which consisted of just the 5.8 Ksi (40 MPa) specimen, was the only one above the 90 degree ply total ply failure line. The theory agrees with the experimental results, since the 5.8 Ksi (40 MPa) stress was experimentally determined to be the first ply failure stress for the material by Mall and Kim (7). The theory also coincided with the observations of the replications, in which there was only evidence of total failure in the 90 degree plies, with some minor damage in the 45^0 plies, and no damage done to the 0^0 plies.

The second grouping of specimens fell between the line of the theoretical 90^0 total ply failure and the line of the theoretical 45^0 and 90^0 ply failure. Once again the classical laminated plate theory was consistant with the experimental results. The four specimens; 8.7 Ksi (60 MPa), 10.15 Ksi (70 MPa), 11.6 Ksi (80 MPa) and 12.33 Ksi (85 MPa), that fell in this region exhibited various degrees of damage in the off-axis plies that increased as a function of applied stress. Damage in the 0^0 plies was limited, as shown in the replication micrographs. All of these specimens lasted for one million cycles or more.

Finally, the last grouping of specimens will be consid-

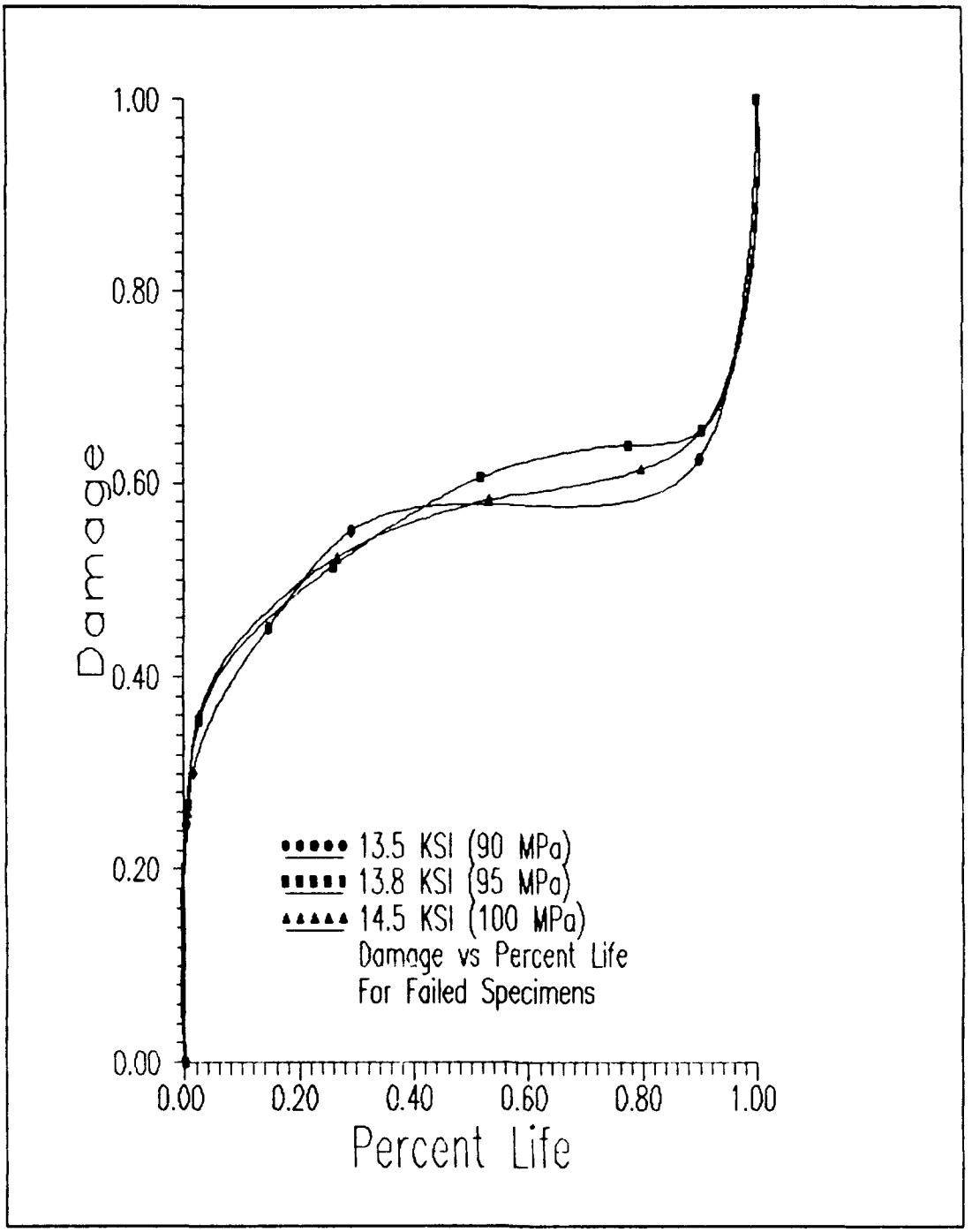

Figure 55 **Damage Vs. Percent Life Curves 13.0 KSI, 13.8 KSI, 14.5 KSI Specimens**

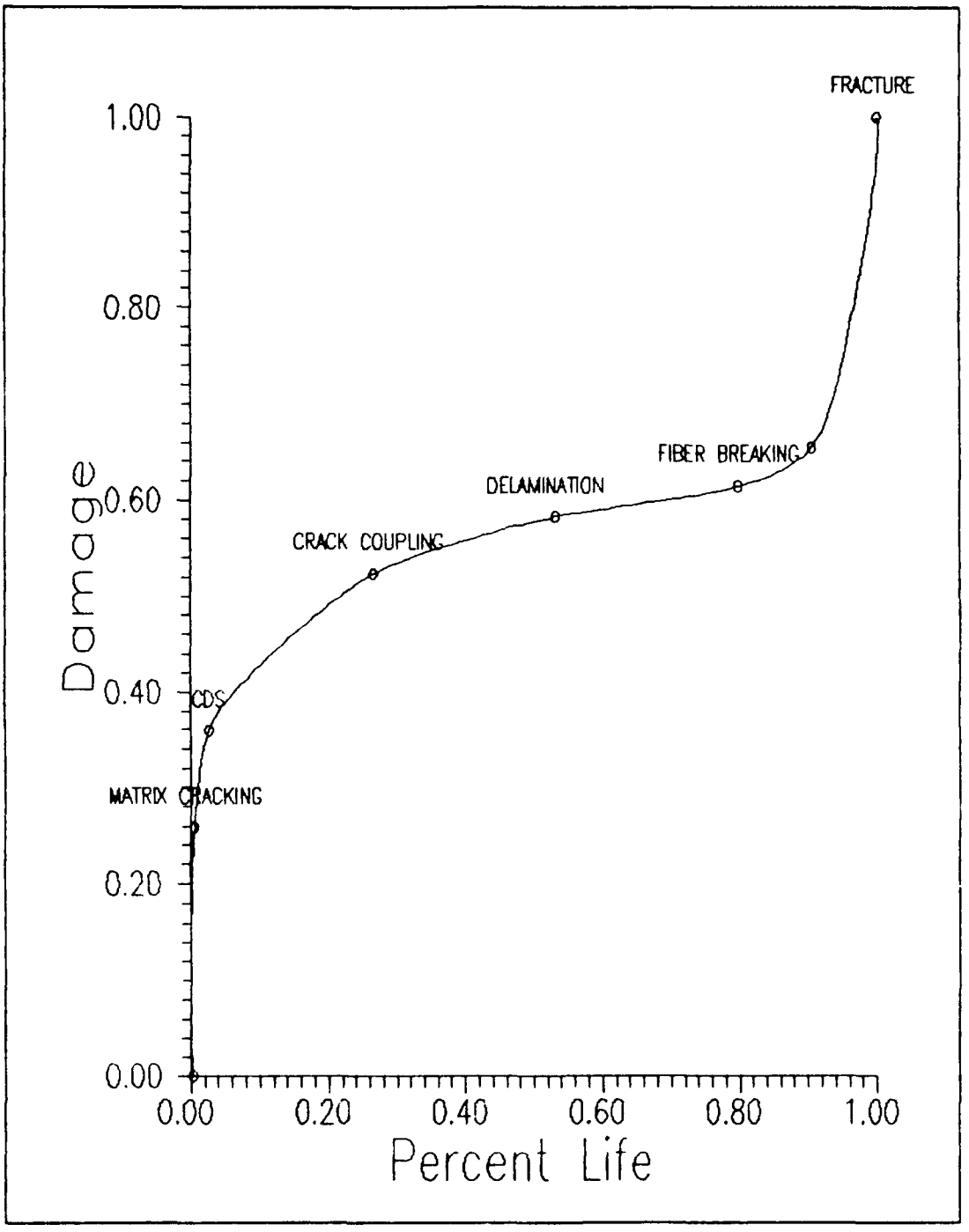

Figure 56 Fatigue Damage Modes in Composite Laminates (From Reifsnider et al. [8])

ered. All of these specimens; 13.0 Ksi (90 MPa), 13.78 Ksi (95 MPa) and 14.5 Ksi (100 MPa), failed within 700 cycles. Significant damage in the 0^0 plies did not appear immediately, but within 10 to 50 cycles, depending upon the applied stress level of the test, substantial cracking had begun in this ply.

When the damage parameter was plotted as a function of the percent of life for each sample (Figure 55), the resulting curves were similar to the schematic that Reifsnider et al. (8) had used to illustrate fatigue damage development for polymer composites (Figure 56). The stages of the curves that were noted in the results corresponded with the five modes that Reifsnider et al. had used to describe the state of damage progression in the model that was developed. The first stage of the curve coincided with the off-axis matrix cracking, which lead to a steep increase in the damage parameter during the first few cycles. After this first large increase in the damage parameter the curve stabilized, where Reifsnider et al. stated that the composite would reach a characteristic damage state (CDS). The second slope of the curves concurred with the next two modes of crack coupling and delamination and finally the last part of the curves concurred with the last two modes of fiber breaking in the 90^0 plies, and fracture.

The results of this test also confirmed that the "Critical Element" approach for residual fatigue life estima-

tion proposed by Reifsnider et al., can be used with some degree of accuracy for this class of ceramic matrix composites. In this case the critical elements have been identified as the 0^0 plies and the sub-critical elements have been identified as the 90^0 and 45^0 plies. As stated before, the critical elements directly limit the life of the composite, the sub-critical elements define the the changing state of stress in the critical element. If the material is stressed below a certain fatigue limit, that is, as long as the critical elements, the 0^0 plies, are not significantly damaged, the material remained intact indefinitely. But if that threshold was exceeded, and the critical elements are damaged, the material had a very limited lifespan.

Figure 57 illustrates the dichotomous nature of this material. Any specimen tested at 12.33 Ksi (85 MPa) or below remained intact for more than 1 million cycles, while any test conducted at 13.0 Ksi (90 MPa) or above failed in less than 700 cycles. Therefore, for this material, the fatigue stress limit occurred at 13.0 Ksi (90 MPa).

When compared with other Nicalon/CAS fatigue studies done previously, the results of this study were similar. In the research done by Zawada and Butkus (6), the results of that study depicted the dichotomous behavior of $(0/90)_{3S}$ and $(0)_{10}$ specimens. The results of these test indicated a fatigue

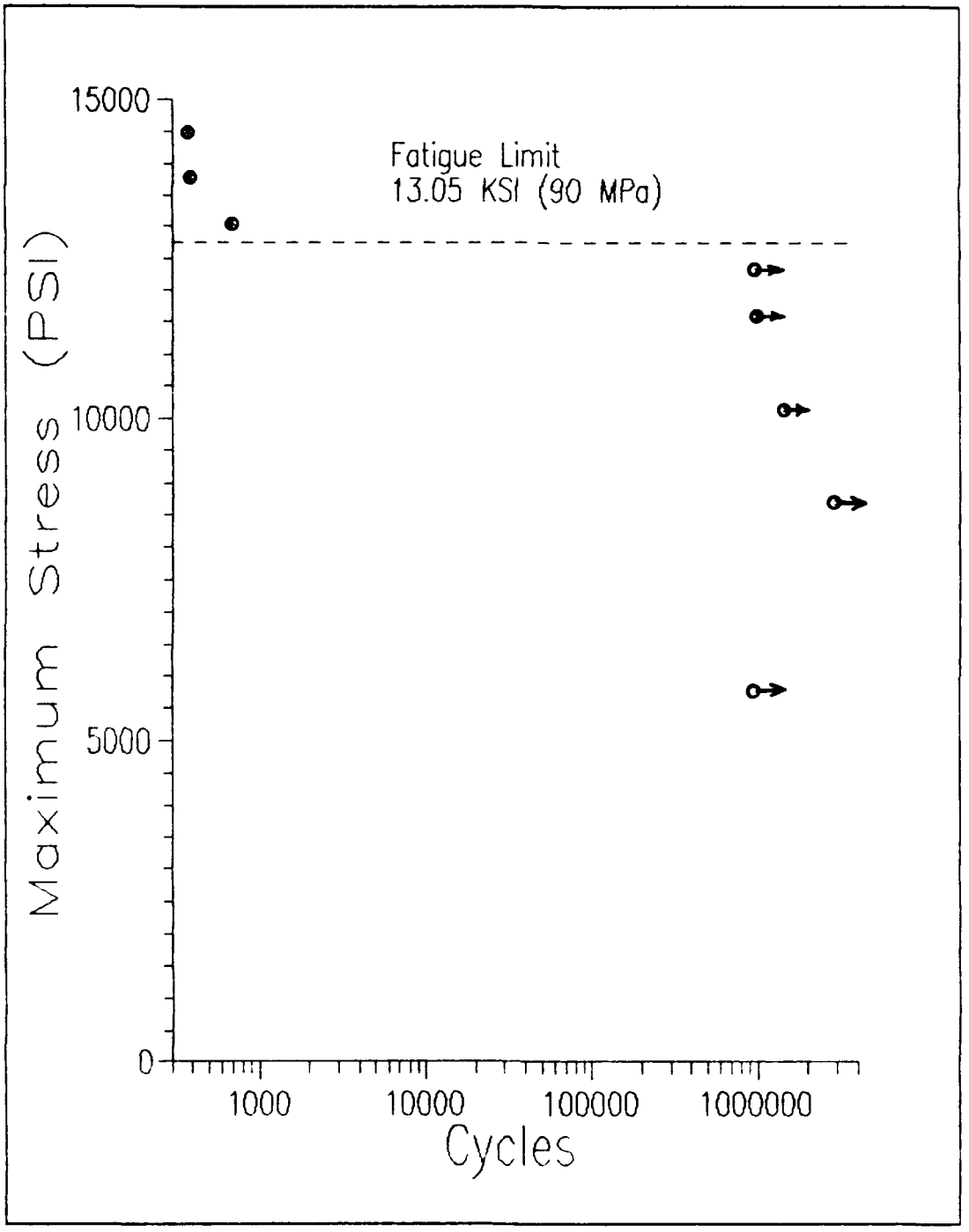

Figure 57 **Fatigue Life Vs. Maximum Applied Stress**

limit of 440 MPa for a $(0)_{10}$ SiC/1723 lay-up, and a fatigue limit of 200 MPa for a $(0/90)_{3S}$ Sic/1723 lay-up. Rousseau (2) validated the use of the critical element approach for brittle matrix ceramic composites and demonstrated that the 0 degree plies were the critical elements in fatigue testing of $(0/90)_{2S}$ Nicalon/CAS laminates. These tests indicated that the fatigue limit for a $(0/90)_{2S}$ lay-up was between 125 MPa to 150 MPa, depending upon the lot tested.

The residual strengths of the of intact specmiens were plotted against applied fatigue stress level in Figure 58. The theoretical values of residual strength were determined using the Tsai-Wu failure criterion for the 0 degree plies, in conjunction with the classical plate theory and ply discount methods described by Jones (11:48-186). These values are recorded in Table 12 of the appendix along with the test results. The comparison between the theoretical and experimental values is presented in Figure 58 where the correlation between the theory and the experimental results can be observed.

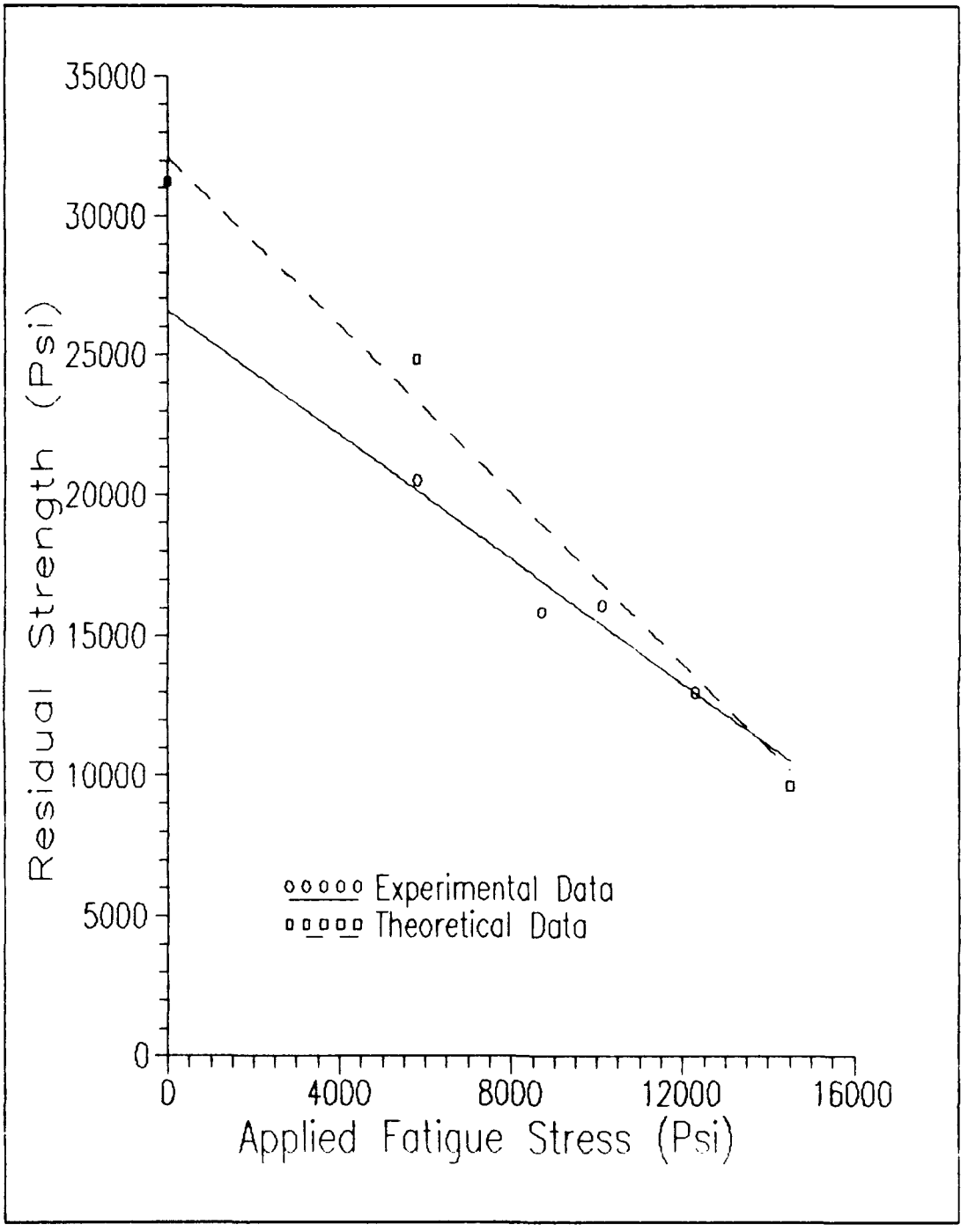

Figure 58 Residual Strength Vs. Applied Fatigue Stress

V. Conclusions

A study was conducted to investigate in a systematic way, the tensile fatigue damage machanisms in a quasi-isotropic ceramic matrix composite. A grip fixture capable of fatigue testing a small ceramic test sample with a minimum of bending moments was developed and integrated into an MTS servo-hydraulic test machine.

A series of tensile fatigue tests were performed with $(0/\pm 45/90)_S$ Nicalon fiber calcium-alumino-silicate matrix composites samples. The composite panel had a fiber volume of .34 and was manufactured by Corning Glass Works. The material was tested in three regions of stress.

The first region test conducted at 5.8 Ksi (40 MPa) which led to initial damage of the 90 degree plies.

The second region tests were performed at 8.7 Ksi (60 MPa), 10.2 Ksi (70 MPa), 11.6 Ksi (80 MPa), and 12.33 Ksi (85 MPa) in which there was initial damage in the 90 degree plies and varying degrees of damage in the 45 degree plies.

The last series of tests were performed at 13.1 Ksi (90 MPa), 13.8 Ksi (95 MPa), and 14.5 Ksi (100 MPa) stress levels in which there was initial damage in all plies.

The tension-tension tests were conducted at ambient room temperature and pressure, with a minimum stress to maximum

stress (σ_{min} / σ_{max}) ratio R = 1 / 10, and a sinusoidal cycling frequency of 10 hertz.

An extensometer was used to monitor the displacement over a one inch gage length, which provided the elastic modulus (E_1) as a function of applied fatigue cycles. Acetate film replications were used to monitor the initiation and progression of damage.

Cracking initiated at the ply boundaries due to strain differentials between the plies. In the first region tested (40 MPa), most of the damage occured on the 90^0 plies due to cracks that initiated in the $45^0/90^0$ bcundaries. In the second stress region (60-85 MPa), more damage occurred in the 45^0 plies due to increased crack initiation in the $45^0/45^0$ and $45^0/90^0$ boundaries. In the region above 90 MPa, the specimens failed as a result of fiber breakage in the 0^0 plies.

The material followed the same trend of fatigue damage modes suggested by Reifsnider et al (8). These modes, in order of occurrence were, matrix cracking in the off-axis plies, secondary cracking and crack coupling, delamination between plies, fiber breakage in the on-axis plies and finally failure.

Static classical laminated plate theory with total ply discount methods were used to predict modulus decrease and residual fatigue life in a simplified fashion. The values

determined with this method corresponded with the experimentally derived modulus values and also with the visual history of damage from the replications.

The experimental residual strength test results corelated well with the theoretical values determined using the Tsai-Wu failure criterion in conjunction with the Classical plate theory using total ply discount methods.

The critical element approach was used to model damage initiation and progression in the material. The 0^0 plies were identified as the critical elements of the laminate, and the off-axis 45^0 and 90^0 plies were identified as the sub-critical elements. If the material was fatigue cycled below the fatigue limit, the 0^0 plies remained intact, and the material had an indefinite lifespan, but once the applied stress exceeded the fatigue limit, the material failed within 700 cycles. This fatigue limit for this material was experimentally determined to be 90 MPa.

VI. Recommendations

In the present study, there was not enough time to address many of the issues in ceramic matrix composite fatigue damage mechanisms that need further study. The following areas merit consideration for future research.

First, a better design for the anti-rotation device in the grip system needs to be developed. Difficulty was encountered with the present device binding when specimens failed. This is not an immediate concern, but one that should be addressed.

Second, a new set of high strength, nickel alloy grip fixtures should be obtained to allow high temperature testing to take place. The present stainless steel grip fixtures are worn and will not withstand high temperatures.

Third, different laminate lay-ups should be tested. In particular, fatigue testing of a $(+45/-45)_n$ laminate would answer many questions concerning ceramic composite fatigue damage mechanisms.

Finally, high temperature testing should be performed. Since the room temperature damage mechanisms have been identified, this composite material should be examined for its fatigue behavior at the elevated temperatures where it will be commonly used.

Bibliography

1. Reifsnider, K.L. and Stinchcomb, W.W., "Fatigue Damage Mechanisms in Composite Materials," Fatigue Mechanisms, Proceedings of ASTM-NBD-NSF Symposium, Kansas City, Missouri: ASTM STP 675, May 1978 762-785

2. Rousseau, C.Q., "Fatigue Damage in Nicalon/CasII Ceramic Composites," General Electric Technical Memorandum TM-88-465: October 23 1988

3. Prewo, K.M., Layden, G.K., Minford, E.J. and Brennan, J.J., "Advanced Characterization of Silicon Carbide Fiber Reinforced Glass-Ceramic Matrix Composites" United Technologies Research Center Technical Report R85-916629-1 June 1985

4. Mandell, J.F., Grande, D.H., and Edwards, B.."Test Method Characterization of Fiber Composites At High Temperatures" Proceedings, 9th Annual Conference on Composites and Advanced Ceramic Materials American Ceramic Society, publisher, Columbus, Ohio 1985 524-535

5. Hartman, G.A. and Russ, S.M., "Techniques For Mechanical And Thermal Testing of Ti_3AL/SCS-6 Metal Matrix Composites" Metal Matrix Composites: Testing, Analysis, and Failure Modes ASTM STP 1032 American Society for Testing And Materials, publisher, Philadelphia, Pa. 1989 43-53

6. Zawada, L.P. and Butkus, L.M., "Room Temperature Tensile and Fatigue Properties of Silicon Carbide Fiber-Reinforced Aluminosilicate Glass" Proceedings, 14th Annual Conference on Composites and Advanced Ceramics, Coca Beach, Fl. 1990

7. Mall, S. and Kim, R.Y., "Damage Initiation and Growth in a Quasi-Isotropic Laminate of Ceramic Matrix Composite" Wright Research and Development Center, USAF Materials Laboratory Report, 1989

8. Reifsnider, K.L. and Stinchcomb, W.W. Composite Materials: Fatigue and Fracture, ASTM STP 907. American Society for Testing and Materials, Philadelphia, Pa., 1986 298-313

9. Daniel, I.M., Anastassopoulos, G., and Lee, J.W., "Failure Mechanisms In Ceramic Matrix Composites," Proceedings, of the 1989 Spring Conference of Experimental Mechanics Cambridge, Ma,. 1989 832-838

10. Fink, W.E., "Investigation of Failure Modes in a Ceramic Composite Under Off-Axis Loading," AFIT/GAE/ENY/89D-9, Air Force Institute of Technology, 1989

11. Jones, Robert M. Mechanics of Composite Materials. New York: Hemisphere Publishing Corporation, 1975.

12. Talreja, R. Fatigue of Composite Materials. Technomic Publishing Co., Inc. Lancaster, Pa. 1989

13. O'Brien, T.K. Damage in Composite Materials. ASTM STP 775. American Society for Testing and Materials, Philadelphia, Pa., 1982 140-167

14. Miller, H.R. "Cumulative Damage Model for Advanced Composite Materials." General Dynnamics Final Report, Contract F33615-81-C-5049. Ft. Worth, Tx., 1985

Appendix

Modulus and Damage Tables

Cycle Count	Modulus (Psi)	Damage
1	17880000	0
2	16056000	.102
10	15750000	.119
100	15500000	.133
1000	15250000	.147
10000	14940000	.165
100000	14870000	.168
1000000	14799000	.172

Table 3 Linear Modulus And Damage Data
5.8 KSI (40 MPa) Specimen

Cycle Count	Modulus (Psi)	Damage
1	18150000	0
2	13640000	.248
10	13180000	.274
100	12150000	.331
1000	11570000	.362
10000	11250000	.380
100000	10270000	.434
1000000	9470000	.478

Table 4 Linear Modulus and Damage Data
8.7 KSI (60 MPa) Specimen

Cycle Count	Modulus (Psi)	Damage
1	17570000	0
2	12560000	.285
10	11840000	.326
100	11090000	.369
1000	10310000	.413
10000	9670000	.449
100000	8600000	.510
1000000	8520000	.515

Table 5 Linear Modulus and Damage Data
10.2 KSI (70 MPa)

Cycle Count	Modulus (Psi)	Damage
1	16730000	0
2	12676000	.242
10	10900000	.351
100	9550000	.429
1000	8600000	.486
10000	7370000	.559
100000	7220000	.569
1000000	7200000	.570

Table 6 Linear Modulus and Damage Data
11.6 KSI (80 MPa)

Cycle Count	Modulus (Psi)	Damage
1	16270000	0
2	12140000	.254
10	10660000	.345
100	8830000	.457
1000	6970000	.572
10000	6250000	.616
100000	6060000	.627
1000000	6000000	.631

Table 7 Linear Modulus and Damage Data
12.3 KSI (85 MPa) Specimen

Cycle Count	Modulus (Psi)	Damage
1	15980000	0
2	12030000	.247
10	10400000	.309
100	8020000	.498
200	6644000	.585
600	6000000	.624
687	0	1.0

Table 8 Linear Modulus and Damage Data
13.1 KSI (90 MPa) Specimen

Cycle Count	Modulus (Psi)	Damage
1	17414000	0
2	12770000	.267
10	11240000	.354
100	8460000	.514
200	6860000	.605
300	6280000	.639
383	0	1.0

Table 9 Linear Modulus and Damage Data
13.8 KSI (95 MPa) Specimen

Cycle Count	Modulus (Psi)	Damage
1	17325000	0
2	12860000	.258
10	11100000	.359
100	8260000	.523
200	7234000	.582
300	6683000	.614
376	0	1.0

Table 10 Linear Modulus and Damage Data
14.5 KSI (100 MPa) Specimen

Cycle Count	5.81 KSI Modulus (Psi)	8.70 KSI Modulus (Psi)	10.1 KSI Modulus (Psi)	13.1 KSI Modulus (Psi)
1	17885000	18150000	17570000	15980000
2	7053000	12470000	12053000	13232000
10	16750000	10980000	9797000	11137000
100	16200000	9800000	9250000	10191000
200	-	-	-	9556000
600	-	-	-	8500000
687	-	-	-	0
1000	16200000	9380000	8680000	-
10000	15800000	9300000	8085000	-
100000	14800000	8300000	7339000	-
1000000	14100000	7700000	6951000	-

Table 11 Full Cycle Unloading Modulus Data
5.8, 8.7, 10.1 and 13.1 KSI Specimens

Applied Fatigue Stress (Psi)	Experimental Residual Strength (Psi)	Theoretical Residual Strength (Psi)
0	-	31212
5800	20530	24840
8700	15860	-
10100	16100	-
12300	13000	-
14500	-	9650

Table 12 Experimental and Theoretical
Residual Strength Data

Vita

Captain Gregory D. Tracy was born on 26 September 1957 in Louisville, Kentucky. He graduated from Bellevue High School, Bellevue, Kentucky in 1975. He then attended Cincinnati Technical College from which he received an Associates Degree in Electronics in June 1977. Upon graduation, he enlisted in the US Air Force as an computer technician. In 1982, he was selected for the Airman Education and Commission Program (AECP) and attended California State Polytechnic University in Pomona, from which he received a Bachelor of Science Degree in Aerospace Engineering in June 1985. He then attended and received his commission from Officer Training School and was assigned to Falcon AFB where he worked as a Satellite Vehicle Engineer. He entered the School of Engineering, Air Force Institute of Technology in May 1989.

Permanent address: 17 South Sherry Lane
Bellevue, Kentucky 41073

REPORT DOCUMENTATION PAGE

Form Approved
OMB No 0704-0188

1. AGENCY USE ONLY (Leave blank)	2. REPORT DATE	3. REPORT TYPE AND DATES COVERED
	December 1990	Master's Thesis

4. TITLE AND SUBTITLE
FAILURE MECHANISMS IN A QUASI-ISOTROPIC CERAMIC COMPOSITE LAMINATE UNDER TENSILE FATIGUE LOADING

5. FUNDING NUMBERS

6. AUTHOR(S)
Gregory D. Tracy, Captain, USAF

7. PERFORMING ORGANIZATION NAME(S) AND ADDRESS(ES)
Air Force Institute of Technology, WPAFB OH 45433

8. PERFORMING ORGANIZATION REPORT NUMBER
AFIT/GAE/ENY/90D-30

9. SPONSORING MONITORING AGENCY NAME(S) AND ADDRESS(ES)

10. SPONSORING MONITORING AGENCY REPORT NUMBER

11. SUPPLEMENTARY NOTES

12a DISTRIBUTION AVAILABILITY STATEMENT
Approved for public release; distribution unlimited

12b. DISTRIBUTION CODE

13. ABSTRACT *(Maximum 200 words)*

A study was conducted to experimentally investigate the tensile fatigue damage mechanisms in a quasi-isotropic ceramic matrix composite (Corning's Nicalon/CASIII). The goals of this study were to (1) develop a grip fixture for a servo-hydraulic MTS test machine and (2) conduct a series of tests with $(0/\pm 45/90)_s$ specimens subjected to tensile fatigue loading to study their fatigue damage growth mechanisms. Results showed that when the material was subjected to stresses below 90 MPa, it lasted over 1000000 cycles but when stressed at or above 90 MPa, it failed in less than 1000 cycles.

14. SUBJECT TERMS	15. NUMBER OF PAGES
Ceramic Composite, Fatigue, Failure Mechanisms, Tensile Fatigue	120
	16. PRICE CODE

17. SECURITY CLASSIFICATION OF REPORT	18. SECURITY CLASSIFICATION OF THIS PAGE	19. SECURITY CLASSIFICATION OF ABSTRACT	20. LIMITATION OF ABSTRACT
Unclassified	Unclassified	Unclassified	UL